Dispersion forces: Analysis of local-field effects and inclusion of excitation
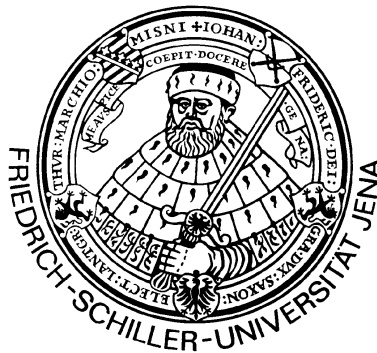
vorgelegt dem Rat der
PHYSIKALISCH-ASTRONOMISCHEN FAKULTÄT
der
FRIEDRICH-SCHILLER-UNIVERSITÄT JENA

von Dipl.-Phys. Agnes Sambale
geboren am 26.12.1982 in Leipzig.

Gutachter:

1. Prof. Dr. rer. nat. habil. Holger Gies, Jena

2. Prof. Dr. rer. nat. habil. Gert-Ludwig Ingold, Augsburg

3. Dr. rer. nat. Stefan Scheel, London

Tag der Disputation: 23. 02. 2012

Contents

Contents

1 Introduction

Out of the four fundamental forces that govern the interaction of matter, in many cases electromagnetic forces are the ones dominating on macroscopic scales. Nevertheless, in classical physics the interaction of neutral, unpolarized objects is governed by gravitation. The situation changes on a quantum level where quantum fluctuations of the electromagnetic field as well as of the charge and current densities of the interacting matter, have to be taken into account. In particular, there is a nonvanishing electromagnetic force – the dispersion force – even if the combined field–matter system is in its ground state and the interacting objects are neutral and unpolarized on a quantum average. We distinguish dispersion forces between macroscopic bodies, known as Casimir forces [1–3], those between a macroscopic body and an atom, called Casimir–Polder (CP) forces [4–6], and finally the forces between atoms, possibly in the presence of media, which are referred to as van der Waals (vdW) forces [5, 7]. Considering the gravitational ($\mathbf{F}_{\mathrm{G}}$) and the vdW force ($\mathbf{F}_{\mathrm{vdW}}$) between two (hydrogen) atoms shows that in the sub-mm regime vdW interactions start to dominate gravitation,

$$\frac{\mathbf{F}_{\mathrm{vdW}}}{\mathbf{F}_{\mathrm{G}}} \propto \left(\frac{0.5\mathrm{mm}}{r}\right)^6, \tag{1.1}$$

where we have employed the $1/r^8$ power law describing the retarded force of two atoms separated by distance r [5] and the ordinary law of gravitation. The two and many-atom vdW interaction may also be interpreted as the microscopic origin of all (ground-state) dispersion forces [8–10]. It should be pointed out that the vdW interaction involving excited atoms has been subject to discussions until now [11–14]. There is a vastness of theoretical work concerning the (static) Casimir force. Many of these studies are based on Lifshitz theory [2] which, in contrast to Casimir's normal-mode approach, allows for the inclusion of arbitrary dispersing and absorbing (linear) bodies as well as temperature effects (for a review see, e.g., [15]). Early investigations on (static) CP forces are usually based on linear response theory [16,17], but can also be obtained from Lifshitz theory by phenomenological treatment of the bodies. In full quantum theories, the electromagnetic field interacting with media may be quantized

in a canonical way based on a semi-microscopic matter model [18], or on using the concept of macroscopic quantum electrodynamics (QED) [19] or, alternatively, within a path-integral approach [20]. In macroscopic QED, all properties of the bodies enter via the classical Green tensor while an atom, subjected to the CP force, is described in terms of its polarizability and its transition frequencies. Conservative CP forces can then be calculated by determining the body-induced energy shifts in leading-order perturbation theory [21].

The impact of (commonly attractive) dispersion forces in science is immense. In biology, dispersion forces contribute to the organization of molecules [22–24] as well as to cell adhesion [22,23,25,26], and to the interaction of molecules with cell membranes [23, 25]. A very fascinating and practically relevant example is the gecko's ability to climb dry and smooth surfaces [27]. There is experimental evidence that vdW forces acting on each of the millions of microstructured hairs on the gecko's toe cause the sticking [28], though it may be influenced by other effects [29–31]. In colloid science, the (primarily dispersion-type) interactions between small clusters of particles in free space [32] and between spherical micro-and macro objects embedded in a liquid or colloidal suspension [33] are investigated. If the interaction is attractive, clustering or flocculation may occur [34] but can be balanced by other (repulsive) forces [35–38]. The consequences of dispersion forces are also noticeable in astronomy where laboratory experiments have shown that vdW forces contribute to the sticking of dust grains in the formation of planetesimals [39]. Furthermore, Casimir energies are controversially discussed to contribute to the cosmology constant [40].

The era of high-precision Casimir force experiments started in 1997 when the force between a metallic plate and a metallic spherical lens has been measured [41]. Corrections due to finite temperature, often referred to as the thermal Casimir effect, were measured in subsequent experiments [42–47] where the correct description of metals has caused a controversy [48–51]. Measurements of the CP energy of excited atoms are typically based on spectroscopic methods [52–54], while ground-state CP forces are measured by means of deflection experiments [55]. To accommodate experiment and theory, the impact of surface roughness has been subject to calculations [56–59]. In the last years, the detection of repulsive dispersion forces has been brought into focus [60, 61]. The possibility to create repulsive dispersion forces is of fundamental interest in micro-electromechanical systems where micro-objects may unintentionally stick to a surface when brought into close vicinity [62–65]. Repulsive dispersion forces may also be utilized for implementing trapping mechanisms [66,67], guiding atomic

beams in atom optics [68], enhancing quantum reflection [69], going towards quantum levitation [70] or facilitating superlubricity [60] by eliminating quantum friction [71].

In the last two decades much progress has been made in fabricating metamaterials [72, 73] with specified properties that might be used to control the strength and the sign of Casimir and CP forces. The frequently used concept of effective permittivity and permeability of materials is only valid on length scales which are sufficiently large in comparison to the elementary building blocks of the material. The material response can be determined theoretically [74, 75] or by means of reflection experiments [76]. Of particular interest are left-handed metamaterials [77, 78] which can be fabricated using periodic arrays of split–ring resonators [79, 80] or two-dimensional metal–insulator–metal waveguide structures [81]. Lefthanded materials have been predicted to lead to a number of unusual optical phenomena [82, 83] such as negative refraction [79, 82], invisibility devices [84, 85] and the possibility of a superlens: a planar left-handed slab is able to focus light with a resolution well beyond the diffraction limit [74]. The superlens concept has been subject to intense discussion [86, 87], and limiting factors such as the finite dimension of the lens [88] or the influence of absorption have been studied [89]. However, passive metamaterials suffer from high absorption which restricts desired metamaterial properties such as left-handedness [82, 83] to a narrow spectral bandwidth [90]. Hence, the influence of such properties on ground-state dispersion forces may be strongly reduced [91–94]. In general, the influence of absorption can be mitigated via introducing amplification as suggested in Refs. [90, 95, 96] and has been achieved recently for a metamaterial in the optical regime [97].

In parallel to these developments in experiments and applications, the possible realization of repulsive dispersion forces has been discussed theoretically. Three main mechanisms can be proposed: 1. Competing effects of electric and magnetic properties of the atoms [91, 93] and/or the bodies are known to lead to repulsive interactions [92, 98–100]. 2. An intervening medium between the Casimir objects [2, 101, 102] or a medium environment of the atom [103] may account for repulsion even for purely electric ground-systems. For atoms embedded in a medium the Onsager real cavity model [104] can be applied to model the difference between the local electromagnetic field at the position of the atom and the macroscopic one. The choice of the correct stress tensor of medium-embedded bodies has been subject to controversial discussion [105–108]. 3. Excitation in the form of excited atoms or active media provides the possibility to turn the sign of the force into repulsion. The vdW interaction was initially studied for excited atoms in free space [12, 13, 109–111], and later the presence

of ground-state media was taken into account [14]. Similarly, the CP interaction of a macroscopic ground-state body and an excited atom has been studied and found to contain (dominating) resonant contributions [112–114], which, depending on the relevant medium and atomic frequencies, can provide repulsive interactions. The CP potential of a ground-state atom in front of an excited dilute gaseous medium, as well as the Casimir interaction between two dilute samples of excited gas atoms has been investigated in Ref. [13]. To calculate the Casimir force on an amplifying body beyond the dilute-medium limit, an inclusion of amplification in the quantization scheme is necessary. An attempt in this direction was made for a slab-like system [115,116] which was later generalized on the basis of macroscopic QED in three dimensions [117]. In particular, the question of whether the Casimir force on an amplifying body can be repulsive as suggested in Ref. [70] has not been solved yet. Thermal excitation may also give rise to resonant force components in non-equilibrium systems [118]. The resonant force may have different signs depending on the temperature difference of the body and the medium-environment [119–122].

Dispersion forces on ground-state objects in free-space have been intensively discussed [6]. Motivated by the above mentioned applications, we investigate in this thesis how CP and Casimir forces can be controlled. Since the magnetic properties created in the context of metamaterials are usually not strong enough to give rise to repulsion [123], we concentrate on the second and third mechanism as introduced above. While excited systems are the most promising candidate for implementing repulsion, dispersion force on objects in media are also of interest to colloid science. We describe the Casimir and Casimir–Polder forces from first principles as Lorentz forces in the framework of macroscopic QED [10, 113]. We start with a review of the quantization procedure of the medium-assisted electromagnetic field in the presence of linear, partially amplifying media. The main part is primarily based on Refs. [AS1]– [AS7] and covers the following problems:

- Impact of the local-field correction on the ground-state CP potential
- Estimation of the ground-state CP potential at the interface between two media
- Dispersion interaction between spherical objects in media
- Resonant CP potential in a realistic superlens scenario
- Casimir force on an arbitrary, partially amplifying body
- Consistency of CP and Casimir force theory for excited matter
- Possibility of repulsive Casimir forces in planar geometries involving amplification

In the last chapter we summarize our results and give ideas for prospective works.

2 Fundamentals

A very successful way to formulate a consistent theory of dispersion forces is provided within the concept of macroscopic quantum electrodynamics, which describes the interaction of the electromagnetic field with nonrelativistic, macroscopic objects (media, bodies) and microscopic objects (atoms, molecules). In this approach, atoms can be described as (usually electric) dipoles, where the response of the medium and the bodies is described macroscopically. This description is valid as long as the distance between the bodies and distances between bodies and external atoms are larger than the inter-atomic length scales inside the bodies. As in classical electrodynamics the medium response is described by causal complex-valued electric permittivity and (para)magnetic permittivity functions. In this work, we restrict our attention to isotropic media that are linearly and locally responding to the electromagnetic field and introduce the permittivity $\varepsilon(\mathbf{r}, \omega)$ and permeability $\mu(\mathbf{r}, \omega)$.

As one of the key features of this thesis the bodies may also be partially amplifying, which is characterized by

$$\operatorname{Im} \varepsilon(\mathbf{r}, \omega) = \varepsilon_I(\mathbf{r}, \omega) < 0 \quad \text{and/or} \quad \operatorname{Im} \mu(\mathbf{r}, \omega) = \mu_I(\mathbf{r}, \omega) < 0 \tag{2.1}$$

for a limited space and frequency regime. The strength of the amplification must be such that the response to the electromagnetic field is still linear, which is particularly important in systems where waves pass through an amplifying medium repeatedly, such as high-Q resonators (details in Ref. [124]). A familiar model for an amplifying dielectric $\varepsilon(\mathbf{r}, \omega)$ [and analogously for $\mu(\mathbf{r}, \omega)$], consistent with the Kramers–Kronig relations, is of Drude–Lorentz type [116],

$$\varepsilon(\omega) = \varepsilon_b(\omega) - \frac{N_l - N_u}{N_l + N_u} \frac{S}{(\omega + \omega_t + i\gamma)(\omega - \omega_t + i\gamma)}, \tag{2.2}$$

where the medium resonance is characterized by the transverse frequency ω_t, strength S, and damping parameter γ, respectively. Other resonances are included in the background contribution $\varepsilon_b(\omega)$. For absorbing media with normal populations of the upper

level N_u and lower level N_l, $N_l > N_u$, we find that $\mathrm{Im}\,\varepsilon > 0$, while for gain-associated frequencies the population is inverted, $N_u > N_l$, implying $\mathrm{Im}\,\varepsilon < 0$. In both cases we find poles in the lower ω half-plane at $\omega = \pm\omega_t - i\gamma$, such that $\varepsilon(\mathbf{r},\omega)$ and $\mu(\mathbf{r},\omega)$ are analytic in the upper half plane including the real axis, apart from a pole at $\omega = 0$ for metals. As follows from causality, the medium becomes transparent for sufficiently high frequencies [6],

$$\lim_{\omega\to\infty} \varepsilon(\mathbf{r},\omega) = 1 + \mathcal{O}\left(\frac{1}{\omega^2}\right) \quad \text{and} \quad \lim_{\omega\to\infty} \mu(\mathbf{r},\omega) = 1 + \mathcal{O}\left(\frac{1}{\omega^2}\right). \tag{2.3}$$

In the following we review the quantization scheme as used in this thesis, where the possibility of amplification is included right from the start.

2.1 Field quantization in linear media

We start with the familiar (macroscopic) Maxwell equations for the operator-valued electric field $\underline{\hat{\mathbf{E}}}(\mathbf{r},\omega)$ and the induction field $\underline{\hat{\mathbf{B}}}(\mathbf{r},\omega)$ in Fourier space,

$$\boldsymbol{\nabla} \cdot \underline{\hat{\mathbf{B}}}(\mathbf{r},\omega) = 0, \tag{2.4}$$

$$\boldsymbol{\nabla} \times \underline{\hat{\mathbf{E}}}(\mathbf{r},\omega) - i\omega\underline{\hat{\mathbf{B}}}(\mathbf{r},\omega) = \mathbf{0}, \tag{2.5}$$

$$\varepsilon_0 \boldsymbol{\nabla} \cdot \underline{\hat{\mathbf{E}}}(\mathbf{r},\omega) = \underline{\hat{\rho}}(\mathbf{r},\omega), \tag{2.6}$$

$$\mu_0^{-1}\boldsymbol{\nabla} \times \underline{\hat{\mathbf{B}}}(\mathbf{r},\omega) + i\omega\varepsilon_0\underline{\hat{\mathbf{E}}}(\mathbf{r},\omega) = \underline{\hat{\mathbf{j}}}(\mathbf{r},\omega), \tag{2.7}$$

where we have introduced the frequency components in a picture-independent manner,

$$\hat{O}(\mathbf{r}) = \int_0^\infty \mathrm{d}\omega\,\underline{\hat{Q}}(\mathbf{r},\omega) + \text{H.c.}, \tag{2.8}$$

with H.c. denoting the hermitian conjugate. In the inhomogeneous Maxwell equations, the $\underline{\hat{\rho}}(\mathbf{r},\omega)$ and $\underline{\hat{\mathbf{j}}}(\mathbf{r},\omega)$ denote the internal charge and current densities, respectively, The charge and current densities are connected via the continuity equation

$$i\omega\underline{\hat{\rho}}(\mathbf{r},\omega) = \boldsymbol{\nabla} \cdot \underline{\hat{\mathbf{j}}}(\mathbf{r},\omega) \tag{2.9}$$

which, together with the solution of Eq. (2.4), $\underline{\hat{\mathbf{B}}}(\mathbf{r},\omega) = (i\omega)^{-1}\boldsymbol{\nabla} \times \underline{\hat{\mathbf{E}}}(\mathbf{r},\omega)$, implies that it is sufficient to consider the electric field and the current density. Hence, we continue with the combination of Eqs. (2.5) and (2.7), and obtain the integro-differential

equation

$$\boldsymbol{\nabla} \times \boldsymbol{\nabla} \times \underline{\hat{\mathbf{E}}}(\mathbf{r}, \omega) - \frac{\omega^2}{c^2} \underline{\hat{\mathbf{E}}}(\mathbf{r}, \omega) = \underline{\hat{\mathbf{j}}}(\mathbf{r}, \omega). \tag{2.10}$$

As in classical electrodynamics, if the internal atomistic structure of the (stationary) medium is not resolved, we introduce the constitutive relation in the form of Ohm's law,

$$\underline{\hat{\mathbf{j}}}(\mathbf{r}, \omega) = \int \mathrm{d}^3 r' \boldsymbol{Q}(\mathbf{r}, \mathbf{r}') \cdot \underline{\hat{\mathbf{E}}}(\mathbf{r}', \omega) + \underline{\hat{\mathbf{j}}}_N(\mathbf{r}, \omega), \tag{2.11}$$

to account for the (linear) response of the medium to the electromagnetic field with $\underline{\hat{\mathbf{j}}}_N$ being the noise current density. For a locally responding medium, the complex macroscopic conductivity tensor $\boldsymbol{Q}$ can be explicitly given as [125, 126]

$$\boldsymbol{Q}(\mathbf{r}, \mathbf{r}', \omega) = \sum_{\lambda=e,m} \boldsymbol{Q}_\lambda(\mathbf{r}, \mathbf{r}', \omega), \tag{2.12}$$

$$\boldsymbol{Q}_e(\mathbf{r}, \mathbf{r}', \omega) = -i\varepsilon_0 \omega [\varepsilon(\mathbf{r}, \omega) - 1] \delta(\mathbf{r} - \mathbf{r}') \boldsymbol{I}, \tag{2.13}$$

$$\boldsymbol{Q}_m(\mathbf{r}, \mathbf{r}', \omega) = -\frac{1}{i\omega\mu_0} \boldsymbol{\nabla} \times \left[1 - \frac{1}{\mu(\mathbf{r}, \omega)} \right] \delta(\mathbf{r} - \mathbf{r}') \boldsymbol{I} \times \overleftarrow{\boldsymbol{\nabla}}'. \tag{2.14}$$

where $\boldsymbol{I}$ is the second-rank unit tensor and $\overleftarrow{\boldsymbol{\nabla}}'$ characterizes the gradient to the left with respect to $\mathbf{r}'$. Note that the notation with the conductivity tensor is very general: In Refs. [10, 127] the quantization scheme has been extended to allow for anisotropic, nonlocal and nonreciprocal media. The fluctuations of the noise current density immediately give rise to fluctuations of the electromagnetic field, which at zero-temperature are a pure quantum effect in agreement with Heisenberg's uncertainty principle. In the high-temperature limit, these fluctuations are consistent with the classical dissipation-fluctuation theorem [128, 129]. Combination of Eqs. (2.10) and (2.11) gives a second-order Helmholtz equation,

$$\left[-\frac{\omega^2}{c^2} + \boldsymbol{\nabla} \times \boldsymbol{\nabla} \times \right] \underline{\hat{\mathbf{E}}}(\mathbf{r}, \omega) - i\mu_0 \omega \int \mathrm{d}^3 r' \boldsymbol{Q}(\mathbf{r}, \mathbf{r}', \omega) \cdot \underline{\hat{\mathbf{E}}}(\mathbf{r}', \omega) = i\mu_0 \omega \underline{\hat{\mathbf{j}}}_N(\mathbf{r}, \omega), \tag{2.15}$$

where the formal solution to Eq. (2.15) can be written in terms of the Green tensor $\boldsymbol{G}(\mathbf{r}, \mathbf{r}', \omega)$

$$\underline{\hat{\mathbf{E}}}(\mathbf{r}, \omega) = i\omega\mu_0 \int \mathrm{d}^3 r' \boldsymbol{G}(\mathbf{r}, \mathbf{r}', \omega) \cdot \underline{\hat{\mathbf{j}}}_N(\mathbf{r}', \omega). \tag{2.16}$$

In addition, we immediately obtain the expansion for the induction field,

$$\underline{\hat{\mathbf{B}}}(\mathbf{r}, \omega) = \mu_0 \int \mathrm{d}^3 r' \boldsymbol{\nabla} \times \boldsymbol{G}(\mathbf{r}, \mathbf{r}', \omega) \cdot \underline{\hat{\mathbf{j}}}_N(\mathbf{r}', \omega). \tag{2.17}$$

In order to accomplish the quantization, the noise current density operator is required to fulfill the commutation relation

$$[\hat{\underline{\mathbf{j}}}_N(\mathbf{r},\omega),\hat{\underline{\mathbf{j}}}_N^\dagger(\mathbf{r}',\omega')] = \frac{\hbar\omega}{\pi}\delta(\omega-\omega')\mathrm{Re}\,\boldsymbol{Q}(\mathbf{r},\mathbf{r}',\omega), \qquad (2.18)$$

such that the commutation relation characteristic for the electromagnetic field is in accordance with free-space QED [8],

$$[\hat{\mathbf{E}}(\mathbf{r}),\hat{\mathbf{B}}(\mathbf{r}')] = i\hbar\varepsilon_0^{-1}\boldsymbol{\nabla}\times\delta(\mathbf{r}-\mathbf{r}')\boldsymbol{I}. \qquad (2.19)$$

The classical (retarded) Green tensor as introduced in Eqs. (2.16) and (2.17) obeys the differential equation with the tensorial δ-function source term

$$\left[-\frac{\omega^2}{c^2}+\boldsymbol{\nabla}\times\boldsymbol{\nabla}\times\right]\boldsymbol{G}(\mathbf{r},\mathbf{s},\omega) = \boldsymbol{I}\delta(\mathbf{r}-\mathbf{r}')+i\mu_0\omega\int\mathrm{d}^3s\,\boldsymbol{Q}(\mathbf{r},\mathbf{s},\omega)\cdot\boldsymbol{G}(\mathbf{s},\mathbf{r}',\omega)$$

$$= \boldsymbol{I}\delta(\mathbf{r}-\mathbf{s})+\frac{\omega^2}{c^2}[\varepsilon(\mathbf{r},\omega)-1]\boldsymbol{G}(\mathbf{r},\mathbf{r}',\omega)+\boldsymbol{\nabla}\times\left[1-\frac{1}{\mu(\mathbf{r},\omega)}\right]\boldsymbol{\nabla}\times\boldsymbol{G}(\mathbf{r},\mathbf{r}',\omega), \qquad (2.20)$$

together with the boundary condition at infinity, $\boldsymbol{G}(\mathbf{r},\mathbf{r}',\omega)\to\boldsymbol{0}$ for $|\mathbf{r}-\mathbf{r}'|\to\infty$. This boundary condition ensures that the partial differential equation (2.20) uniquely determines the Green tensor [130]. In particular, this remains true when amplification in a bounded region is allowed for, as long as the assumption of linear response holds [124]. In practice, the Green tensor is constructed by using the boundary conditions of the geometry. However, a closed expression for the Green tensor is only available for sufficiently simple geometries such as piecewise homogeneous spherical or planar systems [131, 132]. For piecewise homogeneous media with $\mathbf{r},\mathbf{r}'$ being in the same region it is often convenient to decompose the Green tensor into a bulk part and a scattering part,

$$\boldsymbol{G}(\mathbf{r},\mathbf{r}',\omega) = \boldsymbol{G}^{(0)}(\mathbf{r},\mathbf{r}',\omega)+\boldsymbol{G}^{(1)}(\mathbf{r},\mathbf{r}',\omega), \qquad (2.21)$$

where the bulk Green tensor $\boldsymbol{G}^{(0)}$ is a particular solution to the inhomogeneous Helmholtz equation (2.20) with $\varepsilon(\mathbf{r},\omega)=\varepsilon(\omega)$ and $\mu(\mathbf{r},\omega)=\mu(\omega)$, while the scattering Green tensor $\boldsymbol{G}^{(1)}$ solves the homogeneous Helmholtz equation and accounts for the scattering and transmission at the boundaries of the bodies.

The Green tensor has some useful general properties, which will be employed

throughout this thesis, in particular the Schwartz reflection principle

$$\boldsymbol{G}^*(\mathbf{r},\mathbf{r}',\omega) = \boldsymbol{G}(\mathbf{r},\mathbf{r}',-\omega), \tag{2.22}$$

Onsager reciprocity

$$\boldsymbol{G}(\mathbf{r},\mathbf{r}',\omega) = \boldsymbol{G}^{\mathsf{T}}(\mathbf{r}',\mathbf{r},\omega), \tag{2.23}$$

and the integral relation

$$\mu_0\omega \int \mathrm{d}^3s \int \mathrm{d}^3s' \boldsymbol{G}(\mathbf{r},\mathbf{s},\omega) \cdot \mathrm{Re}\,\boldsymbol{Q}(\mathbf{s},\mathbf{s}',\omega) \cdot \boldsymbol{G}^*(\mathbf{s}',\mathbf{r}',\omega) = \mathrm{Im}\,\boldsymbol{G}(\mathbf{r},\mathbf{r}',\omega) \tag{2.24}$$

(for proofs see, e.g., Ref. [129]). We will further require the analytic behavior of the scattering Green tensor in the limit of large and small $|\omega|$ [129],

$$\lim_{|\omega|\to\infty} \frac{\omega^2}{c^2} \boldsymbol{G}^{(1)}(\mathbf{r},\mathbf{r}',\omega) = \boldsymbol{0}, \quad \lim_{|\omega|\to 0} \frac{\omega^2}{c^2} \boldsymbol{G}^{(1)}(\mathbf{r},\mathbf{r}',\omega) = \boldsymbol{0}. \tag{2.25}$$

The analyticity of the Green tensor in the upper half ω plane is a basic requirement for the quantization scheme as it is needed to verify the fundamental commutation relation (2.19). While for absorbing media this assumption is always fulfilled, poles in the upper ω-plane may arise for gain media when the amplification is so strong that the medium response becomes nonlinear [124] (for an example, see Sec. 4.2).

Let us now return to the field quantization. Instead of using the set of noise operators $\hat{\underline{\mathbf{j}}}_N(\mathbf{r},\omega)$ and $\hat{\underline{\mathbf{j}}}_N^\dagger(\mathbf{r},\omega)$, it is convenient to introduce bosonic variables $\hat{\underline{\mathbf{f}}}_\lambda(\mathbf{r},\omega)$ and $\hat{\underline{\mathbf{f}}}_\lambda^\dagger(\mathbf{r},\omega)$, with $\lambda = e, m$, according to

$$\hat{\underline{\mathbf{j}}}_N(\mathbf{r},\omega) = \omega\sqrt{\frac{\hbar\varepsilon_0}{\pi}|\varepsilon_I(\mathbf{r},\omega)|}\left[\Theta[\varepsilon_I(\mathbf{r},\omega)]\hat{\mathbf{f}}_e(\mathbf{r},\omega) + \Theta[-\varepsilon_I(\mathbf{r},\omega)]\hat{\mathbf{f}}_e^\dagger(\mathbf{r},\omega)\right]$$
$$+ \boldsymbol{\nabla} \times \sqrt{\frac{\hbar}{\pi\mu_0}\frac{|\mu_I(\mathbf{r},\omega)|}{|\mu(\mathbf{r},\omega)|^2}}\left[\Theta[\mu_I(\mathbf{r},\omega)]\hat{\mathbf{f}}_m(\mathbf{r},\omega) + \Theta[-\mu_I(\mathbf{r},\omega)]\hat{\mathbf{f}}_m^\dagger(\mathbf{r},\omega)\right], \tag{2.26}$$

with commutation relations

$$\left[\hat{f}_{\lambda i}(\mathbf{r},\omega), \hat{f}_{\lambda' j}(\mathbf{r}',\omega')\right] = 0 = \left[\hat{f}_{\lambda i}^\dagger(\mathbf{r},\omega), \hat{f}_{\lambda' j}^\dagger(\mathbf{r}',\omega')\right] \tag{2.27}$$

$$\left[\hat{f}_{\lambda i}(\mathbf{r},\omega), \hat{f}_{\lambda' j}^\dagger(\mathbf{r}',\omega')\right] = \delta_{\lambda\lambda'}\delta_{ij}\delta(\mathbf{r}-\mathbf{r}')\delta(\omega-\omega'), \quad i,j = 1,2,3 \tag{2.28}$$

and $\Theta(x)$ being the Theta function with $\Theta(0) \equiv 1$. Equation (2.26) shows that the presence of amplification, where ε_I or $\mu_I < 0$, causes an exchange of the roles of the

creation $\hat{\mathbf{f}}$ and annihilation operators $\hat{\mathbf{f}}^{\dagger}$, a fact that is well known [130]. To include amplification in the theory, we assume that the medium-assisted field is in an excited state where the medium is pumped in such a way that a quasi-stationary regime can be established, externally controlled and maintained. This state $|\{0\}\rangle$ is defined by

$$\hat{\mathbf{f}}_{\lambda}(\mathbf{r},\omega)|\{0\}\rangle = \mathbf{0} \quad \forall \lambda, \mathbf{r}, \omega. \tag{2.29}$$

For a purely absorbing medium, Eq. (2.29) defines the ordinary ground-state.

The charge and current densities can be written as functionals of the variables $\hat{\mathbf{f}}_{\lambda}(\mathbf{r},\omega)$ and $\hat{\mathbf{f}}_{\lambda}^{\dagger}(\mathbf{r},\omega)$,

$$\hat{\underline{\mathbf{j}}}(\mathbf{r},\omega) = \left(-\frac{\omega^2}{c^2} + \boldsymbol{\nabla} \times \boldsymbol{\nabla} \times\right) \int \mathrm{d}^3 r' \, \boldsymbol{G}(\mathbf{r}, \mathbf{r}', \omega) \cdot \hat{\underline{\mathbf{j}}}_{N}(\mathbf{r}', \omega), \tag{2.30}$$

$$\hat{\underline{\rho}}(\mathbf{r},\omega) = \frac{i\omega}{c^2} \boldsymbol{\nabla} \cdot \int \mathrm{d}^3 r' \, \boldsymbol{G}(\mathbf{r}, \mathbf{r}', \omega) \cdot \hat{\underline{\mathbf{j}}}_{N}(\mathbf{r}', \omega), \tag{2.31}$$

as can be seen by inserting Eq. (2.26) and (2.16) into Eq. (2.11) and applying Eq. (2.9). To complete the quantization procedure, we introduce the Hamiltonian of the body-assisted electromagnetic field in the form

$$\hat{H} = \sum_{\lambda=e,m} \int \mathrm{d}^3 r \int_0^\infty \mathrm{d}\omega \, \hbar\omega \, \mathrm{sgn}[\kappa_{\lambda}(\mathbf{r},\omega)] \hat{\mathbf{f}}_{\lambda}^{\dagger}(\mathbf{r},\omega) \cdot \hat{\mathbf{f}}_{\lambda}(\mathbf{r},\omega) \tag{2.32}$$

where $\kappa_e = \varepsilon_I, \kappa_m = \mu_I$, in consistency with the quasi-microscopic Huttner–Barnett model [18]. The Hamiltonian can be justified by showing that the Heisenberg equation of motion,

$$\dot{\hat{\mathbf{f}}}_{\lambda}(\mathbf{r},\omega) = i\hbar^{-1}\big[\hat{H}, \hat{\mathbf{f}}_{\lambda}(\mathbf{r},\omega)\big] = -i\omega \, \mathrm{sgn}[\mathrm{Im}\,\kappa_{\lambda}(\mathbf{r},\omega)]\hat{\mathbf{f}}_{\lambda}(\mathbf{r},\omega), \tag{2.33}$$

implies the correct time dependence of the Maxwell's equations. We finally comment on a rather unpleasant feature: The single-quantum Fock state $|\mathbf{1}_{\lambda}(\mathbf{r},\omega)\rangle = \hat{\mathbf{f}}_{\lambda}^{\dagger}(\mathbf{r},\omega)|\{0\}\rangle$ is an eigenstate of the field Hamiltonian whose corresponding eigenvalues can become arbitrarily negative for amplifying media. That means that in the presence of amplification, the state with $\hat{H}|\{0\}\rangle = 0$ is not the state with the lowest energy as would be expected from a true ground-state. As indicated above, the assumed pump mechanism (which, however, is not dynamically included in the theory) defines a quasi-stationary state similar to the ground-state, cf. Eq. (2.29).

2.2 Casimir–Polder forces

The Casimir–Polder force between a neutral, polarizable atom A and a purely absorbing magnetoelectric body can be regarded as the (average) quantum Lorentz force on the atom [113],

$$\mathbf{F} = \int \mathrm{d}^3 r \left\langle \hat{\rho}_A(\mathbf{r})\hat{\mathbf{E}}(\mathbf{r}) + \hat{\mathbf{j}}_A(\mathbf{r}) \times \hat{\mathbf{B}}(\mathbf{r}) \right\rangle, \tag{2.34}$$

where the atomic charge and current densities read

$$\hat{\rho}_A(\mathbf{r}) = \sum_{\alpha \in A} q_\alpha \delta(\mathbf{r} - \hat{\mathbf{r}}_\alpha), \tag{2.35}$$

$$\hat{\mathbf{j}}_A(\mathbf{r}) = \sum_{\alpha \in A} \frac{q_\alpha}{2} \left[\dot{\hat{\mathbf{r}}}_\alpha \delta(\mathbf{r} - \hat{\mathbf{r}}_\alpha) + \delta(\mathbf{r} - \hat{\mathbf{r}}_\alpha)\dot{\hat{\mathbf{r}}}_\alpha \right], \tag{2.36}$$

respectively, and α labels the constituents of the atom with charges q_α. Note that the electric and induction field expansions can still be given in the forms (2.16) and (2.17). The expectation value in Eq. (2.34) is understood to act with respect to the ground-state $|\{0\}\rangle$ of the electromagnetic field coupled to an arbitrary internal state of the atom that will evolve over time.

Equation (2.34) is usually rewritten in long-wavelength approximation which for nonmagnetic (electric-dipole) atoms reads [113]

$$\mathbf{F} = \left[\boldsymbol{\nabla} \left\langle \hat{\mathbf{d}} \cdot \hat{\mathbf{E}}(\mathbf{r}) \right\rangle + \frac{\mathrm{d}}{\mathrm{d}t} \left\langle \hat{\mathbf{d}} \times \hat{\mathbf{B}}(\mathbf{r}) \right\rangle \right]_{\mathbf{r}=\mathbf{r}_A}, \tag{2.37}$$

where $\hat{\mathbf{d}}$ is the dipole operator of the atom given in terms of time-dependent atomic flip operators $\hat{A}_{mn}$,

$$\hat{\mathbf{d}} = \sum_{m,n} \mathbf{d}_{mn}\hat{A}_{mn}, \quad \hat{A}_{mn} = \hat{A}_{mn}(t) = |m\rangle\langle n| \tag{2.38}$$

and m, n counting the atomic energy eigenstates $E_{m,n}$. In Eq. (2.37), $\mathbf{r}_A$ denotes the center-of-mass position of the atom. Effects of the center-of-mass motion are disregarded here and throughout. We further assume that the atom is initially prepared in an energy eigenstate $|n\rangle$. It has been shown that in this case the second term in Eq. (2.37) does not contribute [113]. One now has to derive the time evolution of the internal atomic state which is coupled to the medium-assisted electromagnetic field.

The Hamiltonian in the multipolar coupling scheme [113],

$$\hat{H} = \sum_{\lambda=e,m} \int \mathrm{d}^3r \int_0^\infty \mathrm{d}\omega\, \hbar\omega \hat{\mathbf{f}}_\lambda^\dagger(\mathbf{r},\omega) \cdot \hat{\mathbf{f}}_\lambda(\mathbf{r},\omega) + \sum_n E_n \hat{A}_{nn}$$
$$- \sum_{m,n} \sum_{\lambda=e,m} \int \mathrm{d}^3r \int_0^\infty \mathrm{d}\omega\, \mathbf{d}_{mn} \cdot \boldsymbol{G}_\lambda(\mathbf{r}_A,\mathbf{r},\omega) \cdot \hat{\mathbf{f}}_\lambda(\mathbf{r},\omega)\hat{A}_{mn} + \mathrm{H.c.}, \quad (2.39)$$

consists of the field Hamiltonian (2.32), the atomic Hamiltonian [first line of Eq. (2.39)] and the term accounting for the atom–field coupling [second line of Eq. (2.39)]. For convenience we have introduced

$$\boldsymbol{G}_e(\mathbf{r}_A,\mathbf{r},\omega) = i\frac{\omega^2}{c^2}\sqrt{\frac{\hbar}{\pi\varepsilon_0}\varepsilon_I(\mathbf{r},\omega)}\,\boldsymbol{G}(\mathbf{r}_A,\mathbf{r},\omega), \quad (2.40)$$

$$\boldsymbol{G}_m(\mathbf{r}_A,\mathbf{r},\omega) = i\frac{\omega}{c}\sqrt{\frac{\hbar\mu_I(\mathbf{r},\omega)}{\pi\varepsilon_0|\mu_I(\mathbf{r},\omega)|^2}}\Big[\boldsymbol{\nabla}\times\boldsymbol{G}(\mathbf{r},\mathbf{r}_A,\omega)\Big]^{\mathsf{T}}. \quad (2.41)$$

The field dynamics can be obtained from the Heisenberg equations of motion

$$\dot{\hat{\mathbf{f}}}_\lambda(\mathbf{r},\omega) = i\hbar^{-1}\big[\hat{H},\hat{\mathbf{f}}_\lambda(\mathbf{r},\omega)\big] = -i\omega\hat{\mathbf{f}}_\lambda(\mathbf{r},\omega) + i\hbar^{-1}\sum_{m,n}\boldsymbol{G}_\lambda^{*\mathsf{T}}(\mathbf{r}_A,\mathbf{r},\omega)\cdot\mathbf{d}_{mn}\hat{A}_{mn}, \quad (2.42)$$

where the solution

$$\hat{\mathbf{f}}_\lambda(\mathbf{r},\omega,t) = e^{-i\omega(t-t_0)}\hat{\mathbf{f}}_\lambda(\mathbf{r},\omega) + i\hbar^{-1}\int_{t_0}^t \mathrm{d}t' e^{-i\omega(t-t')}\boldsymbol{G}_\lambda^{*\mathsf{T}}(\mathbf{r}_A,\mathbf{r},\omega)\cdot\mathbf{d}_{mn}\hat{A}_{mn}(t') \quad (2.43)$$

gives, upon using the integral relation (2.24), the time-dependent electric field

$$\hat{\underline{\mathbf{E}}}(\mathbf{r},\omega,t) = e^{-i\omega(t-t_0)}\hat{\underline{\mathbf{E}}}(\mathbf{r},\omega) + \frac{i\mu_0}{\pi}\sum_{m,n}\omega^2\int_{t_0}^t \mathrm{d}t' e^{-i\omega(t-t')}\mathrm{Im}\,\boldsymbol{G}(\mathbf{r},\mathbf{r}_A,\omega)\cdot\mathbf{d}_{mn}\hat{A}_{mn}(t'). \quad (2.44)$$

After some arrangements, the CP force according to Eq. (2.37), can be written in the form

$$\mathbf{F}(t) = \frac{i\mu_0}{\pi}\sum_{m,n,k,l}\int_0^\infty \mathrm{d}\omega\,\omega^2\boldsymbol{\nabla}\mathbf{d}_{mn}\cdot\mathrm{Im}\,\boldsymbol{G}^{(1)}(\mathbf{r}_A,\mathbf{r}_A,\omega)\cdot\mathbf{d}_{kl}\int_{t_0}^t \mathrm{d}t' e^{-i\omega(t-t')}\big\langle\hat{A}_{mn}(t)\hat{A}_{kl}(t')\big\rangle \quad (2.45)$$

where the contribution of the translationally invariant bulk Green tensor $\boldsymbol{G}^{(0)}(\mathbf{r}_A,\mathbf{r}_A,\omega)$ leads to a self force that is not of interest in this thesis.

To calculate the required two-time correlation functions $\big\langle\hat{A}_{mn}(t)\hat{A}_{kl}(t')\big\rangle$, in weak

atom–field coupling, we assume the time-evolution to be Markovian. This basically means that the electric field at a given time is not influenced by the presence of the atom at earlier times. Applying the quantum-regression theorem [133], the correlation functions can be written in the form [113]

$$\langle \hat{A}_{mn}(t)\hat{A}_{kl}(t')\rangle = e^{[i\omega_{mn}-(\Gamma_m+\Gamma_n)/2](t-t')}\delta_{nk}\langle \hat{A}_{ml}(t')\rangle, \quad t \geq t', \qquad (2.46)$$

where we have introduced the spontaneous decay rate accounting for the finite linewidth of the nth energy level,

$$\Gamma_n(\mathbf{r}_A) = \sum_{k<n}\Gamma_{nk} = \sum_{k<n}\frac{2\mu_0}{\hbar}\omega_{nk}^2\mathbf{d}_{nk}\cdot\text{Im}\,\boldsymbol{G}(\mathbf{r}_A,\mathbf{r}_A,\omega_{nk})\cdot\mathbf{d}_{kn} \qquad (2.47)$$

and neglected the influence of the bodies on the atomic transition frequency ω_{nk}. The spontaneous emission of real photons governs the internal dynamics of the atom and manifests in the time-dependence of the (diagonal) atomic level populations

$$\dot{p}_n(t) = -\Gamma_n p_n(t) + \sum_{k>n}\Gamma_{kn}p_k(t). \qquad (2.48)$$

Note that $p_n(t)$ denotes the population probability of the nth state but is also the expectation value of $A_{nn}(t)$. One can show that spontaneous decay transfers an atom initially prepared in the state $\sigma(t_0) = |n\rangle\langle n|$ into an incoherent superposition of (lower) energy eigenstates so that the atomic density matrix $\sigma(t)$ remains diagonal for all times [134],

$$\hat{\sigma}(t) = \sum_{k\leq n}p_k(t)|k\rangle\langle k| \quad \text{for} \quad t \geq t_0. \qquad (2.49)$$

Substituting Eq. (2.46) back into Eq. (2.45), evaluating the time integrals in Markov approximation (i.e., putting $\hat{A}_{mn}(t' = t)$ out of the integral and shifting t_0 towards $-\infty$), we can write the CP force in the form

$$\mathbf{F}(\mathbf{r}_A,t) = \sum_n p_n(t)\mathbf{F}_n(\mathbf{r}_A). \qquad (2.50)$$

In what follows, we assume that $\omega_{nk} \gg \Gamma_n, \Gamma_k \equiv \epsilon$ and neglect the effect of the magnetoelectric bodies on the spontaneous decay. Additionally, we consider only time scales that are short compared to the inverse atomic decay rate. For this purpose, we study the force associated with the nth state which is conservative within these approximations, $F(\mathbf{r}_A,t) \approx F_n(\mathbf{r}_A) = -\boldsymbol{\nabla}U_n(\mathbf{r}_A)$, where the static potential is given

by

$$U_n(\mathbf{r}_A) = -\frac{\mu_0}{\pi} \sum_k \lim_{\epsilon \to 0+} \int_0^\infty \mathrm{d}\omega\, \omega^2 \frac{\mathbf{d}_{nk} \cdot \mathrm{Im}\, \boldsymbol{G}^{(1)}(\mathbf{r}_A, \mathbf{r}_A, \omega) \cdot \mathbf{d}_{kn}}{\omega - \omega_{nk} - i\epsilon} + \mathrm{C.c.}. \qquad (2.51)$$

By means of contour integral techniques, on recalling the analytic properties of the Green tensor, we decompose the CP potential according to

$$U_n(\mathbf{r}_A) = U_e^{\mathrm{res}}(\mathbf{r}_A) + U_e^{\mathrm{nres}}(\mathbf{r}_A). \qquad (2.52)$$

In the nonresonant contribution

$$\begin{aligned}
U_n^{\mathrm{nres}}(\mathbf{r}_A) &= \frac{\hbar\mu_0}{2\pi} \int_0^\infty \mathrm{d}\xi\, \xi^2 \,\mathrm{tr}\big[\boldsymbol{\alpha}_n(i\xi) \cdot \boldsymbol{G}^{(1)}(\mathbf{r}_A, \mathbf{r}_A, i\xi)\big] \\
&= \frac{\hbar\mu_0}{2\pi} \int_0^\infty \mathrm{d}\xi\, \xi^2 \alpha_n(i\xi)\, \mathrm{tr}\, \boldsymbol{G}^{(1)}(\mathbf{r}_A, \mathbf{r}_A, i\xi) \qquad (2.53)
\end{aligned}$$

the Green tensor appears in an integral form and accounts for the magnetoelectric response of the body, while all atomic properties enter via the position-independent polarizability tensor $\boldsymbol{\alpha}_n(\omega)$, which in lowest nonvanishing order of perturbation theory, reads [135],

$$\boldsymbol{\alpha}_n(\omega) = \lim_{\epsilon \to 0+} \frac{1}{\hbar} \sum_k \left[\frac{\mathbf{d}_{nk}\mathbf{d}_{kn}}{\omega_{kn} - \omega - i\epsilon} + \frac{\mathbf{d}_{kn}\mathbf{d}_{nk}}{\omega_{kn} - \omega + i\epsilon}\right] = \lim_{\epsilon \to 0+} \frac{2}{3\hbar} \sum_k \frac{\omega_{kn}|\mathbf{d}_{nk}|^2}{\omega_{kn}^2 - \omega^2 - i\omega\epsilon} \boldsymbol{I}. \qquad (2.54)$$

The second equality in Eqs. (2.53) and (2.54) holds for isotropic atoms, and tr denotes the trace. Equation (2.53) is also valid for left-handed materials. It can, however, be expected that the impact of left-handedness in a limited frequency interval is very weak due to the integration over the full (imaginary) frequency regime. On the other hand the resonant contribution,

$$U_n^{\mathrm{res}}(\mathbf{r}_A) = -\mu_0 \sum_{k<n} \omega_{nk}^2 \mathbf{d}_{nk} \cdot \mathrm{Re}\, \boldsymbol{G}^{(1)}(\mathbf{r}_A, \mathbf{r}_A, \omega_{nk}) \cdot \mathbf{d}_{kn}, \qquad (2.55)$$

is only present for exited atoms and accounts for the emission of real photons. It usually dominates over the off-resonant part. The results (2.53) and (2.55) are consistent with the CP interaction obtained via second-order perturbation theory [21].

In practice, the inclusion of magnetic properties often involves lengthy calculations. As can be shown, the Maxwell equations in the absence of free charges and currents are invariant under an exchange of electric and magnetic field quantities, a symmetry

property which is known as duality. In the presence of magnetoelectric media, duality manifests itself as an invariance of the constitutive relations under the simultaneous exchange of permittivity and permeability $\varepsilon \leftrightarrow \mu$. Such duality transformations, denoted by $\circledast$, can be shown to imply the transformation rules for the Green tensor [136, 137]:

$$\frac{\omega^2}{c^2} \, \boldsymbol{G}^\circledast(\mathbf{r}, \mathbf{r}', \omega) = -\frac{\boldsymbol{\nabla} \times \boldsymbol{G}(\mathbf{r}, \mathbf{r}', \omega) \times \overleftarrow{\boldsymbol{\nabla}}'}{\mu(\mathbf{r}, \omega)\mu(\mathbf{r}', \omega)}, \tag{2.56}$$

$$\boldsymbol{\nabla} \times \boldsymbol{G}^\circledast(\mathbf{r}, \mathbf{r}', \omega) \times \overleftarrow{\boldsymbol{\nabla}}' = -\varepsilon(\mathbf{r}, \omega) \frac{\omega^2}{c^2} \, \boldsymbol{G}(\mathbf{r}, \mathbf{r}', \omega)\varepsilon(\mathbf{r}', \omega), \tag{2.57}$$

$$\boldsymbol{\nabla} \times \boldsymbol{G}^\circledast(\mathbf{r}, \mathbf{r}', \omega) = -\varepsilon(\mathbf{r}, \omega) \frac{\boldsymbol{G}(\mathbf{r}, \mathbf{r}', \omega) \times \overleftarrow{\boldsymbol{\nabla}}'}{\mu(\mathbf{r}', \omega)}, \tag{2.58}$$

$$\boldsymbol{G}^\circledast(\mathbf{r}, \mathbf{r}', \omega) \times \overleftarrow{\boldsymbol{\nabla}}' = -\frac{\boldsymbol{\nabla} \times \boldsymbol{G}(\mathbf{r}, \mathbf{r}', \omega)}{\mu(\mathbf{r}, \omega)} \varepsilon(\mathbf{r}', \omega). \tag{2.59}$$

Equations (2.56)–(2.59) are valid for the scattering parts of the Green tensors and for the bulk Green tensor if $\mathbf{r} \neq \mathbf{r}'$. In general, Lorentz forces are not duality invariant. It can, however, be shown that for dispersion forces on neutral and static objects the duality symmetry is preserved [136]. To recover duality in the presence of atoms it is required that polarizability and magnetizability are connected via [136, 137]

$$\mathbf{d}_{nk}^\circledast = \frac{\mathbf{m}_{nk}}{c^2}, \quad \mathbf{m}_{nk}^\circledast = \mathbf{d}_{nk}c^2, \tag{2.60}$$

$$\boldsymbol{\alpha}_n^\circledast = \frac{\boldsymbol{\beta}_n}{c^2}, \quad \boldsymbol{\beta}_n^\circledast = \boldsymbol{\alpha}_n c^2, \tag{2.61}$$

where $\mathbf{m}_{nk}$ denotes the magnetic dipole matrix elements and

$$\boldsymbol{\beta}_n(\omega) = \lim_{\epsilon \to 0+} \frac{1}{\hbar} \sum_k \left[\frac{\mathbf{m}_{nk}\mathbf{m}_{kn}}{\omega_{kn} - \omega - i\epsilon} + \frac{\mathbf{m}_{kn}\mathbf{m}_{nk}}{\omega_{kn} - \omega + i\epsilon} \right] = \lim_{\epsilon \to 0+} \frac{2}{3\hbar} \sum_k \frac{\omega_{kn}|\mathbf{m}_{nk}|^2}{\omega_{kn}^2 - \omega^2 - i\omega\epsilon} \tag{2.62}$$

is the magnetizability of the atom. Again, the last equality holds for isotropic atoms. Thus, duality arguments provide a strong tool to obtain expressions for dispersion forces from the (usually electric) counterparts that are already known. For example, we may calculate the nonresonant CP potential of a magnetizable atom in free-space from the corresponding electric part (2.53) by carrying out the dual operation

$U_m^{\mathrm{nres}} = U_e^{\mathrm{nres}\circledast} \equiv U_n^{\mathrm{nres}\circledast}$ and, on using Eqs. (2.56) and (2.61), we obtain

$$U_m^{\mathrm{nres}}(\mathbf{r}_A) = \frac{\hbar\mu_0}{2\pi} \int_0^\infty \mathrm{d}\xi \, \mathrm{tr}\big[\boldsymbol{\nabla}_A \times \boldsymbol{\beta}_n(i\xi) \cdot \boldsymbol{G}^{(1)}(\mathbf{r}_A, \mathbf{r}', i\xi) \times \overleftarrow{\boldsymbol{\nabla}}'\big]_{\mathbf{r}'=\mathbf{r}_A}$$

$$= \frac{\hbar\mu_0}{2\pi} \int_0^\infty \mathrm{d}\xi \beta_n(i\xi) \, \mathrm{tr}\big[\boldsymbol{\nabla}_A \times \boldsymbol{G}^{(1)}(\mathbf{r}_A, \mathbf{r}', i\xi) \times \overleftarrow{\boldsymbol{\nabla}}'\big]_{\mathbf{r}'=\mathbf{r}_A}. \qquad (2.63)$$

3 Dispersion forces between ground-state objects in media

In an introductory section, Sec. 3.1, we apply the real-cavity model to account for the local-field correction and review[1] how the Green tensor for this model can be calculated. The first part of the chapter, Sec. 3.2, is concerned with the CP interaction of a (nonmagnetic) ground-state atom near the planar interface between two media, where emphasis is put on the possible creation of repulsive forces, the impact of the local-field correction, and the on-surface potential. In the second part, Sec. 3.3, we allow for an arbitrary background medium instead of the planar system and consider the CP interaction of a ground-state atom with another small spherical object.

3.1 Real-cavity model

We consider an isotropic guest atom placed inside a medium. Note that between the guest atom and the neighboring medium atoms there should be some free space. This is accounted for in the Onsager real-cavity model [104], where the guest atom A is located at the center of a small, empty spherical cavity of radius R_C inside the host medium described by the macroscopic quantities $\varepsilon(\mathbf{r}, \omega)$ and $\mu(\mathbf{r}, \omega)$. Thus, permittivity and permeability of the cavity-medium system can be introduced as

$$\varepsilon_\mathrm{loc}(\mathbf{r}, \omega), \mu_\mathrm{loc}(\mathbf{r}, \omega) = \begin{cases} 1 & \text{if } |\mathbf{r} - \mathbf{r}_A| < R_\mathrm{C}, \\ \varepsilon(\mathbf{r}, \omega), \mu(\mathbf{r}, \omega) & \text{if } |\mathbf{r} - \mathbf{r}_A| \geq R_\mathrm{C}, \end{cases} \tag{3.1}$$

where the radius of the cavity can be regarded as a measure of the distance between the guest atom and the surrounding host atoms [AS1]. The situation is sketched in Fig. 3.6 (i). To apply this model, the medium parameters of the host medium should

---

[1]For details, the reader is referred to my diploma thesis [138] and Ref. [AS1].

not vary appreciably on the microscopic length scale R_C,

$$\left.\begin{aligned}\varepsilon(\mathbf{r},\omega) &= \varepsilon(\mathbf{r}_A,\omega) \equiv \varepsilon_A(\omega)\\ \mu(\mathbf{r},\omega) &= \mu(\mathbf{r}_A,\omega) \equiv \mu_A(\omega)\end{aligned}\right\} \quad \text{for } |\mathbf{r}-\mathbf{r}_A| \lesssim 2R_C, \tag{3.2}$$

and the quantity $\sqrt{|\varepsilon(\mathbf{r},0)\mu(\mathbf{r},0)|}R_C$ should be small compared to the maximum of all characteristic atomic and medium wavelengths as well as to the separation between the guest atom and any surface of the host medium. These assumptions restrict the applicability of the model to dielectrics and excludes metals. We will therefore use the term magnetodielectric instead of magnetoelectric in Chap. 3. The Green tensor in Eq. (2.20) is thus the Green tensor for the electromagnetic field in the medium, disturbed by the (real) cavity, where ε and μ of the unperturbed system are replaced by the local-field quantities given in Eq. (3.1).

The Green tensor in the presence of the cavity can be written as a function of the Green tensor $\boldsymbol{G}^{(1)}(\mathbf{r}_A,\mathbf{r}_A,\omega)$ which accounts for (multiple) transmission through the surface of the cavity and scattering of the electromagnetic field at the inhomogeneities of the (unperturbed) magnetodielectric host medium [AS1],

$$\boldsymbol{G}^{(1)}_{\text{loc}}(\mathbf{r}_A,\mathbf{r}_A,\omega) = \frac{i\omega}{6\pi}C_A(\omega)\boldsymbol{I} + D_A^2(\omega)\boldsymbol{G}^{(1)}(\mathbf{r}_A,\mathbf{r}_A,\omega), \tag{3.3}$$

but neglects multiple reflections at the outer boundaries of the (small) cavity. In Eq. (3.3), the local-field factor can be derived to be

$$\begin{aligned}D_A(\omega) &= \frac{j_1(z_0)\left[z_0 h_1^{(1)}(z_0)\right]' - [z_0 j_1(z_0)]'\, h_1^{(1)}(z_0)}{\mu_A(\omega)\left[j_1(z_0)\left[z h_1^{(1)}(z)\right]' - \varepsilon_A(\omega)\,[z_0 j_1(z_0)]'\, h_1^{(1)}(z)\right]}\\ &= \frac{3\varepsilon_A(\omega)}{2\varepsilon_A(\omega)+1} + \mathcal{O}\!\left(\frac{\omega R_C}{c}\right).\end{aligned} \tag{3.4}$$

The quantity

$$\begin{aligned}C_A(\omega) &= \frac{h_1^{(1)}(z_0)\left[z h_1^{(1)}(z)\right]' - \varepsilon_A(\omega) h_1^{(1)}(z)\left[z_0 h_1^{(1)}(z_0)\right]'}{\varepsilon_A(\omega) h_1^{(1)}(z)\,[z_0 j_1(z_0)]' - j_1(z_0)\left[z h_1^{(1)}(z)\right]'}\\ &= 3\frac{\varepsilon_A(\omega)-1}{2\varepsilon_A(\omega)+1}\frac{c^3}{i\omega^3 R_C^3} + \frac{9}{5}\frac{\varepsilon_A^2(\omega)[5\mu_A(\omega)-1]-3\varepsilon_A(\omega)-1}{[2\varepsilon(\omega)+1]^2}\frac{c}{i\omega R_C}\\ &\quad + 9\frac{\varepsilon_A(\omega)n_A^3(\omega)}{[2\varepsilon(\omega)+1]^2} - 1 + \mathcal{O}\!\left(\frac{\omega R_C}{c}\right)\end{aligned} \tag{3.5}$$

can be shown to arise from the (multiple) scattering processes at the inner surface of the cavity [AS1]. Here, we have introduced the notation $z_0 = \omega R_C/c$, $z = n_A(\omega)z_0$, $n_A(\omega) = \sqrt{\varepsilon_A(\omega)\mu_A(\omega)}$, and $j_1(x)$ and $h_1^{(1)}(x)$ being the first spherical Bessel function and the first spherical Hankel function of the first kind, respectively,

$$j_1(x) = \frac{\sin(x)}{x^2} - \frac{\cos(x)}{x}, \quad h_1^{(1)}(x) = -\left(\frac{1}{x} + \frac{i}{x^2}\right)e^{ix}. \tag{3.6}$$

In the real-cavity model considered, it is sufficient to keep only the leading nonvanishing order in $\sqrt{|\varepsilon_A(0)\mu_A(0)|}\omega_{max}R_C/c$ as given by the factors C_A and D_A, where ω_{max} represents the maximum of the characteristic atomic and medium frequencies. This assumption can also be justified for the CP potentials (for details, cf. [139], [AS1]). Inserting the Green tensor (3.3) into the nonresonant CP potential (2.53) gives the local-field corrected CP potential of a polarizable ground-state atom [AS1],

$$U(\mathbf{r}_A) \equiv U_1^{nres}(\mathbf{r}_A) = U_1(\mathbf{r}_A) + U_2(\mathbf{r}_A), \tag{3.7}$$

where $U_1(\mathbf{r}_A)$ is constant throughout any homogeneous region,

$$\begin{aligned} U_1(\mathbf{r}_A) = &-\frac{\hbar\mu_0}{4\pi^2 c}\int_0^\infty d\xi\,\xi^3\alpha_A(i\xi)C_A(i\xi) \\ = &-\frac{\hbar}{4\pi^2\varepsilon_0}\int_0^\infty d\xi\,\alpha_A\left[3\frac{\varepsilon_A - 1}{2\varepsilon_A + 1}\frac{1}{R_C^3} + \frac{9\xi^2}{c^2}\frac{\varepsilon_A^2\left[1 - 5\mu_A\right] + 3\varepsilon_A + 1}{5\left[2\varepsilon_A + 1\right]^2}\frac{1}{R_C}\right], \end{aligned} \tag{3.8}$$

and $\alpha_A(\omega)$ denotes the ground-state polarizability of the guest atom according to Eq. (2.54). Here and in the following the dependence of ε_A, μ_A and α_A on $i\xi$ is suppressed for brevity. The term $U_2(\mathbf{r}_A)$ involves all interactions associated with the particular shape and size of the magnetodielectric host medium and reads

$$\begin{aligned} U_2(\mathbf{r}_A) = &\frac{\hbar\mu_0}{2\pi}\int_0^\infty d\xi\,\xi^2\alpha_A(i\xi)D_A^2(i\xi)\,\text{tr}\,\boldsymbol{G}^{(1)}(\mathbf{r}_A, \mathbf{r}_A, i\xi) \\ = &\frac{\hbar\mu_0}{2\pi}\int_0^\infty d\xi\,\xi^2\alpha_A\left(\frac{3\varepsilon_A}{2\varepsilon_A + 1}\right)^2\text{tr}\,\boldsymbol{G}^{(1)}(\mathbf{r}_A, \mathbf{r}_A, i\xi). \end{aligned} \tag{3.9}$$

Note that, the second equalities in Eqs. (3.8) and (3.9) hold for the asymptotic limit of small cavity radii. The associated (conservative) CP force is given by

$$\mathbf{F}(\mathbf{r}_A) = -\boldsymbol{\nabla}U(\mathbf{r}_A) = -\frac{\hbar\mu_0}{2\pi}\int_0^\infty d\xi\,\xi^2\alpha_A\left(\frac{3\varepsilon_A}{2\varepsilon_A + 1}\right)^2\boldsymbol{\nabla}\text{tr}\,\boldsymbol{G}^{(1)}(\mathbf{r}_A, \mathbf{r}_A, i\xi). \tag{3.10}$$

It should be pointed out that the cavity-induced part (3.8) does not lead to a force action but to an energy shift.

To obtain the local-field corrected potential for a paramagnetic atom we benefit from the duality invariance of the local-field corrected CP potential of a polarizable and magnetizable atom [136] and apply the transformation rules (2.57) and (2.60) to Eq. (3.10). We find, in accordance with Ref. [140],

$$U_m(\mathbf{r}_A) = -\frac{\hbar\mu_0}{2\pi} \int_0^\infty \mathrm{d}\xi \beta_A(i\xi) \left(\frac{3}{2\mu_A + 1} \right)^2 \mathrm{tr} \left[\boldsymbol{\nabla}_A \times \boldsymbol{G}^{(1)}(\mathbf{r}_A, \mathbf{r}', i\xi) \times \overleftarrow{\boldsymbol{\nabla}}' \right]_{\mathbf{r}'=\mathbf{r}_A} \tag{3.11}$$

with the magnetizability given by Eq. (2.62).

3.2 Casimir–Polder potential near a planar interface

The CP interaction of an atom placed in the vicinity of a rather complex structure, such as a curved surface or a multilayer geometry, can often be modeled by the CP interaction between the same atom and a planar interface. As a typical example in biology one may think of a small molecule inside a cell. In this sense, we study the local-field corrected potential of a (nonmagnetic) ground-state atom in a magnetodielectric two-layer system. Our considerations are primarily based on Ref. [AS4].

We consider two half spaces, as indicated in Fig. 3.1, where the coordinate system is chosen such that the z-direction is perpendicular to the interface between the contacting media. The left region (denoted by layer $j = 1$) is defined by $z < 0$ while the right region ($j = 2$) is given by $z > 0$.
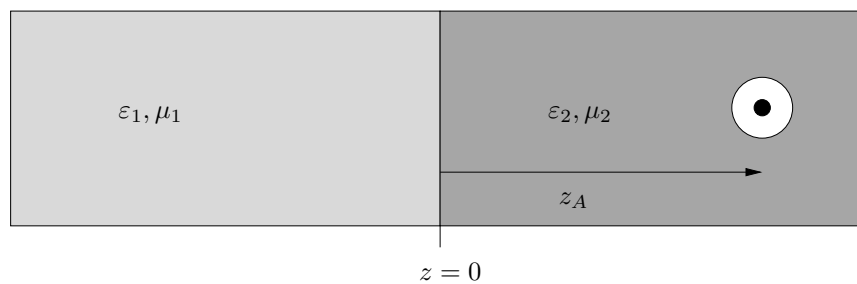
Figure 3.1: Local-field corrected ground-state atom near the interface between two magnetodielectric planar media.

From Eq. (3.7) we expect two contributions to the nonresonant CP potential. We study first the position-dependent nonresonant CP potential with the ground-state

atom located in layer 2 at position z_A from the surface. To that end, we substitute the scattering Green tensor of a half space at equal-position arguments [132]

$$\boldsymbol{G}^{(1)}(z_A, z_A, i\xi) = \frac{\mu_2}{4\pi^2} \int_0^\infty \frac{\mathrm{d}k^\parallel k^\parallel}{\kappa_2} \sum_{\sigma=s,p} e^{-2\kappa_2(i\xi)z} r_{21}^\sigma \mathbf{e}_{2\sigma}^+ \mathbf{e}_{2\sigma}^-, \tag{3.12}$$

into Eq. (3.9), where the single-interface reflection coefficients for s (TE) and p (TM) polarized waves are given by

$$r_{ij}^p = \frac{\kappa_i^\perp \varepsilon_j - \kappa_j^\perp \varepsilon_i}{\kappa_i^\perp \varepsilon_j + \kappa_j^\perp \varepsilon_i}, \quad r_{ij}^s = \frac{\kappa_i^\perp \mu_j - \kappa_j^\perp \mu_i}{\kappa_i^\perp \mu_j + \kappa_j^\perp \mu_i}. \tag{3.13}$$

The wave-vector component perpendicular to the surface is (for imaginary frequencies) given by $k_j^\perp = i\kappa_j^\perp$ where

$$\kappa_j^\perp(i\xi) = \sqrt{\varepsilon_j(i\xi)\mu_j(i\xi)\frac{\xi^2}{c^2} + k^{\parallel 2}}, \tag{3.14}$$

with $\mathbf{k}^\parallel$ being the wave vector parallel to the interface which is preserved across the interface ($k^\parallel = |\mathbf{k}^\parallel|$). The polarization vectors

$$\mathbf{e}_{js}^\pm = \mathbf{e}_{k^\parallel} \times \mathbf{e}_z, \quad \mathbf{e}_{jp}^\pm = -\frac{c}{\sqrt{\varepsilon_j}\xi}\left(ik^\parallel \mathbf{e}_z \pm \kappa_j^\perp \mathbf{e}_{k^\parallel}\right) \tag{3.15}$$

obey the relations

$$\mathbf{e}_{js}^+ \cdot \mathbf{e}_{js}^- = 1, \quad \mathbf{e}_{jp}^+ \cdot \mathbf{e}_{jp}^- = 1, \tag{3.16}$$

which are used to calculate the trace in Eq. (3.9). In the limit of small radius of the real cavity, we eventually arrive at [AS4]

$$U_2(z_A) = \frac{\hbar\mu_0}{8\pi^2} \int_0^\infty \mathrm{d}\xi\, \xi^2 \alpha_A(i\xi) \left(\frac{3\varepsilon_2}{2\varepsilon_2 + 1}\right)^2 \mu_2 \int_0^\infty \mathrm{d}k^\parallel \frac{k^\parallel}{\kappa_2}$$
$$\times \left[\frac{\mu_1\kappa_2 - \mu_2\kappa_1}{\mu_1\kappa_2 + \mu_2\kappa_1} - \frac{\varepsilon_1\kappa_2 - \varepsilon_2\kappa_1}{\varepsilon_1\kappa_2 + \varepsilon_2\kappa_1}\left(1 + 2\frac{k^{\parallel 2}c^2}{\varepsilon_2\mu_2\xi^2}\right)\right] e^{-2\kappa_2 z_A}. \tag{3.17}$$

In the following, we will study the limiting cases of short and large atom–surface separation as well as the case of an isorefractive medium, accompanied by numerical evaluations. Sec. 3.2.3 will then be concerned with the cavity-induced part of the potential according to Eq. (3.8).

3.2.1 Analytical results

Analyzing Eq. (3.17) will help to address the question under which conditions the atom experiences an attractive or repulsive interaction. Let us first change the integration variable according to

$$k^{\parallel} = \sqrt{\kappa_2^2 - \varepsilon_2\mu_2\xi^2/c^2}, \quad k^{\parallel}\mathrm{d}k^{\parallel} = \kappa_2\mathrm{d}\kappa_2, \tag{3.18}$$

$$\kappa_1 = \sqrt{\xi^2/c^2(\varepsilon_1\mu_1 - \varepsilon_2\mu_2) + \kappa_2^2}, \tag{3.19}$$

which gives the potential in the form

$$U_2(z_A) = \frac{\hbar\mu_0}{8\pi^2} \int_0^\infty \mathrm{d}\xi\, \xi^2 \alpha_A \left(\frac{3\varepsilon_2}{2\varepsilon_2 + 1}\right)^2$$
$$\times \mu_2 \int_{\sqrt{\varepsilon_2\mu_2}\xi/c}^\infty \mathrm{d}\kappa_2 \left[\frac{\mu_1\kappa_2 - \mu_2\kappa_1}{\mu_1\kappa_2 + \mu_2\kappa_1} - \frac{\varepsilon_1\kappa_2 - \varepsilon_2\kappa_1}{\varepsilon_1\kappa_2 + \varepsilon_2\kappa_1}\left(-1 + 2\frac{\kappa_2^2 c^2}{\varepsilon_2\mu_2\xi^2}\right)\right] e^{-2\kappa_2 z_A}. \tag{3.20}$$

Note that the quantities $\alpha(i\xi)$, $\varepsilon(i\xi)$, $\mu(i\xi)$ as well as the exponential term $\exp[-2\xi/cz_A]$ are monotonically decreasing functions of ξ.

Close to the surface, in the nonretarded limit, the atom–surface distance z_A is small compared to the typical wavelengths of the medium and the atomic system,

$$z_A \ll \frac{c}{\omega_A^+[n_1(0) + n_2(0)]} \quad \text{and/or,} \quad z_A \ll \frac{c}{\omega_M^+[n_1(0) + n_2(0)]}, \tag{3.21}$$

where ω_A^+ and ω_M^+ denote the maximum of the relevant atomic transition and medium resonance frequencies, respectively, and $n_{1,2}(0) = \sqrt{\varepsilon_{1,2}(0)\mu_{1,2}(0)}$ describe the static refractive indices of the two regions. In this case, the permittivity/permeability-dependent numerators of the reflection coefficients and the polarizability provide an effective cut-off for the ξ-integration. They effectively restrict the ξ-integral to a region where $\xi \lesssim \omega_{A,M}^+$. The conditions (3.21) then imply

$$\frac{z_A\xi}{c}\left(\sqrt{|\varepsilon_1\mu_1 - \varepsilon_2\mu_2|}\right) \leq \frac{z_A\xi}{c}\left(\sqrt{\varepsilon_1\mu_1 + \varepsilon_2\mu_2}\right) \leq \frac{z_A\xi}{c}\left(\sqrt{\varepsilon_1\mu_1} + \sqrt{\varepsilon_2\mu_2}\right)$$
$$\leq \frac{z_A\xi}{c}\left(n_1(0) + n_2(0)\right) \ll 1 \tag{3.22}$$

and further,

$$\frac{z_A\xi}{c} \leq \frac{z_A\omega_{A,M}^+}{c}n_1(0) \leq \frac{z_A\omega_{A,M}^+}{c}\left(n_1(0) + n_2(0)\right) \ll 1. \tag{3.23}$$

To derive the nonretarded CP potential from Eq. (3.20), we perform a leading-order Taylor expansion in $\xi^2/(c^2\kappa_2^2)(\varepsilon_1\mu_1 - \varepsilon_2\mu_2)$, according to the condition (3.22), carry out the integration over κ_2 and set $\exp(-2\sqrt{\varepsilon_2\mu_2}\xi z_A/c) \simeq 1$ as implied by Eq. (3.23). In the nonretarded limit, the potential then decomposes into two terms with different power laws,

$$U_2(z_A) = -\frac{C_3}{z_A^3} + \frac{C_1}{z_A},\tag{3.24}$$

where

$$C_3 = \frac{\hbar}{16\pi^2\varepsilon_0} \int_0^\infty \mathrm{d}\xi\alpha_A \frac{9\varepsilon_2}{(2\varepsilon_2+1)^2}\frac{\varepsilon_1 - \varepsilon_2}{\varepsilon_1 + \varepsilon_2},\tag{3.25}$$

and

$$C_1 = \frac{\hbar\mu_0}{16\pi^2} \int_0^\infty \mathrm{d}\xi\xi^2\alpha_A\mu_2 \left(\frac{3\varepsilon_2}{2\varepsilon_2+1}\right)^2 \left[\frac{\mu_1 - \mu_2}{\mu_1 + \mu_2} + \frac{\varepsilon_1 - \varepsilon_2}{\varepsilon_1 + \varepsilon_2} + \frac{2\varepsilon_1(\varepsilon_1\mu_1 - \varepsilon_2\mu_2)}{\mu_2(\varepsilon_1 + \varepsilon_2)^2}\right].\tag{3.26}$$

Let us briefly discuss the two terms of the potential (3.24). The first term dominates due to the stronger, z_A^{-3}, power law as long as the two contacting media have dissimilar electric properties $\varepsilon_1 \neq \varepsilon_2$. In particular, the atom is repelled from the interface if the region containing the atom has stronger electric properties than the other one ($\varepsilon_2 > \varepsilon_1$), where in the reversed situation, $\varepsilon_1 > \varepsilon_2$, the interaction is attractive. In the case of equal electric properties we have $C_3 = 0$, and the second term gives the leading order, $U_2(z_A) = C_1/z_A$, where

$$C_1 = \frac{\hbar\mu_0}{16\pi^2} \int_0^\infty \mathrm{d}\xi\xi^2\alpha_A \left(\frac{3\varepsilon_2}{2\varepsilon_2+1}\right)^2 (\mu_1 - \mu_2)\left(\frac{\mu_2}{\mu_1 + \mu_2} + 2\right).\tag{3.27}$$

The sign of C_1 clearly shows that the atom experiences a force which points away from the interface if the magnetic properties of the atomic medium environment are weaker than those of the medium on the other side of the interface ($\mu_1 > \mu_2$). Vice versa, the atom is attracted to the interface if $\mu_2 > \mu_1$. Thus the dependence of the direction of the force on the difference in strength of the medium responses is opposite in the two cases of dominantly electric and purely magnetic media. In both cases the strength of the force increases with increasing difference between the electric and magnetic parameters of the contacting media.

Now, we draw our attention to the (long-distance), retarded limit which is characterized by the regime

$$z_A \gg \frac{c}{\omega_A^-} \text{ and } z_A \gg \frac{c}{\omega_M^-},\tag{3.28}$$

where ω_A^- and ω_M^- denote the minimum of all relevant atomic transition and medium resonance frequencies, respectively. In this case, the exponential term in Eq. (3.20) governs the frequency integration. That is to say, for $0 \leq \xi \lesssim c/(2z_A) \ll \omega_{A,M}^-$ the permittivity/permeability and the polarizability are sufficiently approximated by their static counterparts,

$$\alpha(i\xi) \simeq \alpha(0), \quad \varepsilon_{1,2}(i\xi) \simeq \varepsilon_{1,2}(0), \quad \text{and} \quad \mu_{1,2}(i\xi) \simeq \mu_{1,2}(0). \tag{3.29}$$

By introducing a new integration variable in Eq. (3.20), $v = c\kappa_2/\xi$, the integration over ξ can then be performed first, and we end up with

$$U_2(z_A) = \frac{C_4}{z_A^4}, \tag{3.30}$$

where C_4 is given by

$$C_4 = \frac{3\hbar c}{64\varepsilon_0\pi^2}\alpha_A\left(\frac{3\varepsilon_2}{2\varepsilon_2+1}\right)^2\mu_2\int_{\sqrt{\varepsilon_2(0)\mu_2(0)}}^\infty \mathrm{d}v\, \frac{1}{v^4}\left[\frac{\mu_1 v - \mu_2\sqrt{v^2 - \varepsilon_2\mu_2 + \varepsilon_1\mu_1}}{\mu_1 v + \mu_2\sqrt{v^2 - \varepsilon_2\mu_2 + \varepsilon_1\mu_1}}\right.$$
$$\left. + \frac{\varepsilon_1 v - \varepsilon_2\sqrt{v^2 - \varepsilon_2\mu_2 + \varepsilon_1\mu_1}}{\varepsilon_1 v + \varepsilon_2\sqrt{v^2 - \varepsilon_2\mu_2 + \varepsilon_1\mu_1}}\left(1 - 2\frac{v^2}{\varepsilon_2\mu_2}\right)\right]. \tag{3.31}$$

In contrast to the nonretarded case, the dependence of C_4 on the electric and magnetic properties is more involved, where the leading order term depends on the electric properties, only. We first notice that

$$\frac{\partial C_4}{\partial \varepsilon_1(0)} < 0 \quad \text{and} \quad \frac{\partial C_4}{\partial \mu_1(0)} > 0, \tag{3.32}$$

which implies that, for fixed ε_2 and μ_2, the condition $C_4 = 0$ marks the borderline between attractive and repulsive interaction. In particular, we may show this for the case where the contrast between the contacting media is small,

$$\varepsilon_1(0) = \varepsilon_2(0) + \chi(0), \quad \chi(0) \ll \varepsilon_2(0) \tag{3.33}$$

$$\mu_1(0) = \mu_2(0) + \zeta(0), \quad \zeta(0) \ll \mu_2(0). \tag{3.34}$$

We keep only the terms linear in χ and ζ,

$$\frac{\mu_1(0)v - \mu_2(0)\sqrt{v^2 - \varepsilon_2(0)\mu_2(0) + \varepsilon_1(0)\mu_1(0)}}{\mu_1(0)v + \mu_2(0)\sqrt{v^2 - \varepsilon_2(0)\mu_2(0) + \varepsilon_1(0)\mu_1(0)}} \simeq \left(\frac{1}{2\mu_2(0)} - \frac{\varepsilon_2(0)}{4v^2}\right)\zeta(0) - \frac{\mu_2(0)}{4v^2}\chi(0),$$

$$\frac{\varepsilon_1(0)v - \varepsilon_2(0)\sqrt{v^2 - \varepsilon_2(0)\mu_2(0) + \varepsilon_1(0)\mu_1(0)}}{\varepsilon_1(0)v + \varepsilon_2(0)\sqrt{v^2 - \varepsilon_2(0)\mu_2(0) + \varepsilon_1(0)\mu_1(0)}} \simeq -\frac{\varepsilon_2(0)}{4v^2}\zeta(0) + \left(\frac{1}{2\varepsilon_2(0)} - \frac{\mu_2(0)}{4v^2}\right)\chi(0),$$

$$(3.35)$$

and perform the v-integration,

$$C_4 = \frac{9\hbar c}{640\pi^2\varepsilon_0}\alpha(0)\frac{-23\mu_2(0)\chi(0) + 7\varepsilon_2(0)\zeta(0)}{\sqrt{\varepsilon_2(0)\mu_2(0)}\mu_2(0)[2\varepsilon_2(0) + 1]^2}. \tag{3.36}$$

This result generalizes the one obtained in Ref. [91] to the case of an atom embedded in a medium, with local-field correction included. In particular, we find that the interaction is repulsive for $\zeta(0)/\chi(0) > 23\mu_2(0)/(7\varepsilon_2(0))$ and otherwise attractive, e.g., for $\chi(0) = \zeta(0)$ and $\varepsilon_2(0) = \mu_2(0) = 1$.

Let us return to Eq. (3.31) and consider further examples. Assuming that the atom is located in free space where $\mu_2(0) = \varepsilon_2(0) = 1$, it can be shown that, for a purely electric region 1,

$$C_4[\mu_1(0) = 1, \mu_2(0) = 1, \varepsilon_2(0) = 1] < 0, \tag{3.37}$$

and for a purely magnetic region 1 with $\mu_1(0) > 1$,

$$C_4[\varepsilon_1(0) = 1, \mu_2(0) = 1, \varepsilon_2(0) = 1] > 0. \tag{3.38}$$

That is to say, in the retarded limit, the atom is attracted toward an electric half space while it is repelled from a magnetic one. More generally, on recalling the signs of the derivatives given in Eq. (3.32), electric properties tend to make the potential attractive while magnetic ones tend to make the potential repulsive.

If the atom is embedded in a material half space, while the opposite half space is empty, $\mu_1(0) = \varepsilon_1(0) = 1$, it can be shown that, for a purely electric material,

$$C_4[\mu_1(0) = 1, \varepsilon_1(0) = 1, \mu_2(0) = 1] > 0, \tag{3.39}$$

the atom is repelled from the interface, while for a purely magnetic material with $\mu_2(0) > 1$,

$$C_4[\mu_1(0) = 1, \varepsilon_1(0) = 1, \varepsilon_2(0) = 1] < 0, \tag{3.40}$$

the atom is attracted towards the interface. Except for the different power law, the sign of the interaction is the same in each of these limiting cases in the retarded and nonretarded distance regime, cf. Tab. 3.1.

It should be mentioned that the above-given results are consistent with the special case of an atom in vacuum given by $\varepsilon_2 = \mu_2 = 1$ [91]. In particular, the corresponding free-space potential shows qualitatively the same behavior: The atom is attracted to regions of large permittivity and small permeability.

As discussed in the context of several theoretical problems (see, e.g., Ref. [141]), calculations simplify considerably in the special case of an isorefractive medium. Isorefractive media are characterized by the requirement that the refractive index of the two contacting regions is the same,

$$\varepsilon_1\mu_1 = \varepsilon_2\mu_2, \tag{3.41}$$

which immediately implies that the wave vectors also coincide, $\kappa_1(i\xi) = \kappa_2(i\xi)$. If the two half spaces are isorefractive, the potential (3.17) greatly simplifies to

$$U_2(z_A) = -\frac{\hbar}{4\varepsilon_0\pi^2}\int_0^\infty \mathrm{d}\xi\frac{\alpha_A}{\varepsilon_2}\left(\frac{3\varepsilon_2}{2\varepsilon_2+1}\right)^2\frac{\varepsilon_1-\varepsilon_2}{\varepsilon_1+\varepsilon_2}\int_{\sqrt{\varepsilon_2\mu_2}\xi/c}^\infty \mathrm{d}\kappa_2\kappa_2^2 e^{-2\kappa_2 z_A}, \tag{3.42}$$

where we have already changed the integration variable. We carry out the integration over κ_2 and obtain

$$U_2(z_A) = -\frac{\hbar}{16\pi^2\varepsilon_0 z_A^3}\int_0^\infty \mathrm{d}\xi\frac{\alpha_A}{\varepsilon_2}\left(\frac{3\varepsilon_2}{2\varepsilon_2+1}\right)^2\frac{\varepsilon_1-\varepsilon_2}{\varepsilon_1+\varepsilon_2}$$
$$\times e^{-2\sqrt{\varepsilon_2\mu_2}\xi z_A/c}\left[1 + 2z_A\frac{\sqrt{\varepsilon_2\mu_2}\xi}{c} + 2z_A^2\frac{\varepsilon_2\mu_2\xi^2}{c^2}\right]. \tag{3.43}$$

The result in the nonretarded regime can easily be obtained by replacing

$$e^{-2\sqrt{\varepsilon_2\mu_2}\xi z_A/c}\left[1 + 2z_A\frac{\sqrt{\varepsilon_2\mu_2}\xi}{c} + 2z_A^2\frac{\varepsilon_2\mu_2\xi^2}{c^2}\right] \simeq 1, \tag{3.44}$$

thus we have to leading order

$$U_2(z_A) = -\frac{\hbar}{16\pi^2\varepsilon_0 z_A^3}\int_0^\infty \mathrm{d}\xi\frac{\alpha_A}{\varepsilon_2}\left(\frac{3\varepsilon_2}{2\varepsilon_2+1}\right)^2\frac{\varepsilon_1-\varepsilon_2}{\varepsilon_1+\varepsilon_2}, \tag{3.45}$$

in accordance with Eq. (3.24) together with $C_1 = 0$. For the retarded limit we take

$\varepsilon_1 < \varepsilon_2$	$\varepsilon_1 > \varepsilon_2$	$\varepsilon_1\mu_1 = \varepsilon_2\mu_2$
$\mathbf{F}_{\mathrm{nret}} \propto +\frac{1}{z_A^4}$ $\mathbf{F}_{\mathrm{ret}} \propto +\frac{1}{z_A^5}$	$\mathbf{F}_{\mathrm{nret}} \propto -\frac{1}{z_A^4}$ $\mathbf{F}_{\mathrm{ret}} \propto -\frac{1}{z_A^5}$	$\mathbf{F}_{\mathrm{nret}} = -\frac{3\hbar}{16\pi^2\varepsilon_0 z_A^4}\int_0^\infty \mathrm{d}\xi\frac{\alpha_A}{\varepsilon_2}\frac{\varepsilon_1-\varepsilon_2}{\varepsilon_1+\varepsilon_2}\left(\frac{3\varepsilon_2}{2\varepsilon_2+1}\right)^2$
$\mu_1 > \mu_2$ $\mathbf{F}_{\mathrm{nret}} \propto -\frac{1}{z_A^2}$ $\mathbf{F}_{\mathrm{ret}} \propto -\frac{1}{z_A^5}$	$\mu_1 < \mu_2$ $\mathbf{F}_{\mathrm{nret}} \propto +\frac{1}{z_A^2}$ $\mathbf{F}_{\mathrm{ret}} \propto +\frac{1}{z_A^5}$	$\mathbf{F}_{\mathrm{ret}} = -\frac{3\hbar c\alpha_A(0)}{8\pi^2\varepsilon_0\varepsilon_2(0)n_2(0)z_A^5}\frac{\varepsilon_1(0)-\varepsilon_2(0)}{\varepsilon_1(0)+\varepsilon_2(0)}\left(\frac{3\varepsilon_2(0)}{2\varepsilon_2(0)+1}\right)^2$

Table 3.1: Power laws for the CP force on a ground-state atom in a magnetodielectric two-layer system in the nonretarded and the retarded distance regime. The atom is located in layer 2.

the static counterparts of ε, μ and α_A and integrate over ξ,

$$U_2(z_A) = -\frac{3\hbar c\alpha_A}{32\pi^2\varepsilon_0\varepsilon_2\sqrt{\varepsilon_2\mu_2}z_A^4}\left(\frac{3\varepsilon_2}{2\varepsilon_2+1}\right)^2\frac{\varepsilon_1-\varepsilon_2}{\varepsilon_1+\varepsilon_2}, \qquad (3.46)$$

which is in accordance with Eq. (3.30).

3.2.2 Numerical results

To study the local-field corrected potential at moderate distances and to elucidate the combined influence of electric and magnetic properties of the media, we calculate the position dependent part $U_2(z_A)$ in accordance with Eq. (3.17) numerically. We assume a two-level atom of transition frequency ω_{10} and a single resonance Drude–Lorentz model for the permittivities and permeabilities and write Eq. (2.2) in the form

$$\varepsilon_j(i\xi) = 1 + \frac{\omega_{Pej}^2}{\omega_{Tej}^2 + \xi^2 + \xi\gamma_{ej}}, \quad \mu_j(\omega) = 1 + \frac{\omega_{Pmj}^2}{\omega_{Tmj}^2 + \xi^2 + \xi\gamma_{mj}}, \quad j = 1, 2, \quad (3.47)$$

where ω_{Pej}, ω_{Pmj} denote the plasma frequencies of the respective media.

Our analytical results have shown that purely electric or magnetic media, give rise to monotonous potentials of opposite signs and differing power laws. When competing effects of electric and magnetic properties come into play, potential walls or wells can hence be expected. For sufficiently strong magnetic properties, the well is located at short distances where its position and height can be obtained from Eq. (3.24),

$$z_{\min} = \sqrt{\frac{3C_3}{C_1}}, \quad U_{\min} = \frac{2C_1}{9}\sqrt{\frac{C_1}{C_3}} \qquad (3.48)$$

respectively.

The numerical result, as shown in Figure 3.2 (a), illustrates the atom–surface distance dependence of the $U_2(z_A)$ potential. In case (1), $\varepsilon_2 > \varepsilon_1$, the potential at very short atom–surface distances is repulsive in medium 2 and attractive in medium 1, in consistency with the analytical results (3.24) and (3.25). Similarly, in cases (2) and (3), $\varepsilon_2 < \varepsilon_1$, the potential is attractive in medium 2 while repulsive in medium 1. As the atom–surface distance increases, the second term in the potential (3.24) with power law z_A^{-1} gradually comes into play. If the magnetic properties are strong enough they may switch the sign of the potential and create potential walls or wells as can be seen in Fig. 3.2 (2).

In the following we will discuss the impact of the local-field correction. The local-field correction factor $[3\varepsilon_i/(2\varepsilon_i+1)]^2$ of an electric atom depends only on the dielectric properties and is positive, larger than one, and increases with ε_i, where i indicates the layer containing the guest atom. It approaches the maximum value of 9/4 as $\varepsilon_i \to \infty$. Note that a local-field correction factor larger than 1 does not necessarily lead to an enhancement of the potential because the uncorrected factor in the integrand can change sign as the imaginary frequency ξ varies. That is to say, only when the uncorrected integrand is purely repulsive or attractive, the local-field correction increases or decreases the potential. Firstly, we study how the net effect of the local-field correction depends on the distance. In Fig. 3.2 (upper) we indicate the corresponding uncorrected potentials by dashed lines while the difference between the corrected and uncorrected results is shown in the lower part of Fig. 3.2. It reveals quite significant corrections of up to 30% of the uncorrected values. In contrast, in the middle case (2), the two curves with and without local-field correction cross, implying that there exists an atom–surface distance at which the effect of the local-field correction is canceled due to the ξ-integration.

As a second aspect, we study the behavior of the local-field corrected CP potential with respect to the static permittivity of the medium surrounding the atom (region 2). In Figs. 3.3, we have plotted the (corrected and uncorrected) potential for two different values of the atom–surface distance. The curves for the larger distance from the interface peak at certain values of $\varepsilon_2(0)$ where the positions of the peaks are different due to the effects of the local field. Closer inspection verifies that, as $\varepsilon_2(0)$ increases, the ratio between the corrected and uncorrected curves tends to the static value of the local-field correction factor $[3\varepsilon_2/(2\varepsilon_2+1)]^2$ which lies between 1 and 9/4 Note that in general the ratio of the two potentials is not always a good measure since one of the quotients may vanish. For the smaller value of the atom–surface distance
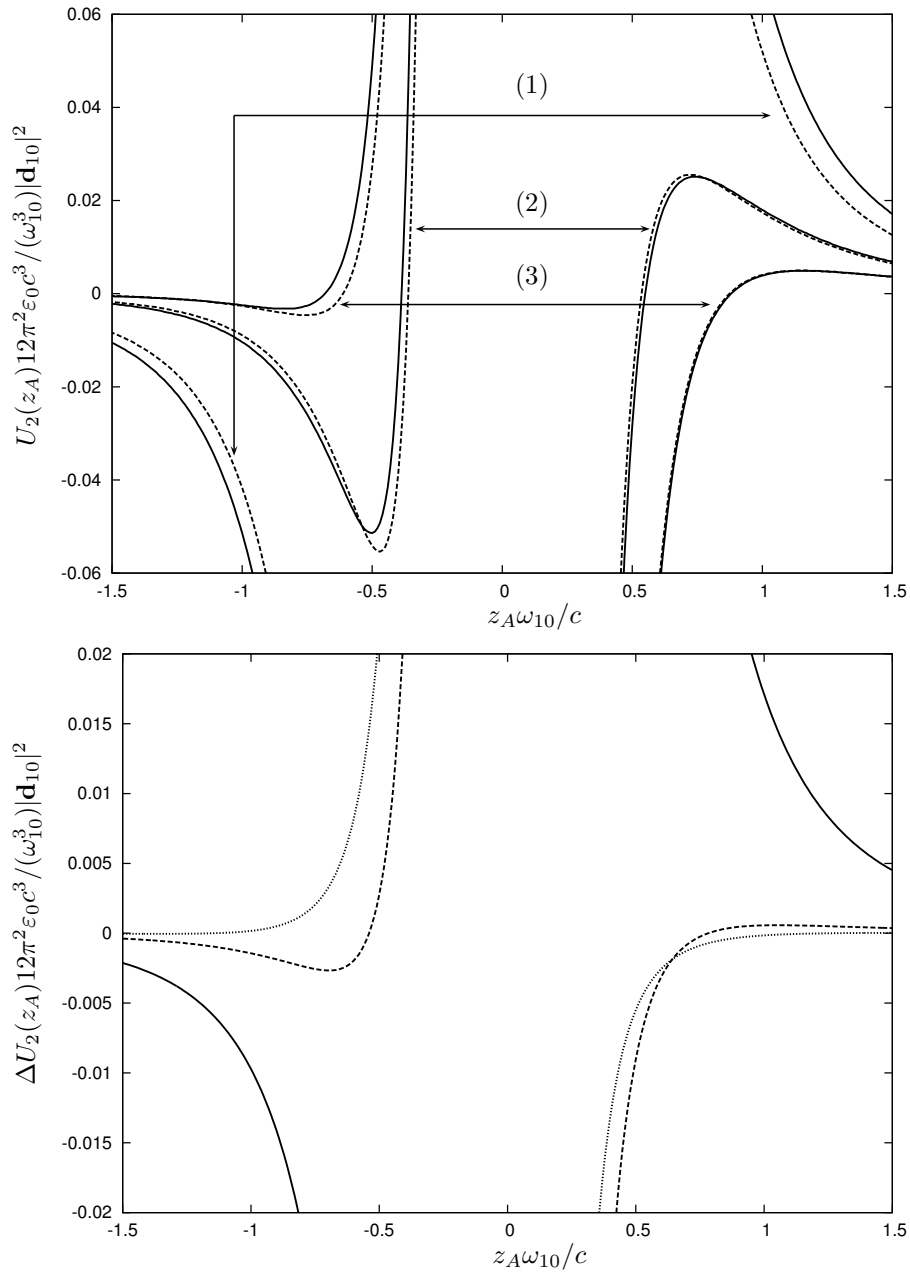
Figure 3.2: (upper) Position-dependent part of the CP potential experienced by a ground-state two-level atom in a magnetodielectric two-layer system as a function of atom–surface distance for fixed ε_1, μ_1, μ_2, and for $\omega_{Pe2}/\omega_{10} = 1$ (1), 0.4 (2), and 0.2 (3). Solid lines denote the potentials with the local-field correction, while dashed lines represent those without. Other parameters are $\omega_{Te1}/\omega_{10} = \omega_{Te2}/\omega_{10} = 1.03$, $\omega_{Pe1}/\omega_{10} = 0.75$, $\omega_{Tm1}/\omega_{10} = \omega_{Tm2}/\omega_{10} = 1$, $\omega_{Pm1}/\omega_{10} = 2.3$, $\omega_{Pm2}/\omega_{10} = 0.4$, $\gamma_{m1,2}/\omega_{10} = \gamma_{e1,2}/\omega_{10} = 0.001$, and the cavity radius is $R_C\omega_{10}/c = 0.01$. (lower) Difference ΔU_2 between local-field corrected and uncorrected (position-dependent) CP potential versus atom–surface distance where the solid, dashed, and dotted lines refer to the curves (1), (2), and (3), respectively.
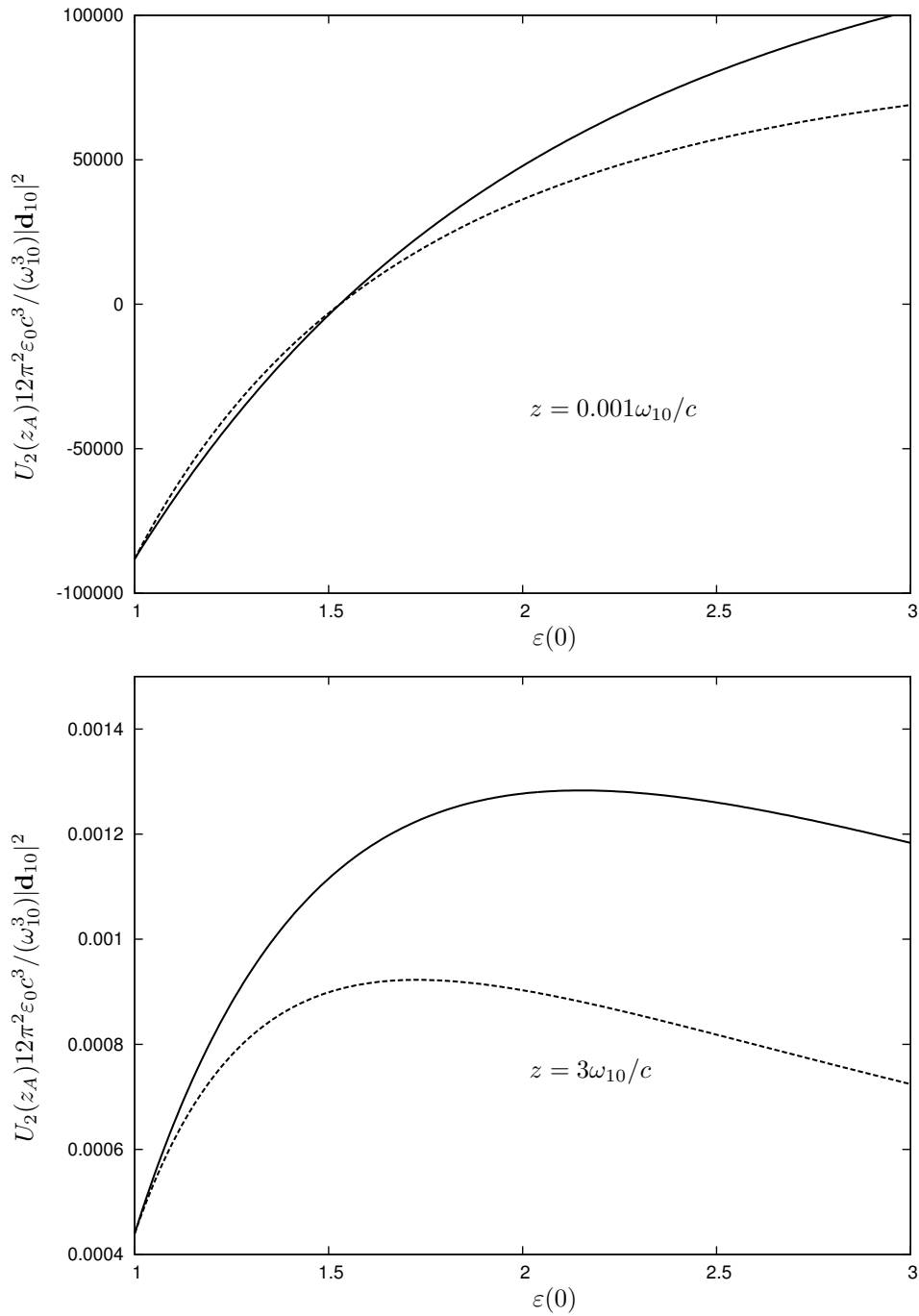
Figure 3.3: Position-dependent part of the CP potential as a function of the static permittivity $\varepsilon_2(0)$ (more specifically ω_{Pe2}/ω_{10}) for two values of the atom–surface distance $z_A\omega_{10}/c = 0.01$ (scale to the left, lower curves) and $z_A\omega_{10}/c = 3$ (scale to the right, upper curves). Solid lines are with the local-field correction while dashed lines are without one. Other parameters are the same as in Fig. 3.2.

$z_A\omega_{10}/c = 0.01$, a crossing point between the corrected and uncorrected curves is observed, where the local-field correction has vanishing net effect.

3.2.3 Potential at the surface

In the following we want to apply our results from the previous section to study the full CP interaction, which is of interest when a small particle is transfered through an interface. Theories of the (long-range) CP interaction are usually incapable of correctly predicting the behavior of the interaction potential at extremely short distances since competing repulsive interactions, arising from the overlap of atomic valence electrons with the surface, are neglected. The calculation of the nonresonant CP potential for very small atom–surface separations has been subject to a number of investigations. There, the CP interaction has been modified to produce a finite potential at the surface [142] by introducing a reference plane [142]; via characterizing the material surface by a more realistic (spatial dispersive) response function [143], or via using an atomic polarizability beyond the dipole approximation [144, 145].

Firstly, we study the layer-dependent, constant part U_1 of the potential which is entirely due to the local-field correction. In Fig. 3.4 we have numerically calculated the dependence of U_1 on the real-cavity radius R_C for a purely electric material and, for comparison, also a purely magnetic material. According to the different leading terms in the analytic result (3.8), the potential $|U_1|$ for a pure electric material is generally larger than that for a pure magnetic material but has opposite sign. The figure also indicates that the magnitude of U_1 decreases with increasing real-cavity radius, that is, the effects of the local field becomes weaker as the medium becomes more dilute, and the average distance between the two atoms increases. Throughout this section, we have assumed that for a small radius of the real cavity it is sufficient to work with the approximate potential as given by the second equality in Eq. (3.8). In Fig. 3.4, we have checked numerically that this assumption is correct; the difference is shown by dashed lines for the approximate result and solid lines for the exact one. On the scale of the plot, the differences are not visible for a purely electric material. The agreement in the case of a purely magnetic material is good for very small $R_C\omega_{10}/c$ but worsens as $R_C\omega_{10}/c$ increases.

In the following, we will propose an estimate of the full CP potential at the interface. Firstly, we recall that for very short distances, $\sqrt{|\varepsilon_j\mu_j|}z_A\omega_{10}/c \ll 1$, the position-dependent part of the potential is dominated by the $C_3 z_A^{-3}$ term, which contains only the difference of the electric medium properties, $\varepsilon_1 - \varepsilon_2$, in the integrand. It can thus
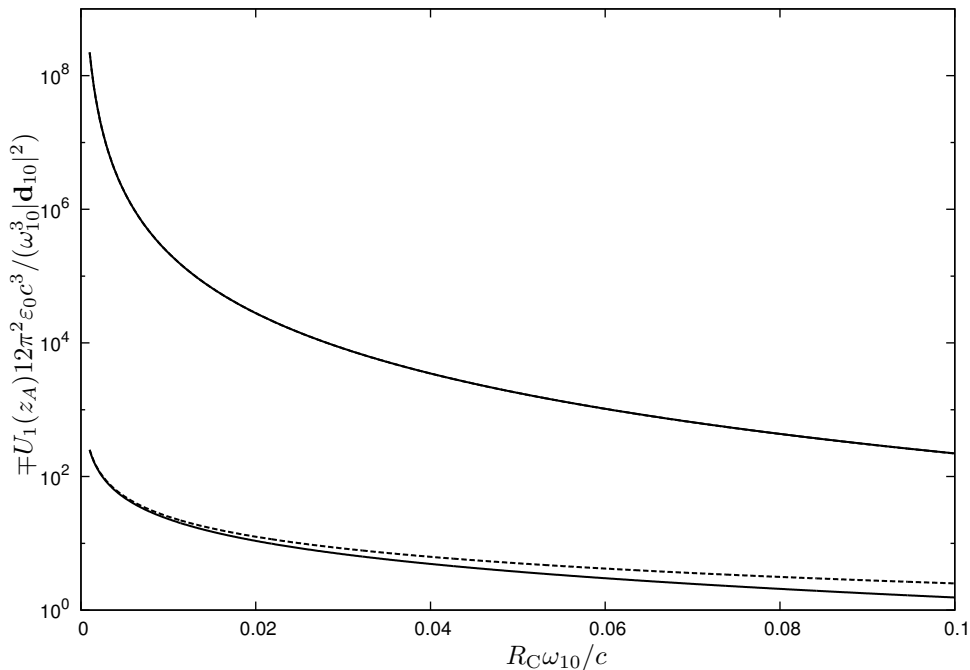
Figure 3.4: The exact layer-dependent constant part of the potential (solid line), and approximate results (dashed line), are shown as functions of the real-cavity radius. The upper (pair of) curves shows $-U_1(z_A)12\pi^2\varepsilon_0 c^3/(\omega_{10}^3|\mathbf{d}_{10}|^2)$ (the sign has been reversed so that a logarithmic scale can be used) for a purely electric material with $\omega_{Pe2}/\omega_{10} = 0.4$, while the lower pair of curves shows $U_1(z_A)12\pi^2\varepsilon_0 c^3/(\omega_{10}^3|\mathbf{d}_{10}|^2)$ for a purely magnetic material with $\omega_{Pm2}/\omega_{10} = 0.4$. All other parameters are the same as in Fig. 3.2. The radius of the cavity $R_C\omega_{10}/c$ starts from 0.001.

be expected that even if the medium has a permeability $\mu_j \neq 1$, it is irrelevant for the total value of the potential at or close to the surface as long as $\varepsilon_1 \neq \varepsilon_2$. In Fig. 3.5 we have calculated the full potential $U_1 + U_2(z_A)$ on both sides of the interface with the properties of medium 1 fixed while those of medium 2 vary from free space to a more dense medium. The case represented by the dashed line is the same as curve (2) in Fig. 3.2, showing that additional structures in U_2, like potential wells or walls, are typically overwhelmed by the magnitude of U_1. As can be seen from the figure, an atom located in layer 2 close to the surface will be attracted to it, and if the atom can cross the interface, it will be pushed further away from the surface into layer 1.

In Fig. 3.5, we have not displayed the results for distances $|z_A| < R_C\sqrt{|\varepsilon\mu|}$ where the real-cavity model can no longer be applied. This gives rise to a gap between the potentials on the two sides of the interface. To estimate the amount of energy needed to push an atom from layer 2 into layer 1, namely the potential exactly at the

interface, we suggest to use the simple interpolation [AS4]

$$U(z_A = 0) = \frac{1}{2}\left[U(R_C) + U(-R_C)\right]$$

$$= -\frac{\hbar}{32\pi^2\varepsilon_0 R_C^3}\int_0^\infty d\xi\,\alpha_A\Bigg\{12\left(\frac{\varepsilon_1 - 1}{2\varepsilon_1 + 1} + \frac{\varepsilon_2 - 1}{2\varepsilon_2 + 1}\right)$$

$$- \frac{\varepsilon_1 - \varepsilon_2}{\varepsilon_1 + \varepsilon_2}\left[\frac{1}{\varepsilon_1}\left(\frac{3\varepsilon_1}{2\varepsilon_1 + 1}\right)^2 - \frac{1}{\varepsilon_2}\left(\frac{3\varepsilon_2}{2\varepsilon_2 + 1}\right)^2\right]\Bigg\} \qquad (3.49)$$

where we have used Eqs. (3.8), (3.24), and (3.25). This means that we first plot the potential as a function of the atomic position up to distances $|z_A| = R_C$. Then we connect the two loose ends on the two sides of the interface by a straight line and read off the value of the potential at $z_A = 0$. In the following we want to show that the proposed estimate, Eq. (3.49), is consistent with an earlier work where the on-surface potential of a molecule of finite size s has been calculated directly [146],

$$U(z_A = 0) = \frac{\hbar}{2\pi^{5/2}\varepsilon_0 s^3}\int_0^\infty d\xi\,\alpha_A\left[\frac{1}{2}\left(\frac{1}{\varepsilon_1} + \frac{1}{\varepsilon_2}\right) + \frac{1}{3}\frac{\varepsilon_1 - \varepsilon_2}{\varepsilon_1 + \varepsilon_2}\left(\frac{1}{\varepsilon_1} - \frac{1}{\varepsilon_2}\right)\right]. \quad (3.50)$$

The results (3.50) and (3.49) look remarkably similar; the second terms in Eqs. (3.49) and (3.50), which represent the interface contribution to the potential, agree when setting $s = (\sqrt[3]{16/3}/\pi^{-1/6})R_C \approx 1.4R_C$ and neglecting the local-field correction in Eq. (3.49) which was not considered in Ref. [146]. The first terms can be regarded as being bulk contributions from the two interfacing media which differ in both approaches. While Eq. (3.50) still contains self-energy contributions which do not vanish in the vacuum case $\varepsilon_j = 1$, the potential (3.49) vanishes in that limit.

Our results may help to understand the transfer of a small molecule through a membrane from one cell to another. In a similar manner, we may also study an atom in a magnetodielectric three-layer planar structure which may serve as a prototype for the problem of a small particle in the middle of a cell membrane of finite thickness [147]. For details, the reader is referred to Ref. [AS4]

# 3.3 Medium-assisted Casimir–Polder potential of spherical objects

Two methods might be envisaged to calculate the CP interaction of a ground-state atom and a magnetodielectric sphere. Firstly, one could take the Green tensor of the
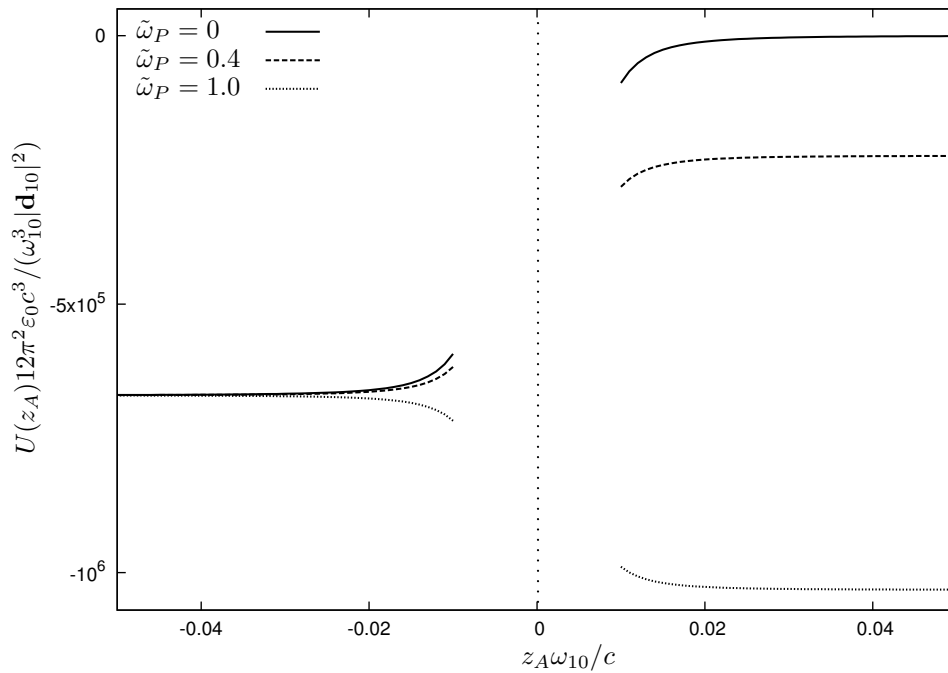
Figure 3.5: Local-field corrected total CP potential of a ground-state two-level atom in a magneto-dielectric two-layer system as a function of the atom–surface distance. Different curves are for different coupling strengths of the medium 2, $\tilde{\omega}_P \equiv \omega_{Pm2}/\omega_{10} = \omega_{Pe2}/\omega_{10}$. Other parameters are the same as in Fig. 3.2. The vertical line indicates the position of the interface.

sphere, as given in Eq. (3.52), and substitute it into the ground-state potential (2.53). Indeed, if the system consists of the sphere and the atom in a homogeneous medium, as sketched in Fig. 3.7 (i), it is possible to derive a closed expression for the CP potential. If, however, other arbitrary (background) bodies are present (cf. Fig. 3.7 (iii)), an analytical expression for the Green tensor of the full system is usually not known. In particular for a sufficiently small radius of the sphere, it is convenient to use another, point-scattering approach to calculate the atom–sphere interaction. We will show how the Green tensor of the sphere–background system can be decomposed into the Green tensor of the system without the sphere and a factor containing the permittivities and permeabilities of the sphere and the ones of the background at the position of the sphere. The results are then used to study the atom–sphere potentials, and are compared to the vdW interaction between two ground-state atoms (Sec. 3.3.1). In a similar manner, we consider the more complex structure of a sphere inside a cavity in the presence of an arbitrary background medium (Sec. 3.3.2). This setup may be regarded as being a model for a molecule of variable size. It reconciles the microscopic description of an atom [Fig. 3.6 (i)] and the macroscopic viewpoint of the

intervening medium and the sphere [Fig. 3.6 (ii)]. With the chosen construction we can continuously interpolate between the two limiting cases of an atom-like sphere and a macroscopic sphere by changing the inner radius of the sphere [Fig. 3.6 (iii)]. Note that our considerations are very different from earlier investigations where the (nonretarded) CP potential of a ground-state atom inside and outside a dielectric or metallic spherical shell [148], as well as that of a perfectly conducting sphere [149] in free-space have been studied. Here, we allow for an arbitrary environment consisting of both a medium and background bodies but exclude metals. Our studies are based on Ref. [AS7].
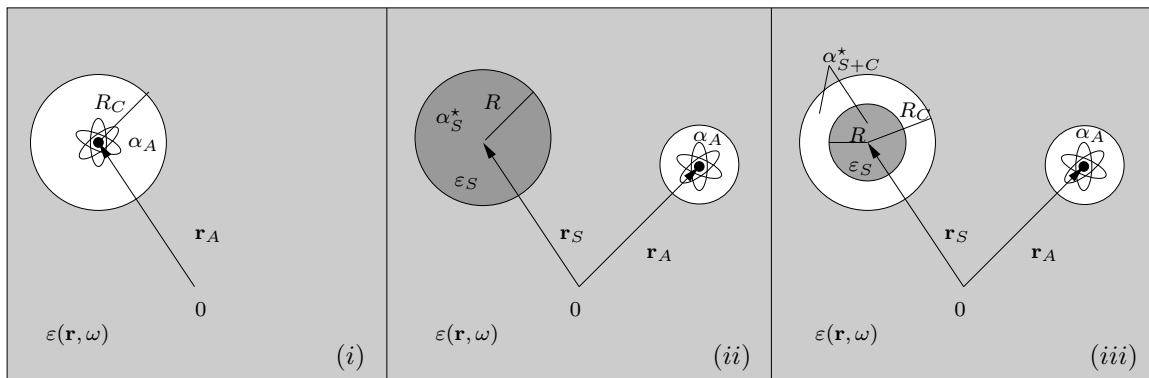
Figure 3.6: Sketch of relevant models and parameters: (i)Atom in an empty cavity surrounded by medium (Onsager real cavity model), (ii) Atom near a dielectric sphere in an arbitrary medium environment (iii) Atom near a dielectric cavity–sphere system surrounded by medium. The magnetic properties of the atoms and the medium are not indicated in the figure.

3.3.1 Full sphere

Decomposition of the Green tensor

Consider a homogeneous magnetodielectric sphere with radius R centered at $\mathbf{r}_S$, and with permittivity $\varepsilon_S(\omega)$ and permeability $\mu_S(\omega)$ placed in a magnetodielectric environment characterized by the functions $\varepsilon(\mathbf{r}, \omega)$ and $\mu(\mathbf{r}, \omega)$. To describe the situation, we introduce the new functions

$$\varepsilon_S(\mathbf{r},\omega), \mu_S(\mathbf{r},\omega) = \begin{cases} \varepsilon_S(\omega), \mu_S(\omega) & \text{for } |\mathbf{r} - \mathbf{r}_S| \leq R, \\ \varepsilon(\mathbf{r},\omega), \mu(\mathbf{r},\omega) & \text{elsewhere.} \end{cases} \tag{3.51}$$

The Green tensor $\boldsymbol{G}_S^{(1)}(\mathbf{r}, \mathbf{r}, \omega)$ of the sphere plus environment is hence the solution to the differential equation (2.20), with $\varepsilon_S(\mathbf{r}, \omega)$ and $\mu_S(\mathbf{r}, \omega)$ in place of $\varepsilon(\mathbf{r}, \omega)$ and

$\mu(\mathbf{r}, \omega)$.
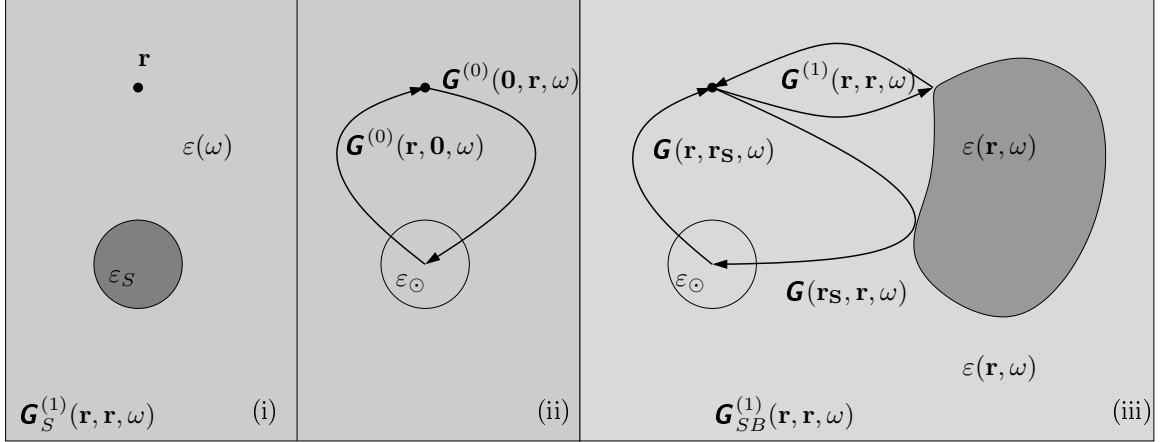
Figure 3.7: (i) Green tensor of the magnetodielectric sphere in the bulk medium $\boldsymbol{G}_S^{(1)}(\mathbf{r}, \mathbf{r}, \omega)$; (ii) Decomposition of the Green tensor from (i), the bulk Green tensor is denoted by $\boldsymbol{G}^{(0)}$; (iii) Decomposition of the Green tensor of the combined system of sphere and arbitrary background environment $\boldsymbol{G}_{SB}^{(1)}(\mathbf{r}, \mathbf{r}, \omega)$. The scattering Green tensor of the background bodies is denoted by $\boldsymbol{G}^{(1)}(\mathbf{r}, \mathbf{r}, \omega)$. Note that the factor accounting for the transmission through the boundaries of the sphere is not explicitly sketched in (ii) and (iii).

We first study the special case of a bulk environment and generalize to arbitrary environments later. The required scattering Green tensor of the sphere with center $\mathbf{r}_S = \mathbf{0}$ inside a bulk medium of permittivity $\varepsilon(\omega)$ and permeability $\mu(\omega)$ can be written in the form [131]

$$
\boldsymbol{G}_S^{(1)}(\mathbf{r}, \mathbf{r}', \omega) = \frac{i\mu k}{4\pi} \sum_{p=\pm} \sum_{l=1}^{\infty} \sum_{m=0}^{l} (2 - \delta_{m0}) \frac{2l+1}{l(l+1)} \frac{(l-m)!}{(l+m)!}
$$
$$
\times \left[B_l^M \mathbf{M}_{lmp}(k, \mathbf{r}) \mathbf{M}_{lmp}(k, \mathbf{r}') + B_l^N \mathbf{N}_{lmp}(k, \mathbf{r}) \mathbf{N}_{lmp}(k, \mathbf{r}') \right], \quad (3.52)
$$

where $k = \sqrt{\varepsilon\mu}\,\omega/c$ and $\mathbf{M}_{lmp}, \mathbf{N}_{lmp}$ denote even $(p = +)$ and odd $(p = -)$ spherical vector wave functions. The numbers l and m parameterize the total angular momentum and and its z-projection, respectively. $B_l^{M,N}$ are the associated Mie coefficients for reflection at the surface of the sphere and read [131],

$$
B_l^M = -\frac{\mu(\omega)k_S(\omega)j_l(z)[z_S j_l(z_S)]' - \mu_S(\omega)k(\omega)j_l(z_S)[z j_l(z)]'}{\mu(\omega)k_S(\omega)h_l^{(1)}(z)[z_S j_l(z_S)]' - \mu_S(\omega)k(\omega)j_l(z_S)[z h_l^{(1)}(z)]'}, \quad (3.53)
$$

and

$$B_l^N = -\frac{\mu(\omega)k_S(\omega)j_l(z_S)[zj_l(z)]' - \mu_S(\omega)kj_l(z)[z_S j_l(z_S)]'}{\mu(\omega)k_S(\omega)j_l(z_S)[zh_l^{(1)}(z)]' - \mu_S(\omega)k(\omega)h_l^{(1)}(z)[z_S j_l(z_S)]'}, \tag{3.54}$$

where $z = kR$, $z_S = k_S R$ with $k_S = \sqrt{\varepsilon_S \mu_S}\,\omega/c$. Here and throughout, we use the limit of a small sphere, where $|k_S R|, |kR| \ll 1$. Additionally, we require the separation between a source point and the center of the sphere to be much greater than the effective radius of the sphere,

$$\sqrt{\varepsilon_S \mu_S}R \ll |\mathbf{r} - \mathbf{r}_S|. \tag{3.55}$$

In this case, we can evaluate the Mie coefficients for small arguments. For small arguments, the lth spherical Bessel and Hankel functions of the first kind read [150]

$$j_l(x) \simeq \frac{x^l}{(2l+1)!!}, \quad h_l^{(1)}(x) \simeq \frac{(2l-1)!!}{x^{l+1}}, \tag{3.56}$$

which implies

$$B_l^{M,N} = \mathcal{O}\left[\left(\frac{\omega R}{c}\right)^{2l+1}\right]. \tag{3.57}$$

Equation (3.57) shows that the dominant contribution to the Green tensor is due to the $l = 1$ terms. The respective vector wave functions are given in spherical coordinates with unit vectors $\mathbf{e}_r$, $\mathbf{e}_\phi$, $\mathbf{e}_\theta$,

$$\mathbf{M}_{1m\pm}(k,\mathbf{r}) = \mp\frac{m}{\sin\theta}h_1^{(1)}(kr)P_1^m(\cos\theta)\begin{pmatrix}\sin m\phi\\\cos m\phi\end{pmatrix}\mathbf{e}_\theta - h_1^{(1)}(kr)\frac{\mathrm{d}P_1^m(\cos\theta)}{\mathrm{d}\theta}\begin{pmatrix}\cos m\phi\\\sin m\phi\end{pmatrix}\mathbf{e}_\phi \tag{3.58}$$

and

$$\mathbf{N}_{1m\pm}(k,\mathbf{r}) = 2\frac{h_1^{(1)}(kr)}{kr}P_1^m(\cos\theta)\begin{pmatrix}\cos m\phi\\\sin m\phi\end{pmatrix}\mathbf{e}_r + \frac{1}{kr}\frac{\mathrm{d}[krh_1^{(1)}(kr)]}{d(kr)}\frac{\mathrm{d}P_1^m(\cos\theta)}{\mathrm{d}\theta}\begin{pmatrix}\cos m\phi\\\sin m\phi\end{pmatrix}\mathbf{e}_\theta$$
$$\mp\frac{m}{\sin\theta}P_1^m(\cos\theta)\frac{1}{kr}\frac{\mathrm{d}[krh_1^{(1)}(kr)]}{d(kr)}\begin{pmatrix}\sin m\phi\\\cos m\phi\end{pmatrix}\mathbf{e}_\phi, \tag{3.59}$$

where the upper (lower) components refer to the upper (lower) sign. Here, $P_1^m(x)$ denote the associated Legendre polynomials, and $j_1(x)$ and $h_1^{(1)}(x)$ are given by Eq. (3.6).

In particular, we need

$$P_1^0(\cos\theta) = \cos\theta \quad \text{and} \quad P_1^1(\cos\theta) = -\sin\theta. \tag{3.60}$$

The $l = 1$ reflection coefficients are given by

$$B_1^M = \frac{2i}{3}\left(\sqrt{\varepsilon\mu}\,\frac{\omega R}{c}\right)^3 \frac{\mu_S - \mu}{\mu_S + 2\mu}, \tag{3.61}$$

$$B_1^N = \frac{2i}{3}\left(\sqrt{\varepsilon\mu}\,\frac{\omega R}{c}\right)^3 \frac{\varepsilon_S - \varepsilon}{\varepsilon_S + 2\varepsilon} \tag{3.62}$$

in the small-sphere limit. We further evaluate the sums over p and m for $l = 1$ for equal arguments $\mathbf{r} = \mathbf{r}'$,

$$\sum_{p=\pm 1}\sum_{m=0}^{1}(2 - \delta_{m0})\frac{(1-m)!}{(1+m)!}\,\mathbf{M}_{1mp}(\mathbf{r})\mathbf{M}_{1mp}(\mathbf{r}) = h^2(\boldsymbol{I} - \mathbf{e}_r\mathbf{e}_r) \tag{3.63}$$

and

$$\sum_{p=\pm 1}\sum_{m=0}^{1}(2 - \delta_{m0})\frac{(1-m)!}{(1+m)!}\,\mathbf{N}_{1mp}(\mathbf{r})\mathbf{N}_{1mp}(\mathbf{r}) = \frac{h'^2}{(kr)^2}\,\boldsymbol{I} + \frac{4h^2 - h'^2}{(kr)^2}\,\mathbf{e}_r\mathbf{e}_r, \tag{3.64}$$

with the notation $h \equiv h_1^{(1)}(kr)$ and $h' \equiv \mathrm{d}[krh_1^{(1)}(kr)]/\mathrm{d}(kr)$. Substituting these expressions into Eq. (3.52), the (equal-position) scattering Green tensor of a small sphere becomes

$$\begin{aligned}
\boldsymbol{G}_S^{(1)}(\mathbf{r},\mathbf{r},\omega) = \frac{\mu e^{2ikr}}{4\pi k^2 r^6}&\Bigg\{\left[1 - 2ikr - 3(kr)^2 + 2i(kr)^3 + (kr)^4\right]\boldsymbol{I} \\
&+ \left[3 - 6ikr - (kr)^2 - 2i(kr)^3 - (kr)^4\right]\mathbf{e}_r\mathbf{e}_r\Bigg\}\frac{\varepsilon_S - \varepsilon}{\varepsilon_S + 2\varepsilon}\,R^3 \\
&+ \frac{\mu e^{2ikr}}{4\pi r^4}\left[1 - 2ikr - (kr)^2\right](\boldsymbol{I} - \mathbf{e}_r\mathbf{e}_r)\frac{\mu_S - \mu}{\mu_S + 2\mu}\,R^3. \tag{3.65}
\end{aligned}$$

The Green tensor $\boldsymbol{G}_S^{(1)}(\mathbf{r},\mathbf{r},\omega)$ of the small sphere describes the propagation of the electric field from a source at $\mathbf{r}$ to the sphere, its scattering from the sphere at $\mathbf{r}_S = \mathbf{0}$ and its return to $\mathbf{r}$, where the sphere acts as a polarizable and magnetizable point scatterer. It is therefore natural to try to relate the electric part of $\boldsymbol{G}_S^{(1)}$ (i.e., the terms proportional to $\varepsilon_S - \varepsilon$) to products of the bulk Green tensor $\boldsymbol{G}^{(0)}$, which describes

the propagation of the electric field through the homogeneous (bulk) medium to an electric scatterer. The magnetic contribution will be disussed after that. For different spatial arguments, the bulk Green tensor [151]

$$\boldsymbol{G}^{(0)}(\mathbf{r}, \mathbf{r}', \omega) = -\frac{\mu e^{ik\rho}}{4\pi k^2 \rho^3}\left\{\left[1 - ik\rho - (k\rho)^2\right]\boldsymbol{I} - \left[3 - 3ik\rho - (k\rho)^2\right]\mathbf{e}_\rho\mathbf{e}_\rho\right\} \quad (3.66)$$

depends on $\boldsymbol{\rho} = \mathbf{r} - \mathbf{r}'$ and $\mathbf{e}_\rho = \boldsymbol{\rho}/\rho$ with $\rho = |\boldsymbol{\rho}|$. From Eq. (3.66) we find that

$$\boldsymbol{G}^{(0)}(\mathbf{r}, \mathbf{0}, \omega) \cdot \boldsymbol{G}^{(0)}(\mathbf{0}, \mathbf{r}, \omega) = \frac{\mu^2 e^{2ikr}}{16\pi^2 k^4 r^6}\left\{\left[1 - 2ikr - 3(kr)^2 + 2i(kr)^3 + (kr)^4\right]\boldsymbol{I}\right.$$
$$\left. + \left[3 - 6ikr - (kr)^2 - 2i(kr)^3 - (kr)^4\right]\mathbf{e}_r\mathbf{e}_r\right\} \quad (3.67)$$

is related to the electric parts of (3.65) as sketched in Fig. 3.7 (ii). In a similar manner, we want to relate the magnetic terms in Eq. (3.65) to $\boldsymbol{G}^{(0)} \times \overleftarrow{\boldsymbol{\nabla}}$ and therefore calculate

$$\boldsymbol{G}^{(0)}(\mathbf{r}, \mathbf{r}_S, \omega) \times \overleftarrow{\boldsymbol{\nabla}}_S \cdot \boldsymbol{\nabla}_S \times \boldsymbol{G}^{(0)}(\mathbf{r}_S, \mathbf{r}, \omega)\big|_{\mathbf{r}_S=\mathbf{0}} = -\frac{\mu^2 e^{2ikr}}{16\pi^2 r^4}\left[1 - 2ikr - (kr)^2\right](\boldsymbol{I} - \mathbf{e}_r\mathbf{e}_r). \quad (3.68)$$

A comparison of Eq. (3.65) with Eqs. (3.67) and (3.68) shows how the Green tensor of a small magnetodielectric sphere in a bulk medium can be decomposed:

$$\boldsymbol{G}_S^{(1)}(\mathbf{r}, \mathbf{r}, \omega) = 4\pi\varepsilon R^3 \frac{\varepsilon_S - \varepsilon}{\varepsilon_S + 2\varepsilon}\frac{\omega^2}{c^2}\boldsymbol{G}^{(0)}(\mathbf{r}, \mathbf{0}, \omega) \cdot \boldsymbol{G}^{(0)}(\mathbf{0}, \mathbf{r}, \omega)$$
$$-\frac{4\pi R^3}{\mu}\frac{\mu_S - \mu}{\mu_S + 2\mu}\boldsymbol{G}^{(0)}(\mathbf{r}, \mathbf{r}_S, \omega) \times \overleftarrow{\boldsymbol{\nabla}}_S \cdot \boldsymbol{\nabla}_S \times \boldsymbol{G}^{(0)}(\mathbf{r}_S, \mathbf{r}, \omega)|_{\mathbf{r}_S=\mathbf{0}}. \quad (3.69)$$

In the next step we allow for a general background environment consisting of arbitrary bodies instead of the bulk medium and introduce the Green tensor of the sphere-background system $\boldsymbol{G}_{SB}^{(1)}$ as sketched in Fig. 3.7 (iii). With the permittivity $\varepsilon(\mathbf{r}, \omega)$ and permeability $\mu(\mathbf{r}, \omega)$ of the environment now being functions of position, it is useful to introduce a notation for their values at the position (but in absence) of the sphere, $\varepsilon_\odot(\omega) \equiv \varepsilon(\mathbf{r}_S, \omega)$, $\mu_\odot(\omega) \equiv \mu(\mathbf{r}_S, \omega)$. In addition to the small-sphere limit $|k_S R| \ll 1$, we assume the effective sphere radius to be much smaller than the distance from the sphere to any of the environment bodies,

$$\sqrt{\varepsilon_S \mu_S} R \ll |\mathbf{r} - \mathbf{r}_B|, \quad (3.70)$$

where $\mathbf{r}_B$ pointing inside the bodies. In this case, multiple scattering between sphere and environment can safely be neglected within leading order of $k_S R$. Our result

(3.69) can thus be generalized from the bulk case to an arbitrary environment by replacing $\varepsilon \mapsto \varepsilon_\odot$, $\mu \mapsto \mu_\odot$ as well as $\boldsymbol{G}^{(0)} \mapsto \boldsymbol{G}$ and adding the scattering Green tensor $\boldsymbol{G}^{(1)}(\mathbf{r},\mathbf{r})$ of the system without the sphere:

$$
\begin{aligned}
\boldsymbol{G}_{SB}^{(1)}(\mathbf{r},\mathbf{r},\omega) = {} & \boldsymbol{G}^{(1)}(\mathbf{r},\mathbf{r},\omega) + \frac{\varepsilon_\odot}{\varepsilon_0}\alpha_S^\star \frac{\omega^2}{c^2}\,\boldsymbol{G}(\mathbf{r},\mathbf{r}_S,\omega)\cdot\boldsymbol{G}(\mathbf{r}_S,\mathbf{r},\omega) \\
& -\frac{\mu_0}{\mu_\odot}\beta_S^\star \boldsymbol{G}(\mathbf{r},\mathbf{r}_S,\omega)\times\overleftarrow{\boldsymbol{\nabla}}_S\cdot\boldsymbol{\nabla}_S\times\boldsymbol{G}(\mathbf{r}_S,\mathbf{r},\omega),
\end{aligned}
\tag{3.71}
$$

where we have introduced the excess (or effective) polarizability, [103, 152]

$$
\alpha_S^\star = 4\pi\varepsilon_0 R^3\,\frac{\varepsilon_S - \varepsilon_\odot}{\varepsilon_S + 2\varepsilon_\odot},
\tag{3.72}
$$

and magnetizability

$$
\beta_S^\star = \frac{4\pi R^3}{\mu_0}\,\frac{\mu_S - \mu_\odot}{\mu_S + 2\mu_\odot}
\tag{3.73}
$$

of the sphere [153], which describe the electric and magnetic response of the sphere with respect to that of the surrounding medium.

The result (3.71) can be proven formally by treating both the sphere and the environment bodies via a Born expansion of the Green tensor [154]. In the following we show this for the terms arising from the electric scattering off the sphere. To that end, we introduce the susceptibility as the difference of the permittivity of the sphere–body system and the permittivity of the bulk background identified with $\varepsilon_\odot(\omega)$,

$$
\chi(\mathbf{r},\omega) = \varepsilon_S(\mathbf{r},\omega) - \varepsilon_\odot(\omega).
\tag{3.74}
$$

This function is non-zero when $\mathbf{r}$ is inside the sphere of volume S or inside one of the bodies (volumes B). For a purely electric sphere, the Born expansion of the scattering Green tensor of the sphere-background system with respect to the bulk medium reads

$$
\begin{aligned}
\boldsymbol{G}_{SB}^{(1)}(\mathbf{r},\mathbf{r},\omega) = {} & \sum_{K=1}^{\infty}\frac{\omega^{2K}}{c^{2K}}\int_{S+B}\mathrm{d}^3 s_1\chi(\mathbf{s}_1,\omega)\cdots\int \mathrm{d}^3 s_K\chi(\mathbf{s}_K,\omega) \\
& \times\,\boldsymbol{G}^{(0)}(\mathbf{r},\mathbf{s}_1,\omega)\cdot\boldsymbol{G}^{(0)}(\mathbf{s}_1,\mathbf{s}_2,\omega)\cdots\boldsymbol{G}^{(0)}(\mathbf{s}_K,\mathbf{r},\omega).
\end{aligned}
\tag{3.75}
$$

According to our condition (3.70), we keep only the terms that correspond to scattering processes starting from $\mathbf{r}$ followed by (multiple) reflections at the boundaries of the bodies and transmission into the sphere, (multiple) scattering inside the sphere, a second transmission through the surface of the sphere followed by scattering at the

bodies and finally return to the position **r** (cf. Fig. 3.8). To account for the desired
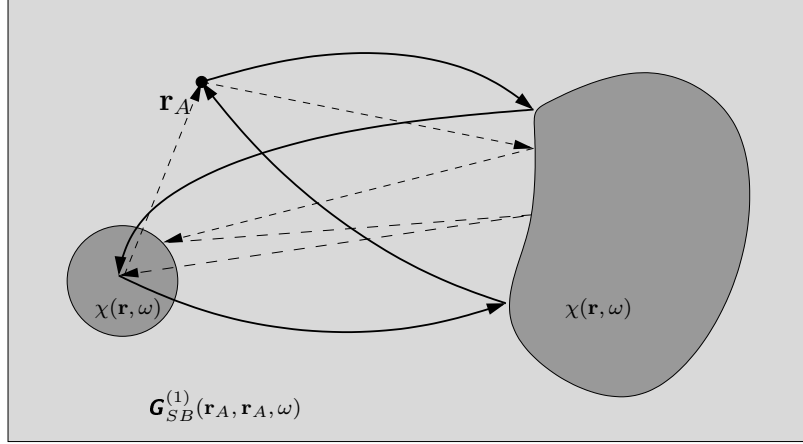
Figure 3.8: A typical processes included in the Born expansion of $G_{SB}(\mathbf{r}_A, \mathbf{r}_A, \omega)$ is indicated by the solid line. Processes involving multiple scattering between background bodies and sphere are discarded (dashed line).

processes, we rewrite Eq. (3.75)

$$
\begin{aligned}
\boldsymbol{G}_{SB}^{(1)}(\mathbf{r}, \mathbf{r}, \omega) = &\sum_{K=1}^{\infty} \frac{\omega^{2K}}{c^{2K}} \int_B \mathrm{d}^3 s_1 \chi(\mathbf{s}_1, \omega) \cdots \int_B \mathrm{d}^3 s_K \chi(\mathbf{s}_K, \omega) \\
&\times \boldsymbol{G}^{(0)}(\mathbf{r}, \mathbf{s}_1, \omega) \cdot \boldsymbol{G}^{(0)}(\mathbf{s}_1, \mathbf{s}_2, \omega) \cdots \boldsymbol{G}^{(0)}(\mathbf{s}_K, \mathbf{r}, \omega) \\
&+ \sum_{K=1}^{\infty} \sum_{i=0}^{K-1} \sum_{j=i+1}^{K} \frac{\omega^{2K}}{c^{2K}} \int_B \mathrm{d}^3 s_1 \chi(\mathbf{s}_1, \omega) \cdots \int_B \mathrm{d}^3 s_i \chi(\mathbf{s}_i, \omega) \\
\times \int_S \mathrm{d}^3 s_{i+1} \chi(\mathbf{s}_{i+1}, \omega) \cdots &\int_S \mathrm{d}^3 s_j \chi(\mathbf{s}_j, \omega) \int_B \mathrm{d}^3 s_{j+1} \chi(\mathbf{s}_{j+1}, \omega) \cdots \int_B \mathrm{d}^3 s_K \chi(\mathbf{s}_K, \omega) \\
&\times \boldsymbol{G}^{(0)}(\mathbf{r}, \mathbf{s}_1, \omega) \cdot \boldsymbol{G}^{(0)}(\mathbf{s}_1, \mathbf{s}_2, \omega) \cdots \boldsymbol{G}^{(0)}(\mathbf{s}_i, \mathbf{s}_{i+1}, \omega) \\
\cdot \boldsymbol{G}^{(0)}(\mathbf{s}_{i+1}, \mathbf{s}_{i+2}, \omega) &\cdots \boldsymbol{G}^{(0)}(\mathbf{s}_{j-1}, \mathbf{s}_j, \omega) \cdot \boldsymbol{G}^{(0)}(\mathbf{s}_j, \mathbf{s}_{j+1}, \omega) \cdots \boldsymbol{G}^{(0)}(\mathbf{s}_K, \mathbf{r}, \omega). \quad (3.76)
\end{aligned}
$$

Here, the first term is nothing but (a Born expansion of) the Green tensor of the background bodies

$$
\begin{aligned}
\boldsymbol{G}^{(1)}(\mathbf{r}, \mathbf{r}, \omega) = &\sum_{K=1}^{\infty} \frac{\omega^{2K}}{c^{2K}} \int_B \mathrm{d}^3 s_1 \chi(\mathbf{s}_1, \omega) \cdots \int_B \mathrm{d}^3 s_K \chi(\mathbf{s}_K, \omega) \\
&\times \boldsymbol{G}^{(0)}(\mathbf{r}, \mathbf{s}_1, \omega) \cdot \boldsymbol{G}^{(0)}(\mathbf{s}_1, \mathbf{s}_2, \omega) \cdots \boldsymbol{G}^{(0)}(\mathbf{s}_K, \mathbf{r}, \omega). \quad (3.77)
\end{aligned}
$$

The second term in Eq. (3.76) has three contributions. The first one arises from a first

group of integrals over the bodies. According to Eq. (3.77), it can be identified with the scattering Green tensor of the background body $\boldsymbol{G}^{(1)}(\mathbf{r}, \mathbf{s}_{i+1}, \omega)$ with $\mathbf{s}_{i+1}$ pointing to the position of the sphere. The second contribution containing the integrals over the sphere, accounts for reflections inside it. The third contribution is due to a second group of integrals over the bodies which can be identified with $\boldsymbol{G}^{(1)}(\mathbf{s}_j, \mathbf{r}, \omega)$ connecting a space point $\mathbf{r}$ with a point inside the sphere with scattering at the boundaries of the body included.

Now, we compare Eq. (3.76) with the Born expansion of the left-hand side of our bulk result (3.69),

$$\boldsymbol{G}_S^{(1)}(\mathbf{r}, \mathbf{r}, \omega) = \sum_{K=1}^{\infty} \frac{\omega^{2K}}{c^{2K}} \int_S \mathrm{d}^3 s_1 \chi(\mathbf{s}_1, \omega) \cdots \int_S \mathrm{d}^3 s_K \chi(\mathbf{s}_K, \omega) \tag{3.78}$$

$$\times \, \boldsymbol{G}^{(0)}(\mathbf{r}, \mathbf{s}_1, \omega) \cdot \boldsymbol{G}^{(0)}(\mathbf{s}_1, \mathbf{s}_2, \omega) \cdots \boldsymbol{G}^{(0)}(\mathbf{s}_K, \mathbf{r}, \omega) \tag{3.79}$$

$$= \alpha_S^\star \frac{\omega^2}{c^2} \frac{\varepsilon_\odot}{\varepsilon_0} \boldsymbol{G}^{(0)}(\mathbf{r}, \mathbf{0}, \omega) \cdot \boldsymbol{G}^{(0)}(\mathbf{0}, \mathbf{r}, \omega). \tag{3.80}$$

Substituting Eqs. (3.78) and (3.77) into Eq. (3.76) gives the electric part of Eq. (3.71). There, it also reveals the meaning of the factor $\omega^2/c^2 \alpha_S^\star \varepsilon_\odot/\varepsilon_0$: it arises from reflections at the inner boundary of the sphere. For a magnetizable sphere, a similar Born expansion can be applied to prove the relation for the magnetic terms.

So far we have studied the Green tensor as needed for the CP potential of a polarizable atom (2.53). To study also CP potential of a magnetizable atom (2.63), we require an analogous relation for the combination $\boldsymbol{\nabla} \times \boldsymbol{G}_{SB}^{(1)} \times \overleftarrow{\boldsymbol{\nabla}}'$. Applying the duality transformations (2.56)–(2.59) together with $\alpha_S^{\star \circledast} = \beta_S^\star/c^2$ to both sides of Eq. (3.71), we obtain the desired relation,

$$\boldsymbol{\nabla} \times \boldsymbol{G}_{SB}^{(1)}(\mathbf{r}, \mathbf{r}', \omega) \times \overleftarrow{\boldsymbol{\nabla}}'\big|_{\mathbf{r}'=\mathbf{r}} = \boldsymbol{\nabla} \times \boldsymbol{G}^{(1)}(\mathbf{r}, \mathbf{r}', \omega) \times \overleftarrow{\boldsymbol{\nabla}}'\big|_{\mathbf{r}'=\mathbf{r}}$$
$$-\frac{\mu_0}{\mu_\odot} \beta_S^\star \boldsymbol{\nabla} \times \boldsymbol{G}(\mathbf{r}, \mathbf{r}_S, \omega) \times \overleftarrow{\boldsymbol{\nabla}}_S \cdot \boldsymbol{\nabla}_S \times \boldsymbol{G}(\mathbf{r}_S, \mathbf{r}', \omega) \times \overleftarrow{\boldsymbol{\nabla}}'\big|_{\mathbf{r}'=\mathbf{r}}$$
$$+\frac{\varepsilon_\odot}{\varepsilon_0} \alpha_S^\star \frac{\omega^2}{c^2} \boldsymbol{\nabla} \times \boldsymbol{G}(\mathbf{r}, \mathbf{r}_S, \omega) \cdot \boldsymbol{G}(\mathbf{r}_S, \mathbf{r}', \omega) \times \overleftarrow{\boldsymbol{\nabla}}'\big|_{\mathbf{r}'=\mathbf{r}}. \tag{3.81}$$

CP potential

Using our general results for the electric Green tensor $\boldsymbol{G}_S^{(1)}$ and the magnetic Green tensor $\boldsymbol{\nabla} \times \boldsymbol{G}_S^{(1)} \times \overleftarrow{\boldsymbol{\nabla}}'$ in the presence of a small magnetodielectric sphere, we can now evaluate the CP potential of a polarizable and magnetizable ground-state atom with such a sphere in an arbitrary environment. To apply the proposed decompositions

(3.71) and (3.81) of the Green tensor we have assumed that the cavity radius is small compared to the characteristic wavelength of the medium environment. Now, if an atom is placed in the system we recall the condition (3.55). Substituting Eq. (3.71) into Eq. (2.53) gives the interaction of an electric atom with a magnetodielectric sphere,

$$U_e(\mathbf{r}_A, \mathbf{r}_S) = U_{ee}(\mathbf{r}_A, \mathbf{r}_S) + U_{em}(\mathbf{r}_A, \mathbf{r}_S), \qquad (3.82)$$

where

$$U_{ee}(\mathbf{r}_A, \mathbf{r}_S) = -\frac{\hbar\mu_0^2}{2\pi} \int_0^\infty \mathrm{d}\xi\, \xi^4 \alpha_A \left(\frac{3\varepsilon_A}{2\varepsilon_A + 1}\right)^2 \alpha_S^\star \varepsilon_\odot \mathrm{tr}\big[\boldsymbol{G}(\mathbf{r}_A, \mathbf{r}_S, i\xi) \cdot \boldsymbol{G}(\mathbf{r}_S, \mathbf{r}_A, i\xi)\big] \qquad (3.83)$$

and

$$U_{em}(\mathbf{r}_A, \mathbf{r}_S) = -\frac{\hbar\mu_0^2}{2\pi} \int_0^\infty \mathrm{d}\xi\, \xi^2 \alpha_A \left(\frac{3\varepsilon_A}{2\varepsilon_A + 1}\right)^2 \frac{\beta_S^\star}{\mu_\odot}$$
$$\times \mathrm{tr}\left[\boldsymbol{G}(\mathbf{r}_A, \mathbf{r}_S, i\xi) \times \overleftarrow{\boldsymbol{\nabla}}_S \cdot \boldsymbol{\nabla}_S \times \boldsymbol{G}(\mathbf{r}_S, \mathbf{r}_A, i\xi)\right] \quad (3.84)$$

are associated with the electric and magnetic properties of the sphere, respectively. Similarly, combining Eqs. (3.81) and (2.63) gives the CP interaction of a magnetic atom and a magnetodielectric sphere,

$$U_m(\mathbf{r}_A, \mathbf{r}_S) = U_{me}(\mathbf{r}_A, \mathbf{r}_S) + U_{mm}(\mathbf{r}_A, \mathbf{r}_S), \qquad (3.85)$$

with

$$U_{me}(\mathbf{r}_A, \mathbf{r}_S) = -\frac{\hbar\mu_0^2}{2\pi} \int_0^\infty \mathrm{d}\xi\, \xi^2 \beta_A \left(\frac{3}{2\mu_A + 1}\right)^2 \alpha_S^\star \varepsilon_\odot$$
$$\times \mathrm{tr}\left\{\left[\boldsymbol{\nabla}_A \times \boldsymbol{G}(\mathbf{r}_A, \mathbf{r}_S, i\xi)\right] \cdot \left[\boldsymbol{G}(\mathbf{r}_S, \mathbf{r}_A, i\xi) \times \overleftarrow{\boldsymbol{\nabla}}_A\right]\right\} \quad (3.86)$$

and

$$U_{mm}(\mathbf{r}_A, \mathbf{r}_S) = -\frac{\hbar\mu_0^2}{2\pi} \int_0^\infty \mathrm{d}\xi\, \beta_A \left(\frac{3}{2\mu_A + 1}\right)^2 \frac{\beta_S^\star}{\mu_\odot}$$
$$\times \mathrm{tr}\left\{\left[\boldsymbol{\nabla}_A \times \boldsymbol{G}(\mathbf{r}_A, \mathbf{r}_S, i\xi) \times \overleftarrow{\boldsymbol{\nabla}}_S\right] \cdot \left[\boldsymbol{\nabla}_S \times \boldsymbol{G}(\mathbf{r}_S, \mathbf{r}_A, i\xi) \times \overleftarrow{\boldsymbol{\nabla}}_A\right]\right\}. \quad (3.87)$$

Let us make two remarks on the results (3.82)–(3.87). Firstly, as can already be seen in the decomposition of the Green tensor, the electric and magnetic properties of the

sphere completely decouple and give rise to the separate potentials U_{ee}, U_{me} and U_{em}, U_{mm}. This is only true in the limit of small spheres. Secondly, the total atom–sphere CP potential is duality-invariant by construction,

$$U(\mathbf{r}_A, \mathbf{r}_S) = U_{ee}(\mathbf{r}_A, \mathbf{r}_S) + U_{em}(\mathbf{r}_A, \mathbf{r}_S) + U_{me}(\mathbf{r}_A, \mathbf{r}_S) + U_{mm}(\mathbf{r}_A, \mathbf{r}_S) = U^{\circledast}(\mathbf{r}_A, \mathbf{r}_S). \tag{3.88}$$

In particular note that the duality invariance is ensured by the presence of the factors $\varepsilon_{\odot}$ and $1/\mu_{\odot}$ in the potentials.

It is instructive to compare our findings with the vdW interaction between two magnetoelectric ground-state atoms A and B in the presence of an arbitrary magnetodielectric environment. The vdW interaction between two (isotropic) polarizable ground-state atoms in free-space can be obtained from fourth-order perturbation theory [155] To account for a medium-environment of the atoms, two local-field factors are to be introduced [AS1],

$$U_{ee}^{\mathrm{vdW}}(\mathbf{r}_A, \mathbf{r}_B) = -\frac{\hbar\mu_0^2}{2\pi}\int_0^\infty \mathrm{d}\xi \xi^4 \alpha_A \alpha_B \left(\frac{3\varepsilon_A}{2\varepsilon_A+1}\right)^2 \left(\frac{3\varepsilon_B}{2\varepsilon_B+1}\right)^2$$
$$\times \mathrm{tr}\Big[\boldsymbol{G}(\mathbf{r}_A,\mathbf{r}_B,i\xi)\cdot \boldsymbol{G}(\mathbf{r}_B,\mathbf{r}_A,i\xi)\Big]. \tag{3.89}$$

The respective potential between two magnetizable atoms can be obtained by applying the transformation (2.56) and (2.61),

$$U_{mm}^{\mathrm{vdW}}(\mathbf{r}_A, \mathbf{r}_B) = -\frac{\hbar\mu_0^2}{2\pi}\int_0^\infty \mathrm{d}\xi \beta_A \beta_B \left(\frac{3}{2\mu_A+1}\right)^2 \left(\frac{3}{2\mu_B+1}\right)^2$$
$$\times \mathrm{tr}\Big\{\big[\boldsymbol{\nabla}_A \times \boldsymbol{G}(\mathbf{r}_A,\mathbf{r}_B,i\xi)\times \overset{\leftarrow}{\boldsymbol{\nabla}}_B\big]\cdot \big[\boldsymbol{\nabla}_B \times \boldsymbol{G}(\mathbf{r}_B,\mathbf{r}_A,i\xi)\times \overset{\leftarrow}{\boldsymbol{\nabla}}_A\big]\Big\}. \tag{3.90}$$

If only one of the atoms (say B) is magnetizable the vdW potential reads [140]

$$U_{em}^{\mathrm{vdW}}(\mathbf{r}_A, \mathbf{r}_B) = -\frac{\hbar\mu_0^2}{2\pi}\int_0^\infty \mathrm{d}\xi \xi^2 \alpha_A \beta_B \left(\frac{3\varepsilon_A}{2\varepsilon_A+1}\right)^2 \left(\frac{3}{2\mu_B+1}\right)^2$$
$$\times \mathrm{tr}\Big\{\big[\boldsymbol{G}(\mathbf{r}_A,\mathbf{r}_B,i\xi)\times \overset{\leftarrow}{\boldsymbol{\nabla}}_B\big]\cdot \big[\boldsymbol{\nabla}_B \times \boldsymbol{G}(\mathbf{r}_B,\mathbf{r}_A,i\xi)\big]\Big\}, \tag{3.91}$$

where the opposite case of atom A being magnetizable, U_{me}^{vdW}, can be easily obtained by interchanging A and B in Eq. (3.91). Clearly, the full vdW interaction of two atoms is given by summation of U_{ee}^{vdW}, U_{mm}^{vdW}, U_{em}^{vdW}, and U_{me}^{vdW}. In order to connect

our results to the vdW potentials, one has to perform the substitutions

$$\alpha_S^\star \varepsilon_\odot \mapsto \alpha_B \Big(\frac{3\varepsilon_B}{2\varepsilon_B + 1}\Big)^2 \tag{3.92}$$

$$\frac{\beta_S^\star}{\mu_\odot} \mapsto \beta_B \Big(\frac{3}{2\mu_B + 1}\Big)^2. \tag{3.93}$$

The atom–atom and the atom–sphere potentials look very similar, and in particular lead to the same power laws in the nonretarded and retarded regime. This can be understood from the fact that the magnetodielectric response of point-like objects, such as the isotropic atom and the small sphere, enters only via the respective polarizability and magnetizability. Note that a (frequency-dependent) correction factor accounting for the surrounding medium does not change the power laws. For example, if the atom and the sphere are purely electric and embedded in free space, we immediately expect the familiar $|\mathbf{r}_A - \mathbf{r}_S|^{-6}$ power law to hold in the nonretarded regime and $|\mathbf{r}_A - \mathbf{r}_S|^{-7}$ in the retarded regime [7]. The difference between the case of a sphere as given in the left-hand sides of Eqs. (3.92) and (3.93), and an atom, given by the corresponding right-hand sides, are due to the different natures, macroscopic versus microscopic, of the two objects. The sphere and the background medium consist of a large number of atoms and can therefore be described macroscopically, by (separate) average permittivity and permeability functions. The sphere is in immediate contact with the surrounding medium, which leads to the factors $\varepsilon_\odot$ and $1/\mu_\odot$. Note that the polarizability (3.72) and magnetizability (3.73) of the sphere depend on the difference $\varepsilon_S - \varepsilon_\odot$ and $\mu_S - \mu_\odot$, respectively, and can be either positive or negative. In contrast, the polarizability and magnetizability of an atom depends on the transition frequencies and dipole matrix elements, as given by Eqs. (2.54) and (2.62). They are strictly positive on the positive imaginary frequency axis. Since an atom is a microscopic object, the interspace between the atom and the neighboring medium atoms needs to be taken into account. This gives rise to the local-field correction factors $[3\varepsilon_B/(2\varepsilon_B + 1)]^2$ and $[3/(2\mu_B + 1)]^2$ on the right-hand sides of Eqs. (3.92) and (3.93).

3.3.2 Sphere inside an Onsager cavity.

In the following we compare and interpolate between the homogeneous sphere placed inside a medium and a local-field corrected atom.

Decomposition of the Green tensor

To that end, we consider a homogeneous magnetodielectric sphere with radius R centered around $\mathbf{r}_S$, with permittivity $\varepsilon_S(\omega)$ and permeability $\mu_S(\omega)$, which is not in immediate contact with the surrounding medium, but placed inside a small spherical cavity of radius R_C, also centered around $\mathbf{r}_S$. The cavity implements the interspace between the atoms contained in the sphere and the surrounding medium atoms. We again study the limit of small cavity/sphere radii and assume $|k_S R|, |k R_C|, |k_0 R_C| \ll 1$ where $k_0 = \omega/c$. The situation is sketched in Fig. 3.6 (iii).

The scattering Green tensor $\mathbf{G}^{(1)}_{S+C}$ of the sphere–cavity system in a homogeneous bulk medium is again given by an equation of the form (3.52), where the reflection coefficients now take a more complex form [151]. The required $l = 1$ terms are given by

$$B_1^M = \frac{2i}{3}\left(\sqrt{\varepsilon\mu}\,\frac{\omega}{c}\right)^3\left[R_C^3\,\frac{1-\mu}{1+2\mu} + \frac{9\mu R^3(\mu_S-1)/(2\mu+1)}{(\mu_S+2)(2\mu+1) + 2(\mu_S-1)(1-\mu)R^3/R_C^3}\right],$$

$$(3.94)$$

$$B_1^N = \frac{2i}{3}\left(\sqrt{\varepsilon\mu}\,\frac{\omega}{c}\right)^3\left[R_C^3\,\frac{1-\varepsilon}{1+2\varepsilon} + \frac{9\varepsilon R^3(\varepsilon_S-1)/(2\varepsilon+1)}{(\varepsilon_S+2)(2\varepsilon+1) + 2(\varepsilon_S-1)(1-\varepsilon)R^3/R_C^3}\right] \quad (3.95)$$

in the small-sphere/cavity limit. We can then follow exactly the same steps as in Sec. 3.3.1. We again arrive at Eqs. (3.71) and (3.81) with $\alpha^\star_{S+C}$, $\beta^\star_{S+C}$ in place of $\alpha^\star_S$, $\beta^\star_S$. A comparison of Eqs. (3.61) and (3.62) with Eqs. (3.94) and (3.95) shows that the relevant excess polarizability and magnetizability of the sphere–cavity system read

$$\alpha^\star_{S+C} = 4\pi\varepsilon_0\left[R_C^3\,\frac{1-\varepsilon_\odot}{1+2\varepsilon_\odot} + \frac{9\varepsilon_\odot R^3(\varepsilon_S-1)/(2\varepsilon_\odot+1)}{(\varepsilon_S+2)(2\varepsilon_\odot+1) + 2(\varepsilon_S-1)(1-\varepsilon_\odot)R^3/R_C^3}\right] \quad (3.96)$$

and

$$\beta^\star_{S+C} = \frac{4\pi}{\mu_0}\left[R_C^3\,\frac{1-\mu_\odot}{1+2\mu_\odot} + \frac{9\mu_\odot R^3(\mu_S-1)/(2\mu_\odot+1)}{(\mu_S+2)(2\mu_\odot+1) + 2(\mu_S-1)(1-\mu_\odot)R^3/R_C^3}\right], \quad (3.97)$$

respectively. By introducing the free-space polarizability and magnetizability of the sphere

$$\alpha_S = 4\pi\varepsilon_0 R^3\,\frac{\varepsilon_S - 1}{\varepsilon_S + 2} \quad (3.98)$$

and

$$\beta_S = \frac{4\pi R^3}{\mu_0} \frac{\mu_S - 1}{\mu_S + 2}, \tag{3.99}$$

respectively, as well as the excess polarizability and magnetizability of the cavity

$$\alpha_C^\star = 4\pi\varepsilon_0 R_C^3 \frac{1 - \varepsilon_\odot}{1 + 2\varepsilon_\odot} \tag{3.100}$$

and

$$\beta_C^\star = \frac{4\pi R_C^3}{\mu_0} \frac{1 - \mu_\odot}{1 + 2\mu_\odot}, \tag{3.101}$$

respectively, we can rewrite Eqs. (3.96) and (3.97) more transparently as

$$\alpha_{S+C}^\star = \alpha_C^\star + \frac{\alpha_S}{\varepsilon_\odot} \left(\frac{3\varepsilon_\odot}{2\varepsilon_\odot + 1}\right)^2 \frac{1}{1 + \alpha_C^\star \alpha_S/(8\pi^2\varepsilon_0^2 R_C^6)}, \tag{3.102}$$

$$\beta_{S+C}^\star = \beta_C^\star + \beta_S\mu_\odot \left(\frac{3}{2\mu_\odot + 1}\right)^2 \frac{1}{1 + \beta_C^\star \beta_S\mu_0^2/(8\pi^2 R_C^6)}. \tag{3.103}$$

Equation (3.102) shows that the response of the sphere–cavity system to an electromagnetic field is due to reflection at the cavity surface from the outside given by $\alpha_C^\star, \beta_C^\star$, plus reflections at the sphere given by $\alpha_S^\star, \beta_S^\star$. The local-field correction factors in large parentheses account for the transmission of the field into and out of the cavity and the denominators account for multiple reflections between the cavity and sphere surfaces. Note that in the leading-order approximation made (with respect to the sphere and cavity radii), the factors accounting for reflections at the sphere [Eqs. (3.72), (3.73)] and cavity surface [Eqs. (3.100), (3.101)] are proportional to the third power of these radii, while the transmission properties of the cavity as described by the local-field correction factors become independent of R_C. Our equation (3.102) determines the correct polarizability/magnetizability of a small medium-embedded spherical object.

Casimir–Polder potential

In order to interpolate between the two extreme cases of a single atom and a sphere consisting of a very large number of atoms, we now consider the CP interaction of an atom with the sphere-cavity system and assume $\sqrt{\varepsilon_\odot\mu_\odot}R_C \ll |\mathbf{r}_A - \mathbf{r}_S|$ in addition to the condition (3.55). Since expressions of the type (3.71) and (3.81) remain valid, their substitution into Eqs. (2.53) and (2.63) again leads to Eqs. (3.82)–(3.87), where

now $\alpha^\star_{S+C}$ and $\beta^\star_{S+C}$ as given by Eqs. (3.96) and (3.97) appear in place of $\alpha^\star_S$ and $\beta^\star_S$.

As an example, let us consider the CP interaction of a nonmagnetic atom with a purely electric sphere of radius $R > 0$ in a bulk medium ($\varepsilon_\odot = \varepsilon_A = \varepsilon$). Substituting the required bulk Green tensor (3.66) into Eq. (3.83), one finds

$$U_{ee}(\mathbf{r}_A, \mathbf{r}_S) = -\frac{\hbar}{16\pi^3 \varepsilon_0^2 r_{AS}^6} \int_0^\infty \mathrm{d}\xi \left(\frac{3\varepsilon}{2\varepsilon + 1}\right)^2 \alpha_A \varepsilon \alpha^\star_{S+C} g\left(\sqrt{\varepsilon}\,\xi\,r_{AS}/c\right), \quad (3.104)$$

with $r_{AS} = |\mathbf{r}_A - \mathbf{r}_S|$ and

$$g(x) = e^{-2x}(3 + 6x + 5x^2 + 2x^3 + x^4). \quad (3.105)$$

Figure 3.9 shows the potential U_{ee} for a two-level atom as a function of the ratio $q = R/R_C$ for various atom–sphere separations while Fig. 3.10 shows the potential U_{ee} as a function of the atom-sphere separation for different (fixed) relative sphere radii q. We have used single-resonance models for the permittivities of the sphere
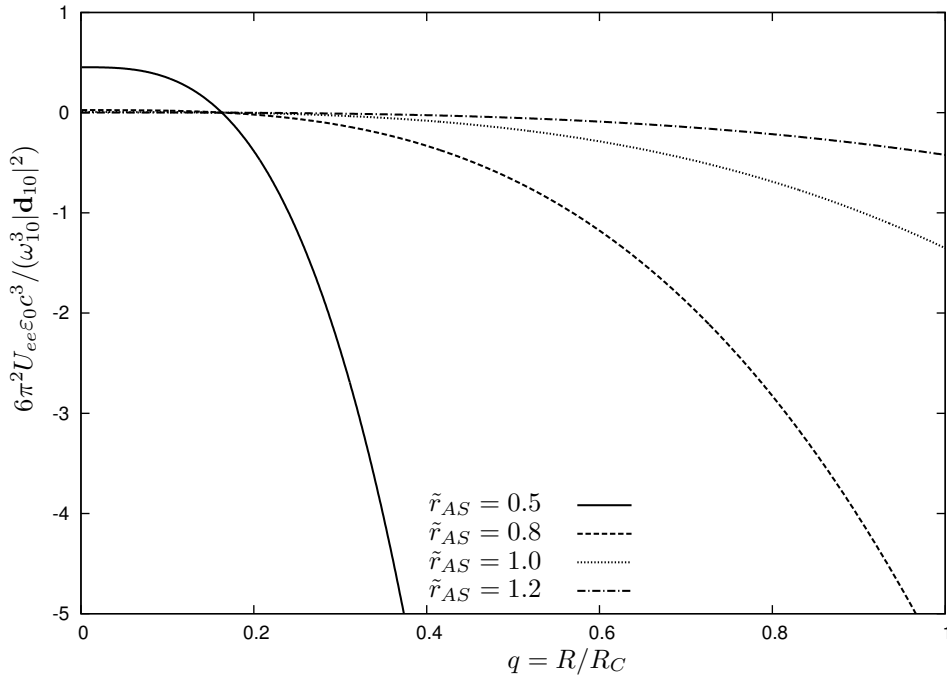
Figure 3.9: CP potential U_{ee} of a nonmagnetic atom in front of a dielectric sphere in an empty cavity embedded in bulk material vs. $q = R/R_C$. The curves correspond to different atom–sphere separations $\tilde{r}_{AS} \equiv r_{AS}\omega_{10}/c$. Other parameters are $\omega_T/\omega_{10} = 1.03$, $\omega_{TS}/\omega_{10} = 1.0$, $\omega_{PS}/\omega_{10} = 1.2$, $\omega_P/\omega_{10} = 0.75$, $\gamma_{(S)}/\omega_{10} = 0.001$.

and the medium as given in Eq. (3.47). Both figures reveal that for the constant ε_S

considered here, larger spheres lead to a stronger CP attraction between the atom and the sphere. As can be seen in Fig. 3.9, all curves cross at a particular value of the relative sphere radius, indicating the critical ratio where the sign of the interaction is turned into repulsion, i.e., for $q \lesssim 0.16$.
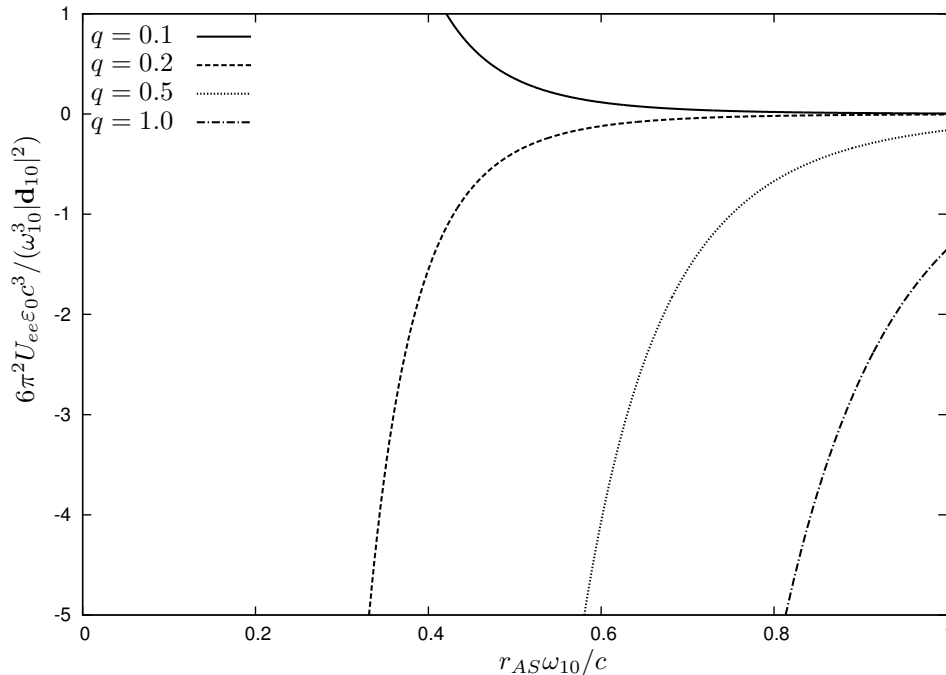
Figure 3.10: U_{ee} vs. $r_{AS}\omega_{10}/c$ for different ratios q. Other parameters are the same as in Fig. 3.9.

Apart from the polarizability $\alpha^{\star}_{S+C}$, all quantities appearing in the integrand of Eq. (3.104) are monotonic functions in ξ. Thus, on recalling Eq. (3.102), the polarizability of the sphere gives rise to attractive forces while the cavity leads to a reduction of these forces. On calculating the zeros of $\alpha^{\star}_{S+C}$, we find the frequency-dependent critical ratio of the two radii, R/R_C,

$$q_{\mathrm{crit}} \equiv \left(\frac{R}{R_C}\right)_{\mathrm{crit}} = \sqrt[3]{\frac{(2+\varepsilon_{\odot})(\varepsilon_{\odot}-1)(1+2\varepsilon_{\odot})}{9\varepsilon_{\odot}(\varepsilon_S-1)+2(\varepsilon_{\odot}-1)^2(\varepsilon_S-1)}}. \qquad (3.106)$$

In practice, one could estimate the critical ratio by evaluating Eq. (3.106) for static medium response, or if available, by using an effective frequency to evaluate the medium response. The unexpected repulsion for a purely electric system can be explained from the fact that the sphere–cavity system contains only little polarizable matter, but the volume is the same as in the full sphere situation, i.e., it displaces the medium and gives rise to a bouyancy-type force opposite to the CP interac-

tion/force. Such effects are known from the field of ionic dispersion forces as discussed in Ref. [156]. For example, when a molecule is embedded in bulk water, a layer of water atoms (hydration layer) encloses the molecule and has a permittivity distinct from the surrounding water. One can think of the hydration layer as being part of the cavity. In particular, it has been shown that the volume of the hydration layer is impenetrable to many ions and short-range repulsion may occur [156].

In the following, we show how the two extreme cases of a full sphere and an atom can be recovered from Eqs. (3.102) and (3.103). For a macroscopic sphere, the interspace between the sphere and medium atoms becomes irrelevant as implemented by $R \to R_C$. In this case, it is almost trivial to verify that, for $R = R_C$, Eqs. (3.96) and (3.97) reduce to the results (3.72) and (3.73) for the full sphere. We thus recover Eqs. (3.82)–(3.87) in their original form. The opposite limit of a single atom can be obtained as follows. If the sphere consists of only very few atoms or a single atom, the interspace becomes very large in comparison to the sphere, $R \ll R_C$. Note that the single-atom result cannot be obtained by simply setting $R = 0$ in the response functions since this case corresponds to an empty cavity and not to a single atom with finite polarizability. What we can do is to neglect the effect of multiple scattering between the surfaces of sphere and cavity for sufficiently small R ($R \ll R_C$). In this case, the polarizability (3.102) and magnetizability (3.103) reduce to

$$\alpha^{\star}_{S+C} = \alpha^{\star}_C + \frac{\alpha_S}{\varepsilon_\odot} \left(\frac{3\varepsilon_\odot}{2\varepsilon_\odot + 1} \right)^2, \tag{3.107}$$

$$\beta^{\star}_{S+C} = \beta^{\star}_C + \beta_S \mu_\odot \left(\frac{3}{2\mu_\odot + 1} \right)^2. \tag{3.108}$$

Furthermore, if the sphere consists of a single atom (say B) only, the Clausius–Mossotti laws [157]

$$\frac{\varepsilon_S - 1}{\varepsilon_S + 2} = \frac{\alpha_B}{3\varepsilon_0 V}, \qquad \frac{\mu_S - 1}{\mu_S + 2} = \frac{\mu_0 \beta_B}{3V}, \tag{3.109}$$

where $V = (4\pi/3)R^3$ denotes the volume of the sphere, together with Eqs. (3.98) and (3.99), show that $\alpha_S = \alpha_B$ and $\beta_S = \beta_B$.

So far we have considered an atom in a cavity interacting with a second atom. To make contact with the real-cavity model of the local-field corrected atom, we have to consider a sufficiently small cavity radius R_C, such that multiple scattering at the

outer surface of the cavity can be neglected. In this case, we obtain

$$\alpha^\star_{S+C}\varepsilon_\odot = \alpha_B \left(\frac{3\varepsilon_B}{2\varepsilon_B + 1}\right)^2 , \tag{3.110}$$

$$\frac{\beta^\star_{S+C}}{\mu_\odot} = \beta_B \left(\frac{3}{2\mu_B + 1}\right)^2 , \tag{3.111}$$

where the notation $\varepsilon_\odot = \varepsilon_B$, $\mu_\odot = \mu_B$ has been introduced in accordance with Sec. 3.1. Substituting these polarizabilities into Eqs. (3.82)–(3.87) leads to the local-field corrected two-atom potentials (3.89), (3.84), (3.90), as expected. For intermediate radii, our model provides a formula for the polarizability of the medium-embedded sphere where the correct amount of local-field correction is automatically included.

4 Dispersion forces on excited systems

So far we have considered ground-state dispersion forces which can be expressed as an integral over the full imaginary frequency axis. Excited systems allow for a more flexible manipulation of dispersion forces because they depend on the medium properties in a narrow frequency region. By suitably choosing the medium properties in this frequency window, one can probe effects of left-handed metamaterials (LHM) or realize repulsive dispersion forces.

In this chapter we investigate two configurations: Firstly, in Sec. 4.1, we will study the CP potential and the spontaneous decay of an excited atom in a planar magnetoelectric metamaterial system and secondly, in Sec. 4.2, we consider the Casimir force on a system of magnetoelectric bodies that is amplifying in a limited space and frequency regime. Note that in this chapter we explicitly allow also for metallic bodies and use the term magnetoelectric instead of magnetodielectric (as used in Chap. 3).

4.1 Resonant Casimir–Polder potential of an excited atom

In the following, we briefly investigate the CP potential of an excited atom in front of a magnetoelectric metamaterial half space, as based on Ref. [AS3]. In Sec. 4.1.2, basing on Ref. [AS2], the same atom is placed in a superlens-type geometry consisting of a left-handed slab mounted on a perfect mirror.

4.1.1 Discussion of planar metamaterials

Consider an excited atom prepared in an energy eigenstate $|n\rangle$ with (excited-state) polarizability $\boldsymbol{\alpha}_n$, transition frequencies ω_{nk} and electric-dipole transition matrix elements $\mathbf{d}_{nk}$. The atom is placed in a free-space region in front of a magnetoelectric

half space of permittivity $\varepsilon(\omega)$ and permeability $\mu(\omega)$ at distance $z_A \geq 0$ from the interface, where the coordinate system is chosen in the same way as in Sec. 3.2. Rewriting Eqs. (3.12) and (3.15) for real frequencies gives the required Green tensor in the form [AS2]

$$\boldsymbol{G}^{(1)}(z_A, z_A, \omega_{nk}) = \frac{i}{8\pi} \int_0^\infty \mathrm{d}k^\| \frac{k^\|}{k^\perp} e^{2ik^\perp z_A}$$
$$\times \left[\left(r_{21}^s - \frac{k^{\perp 2}c^2}{\omega^2} r_{21}^p \right) (\mathbf{e}_x\mathbf{e}_x + \mathbf{e}_y\mathbf{e}_y) + 2 \frac{k^{\|2}c^2}{\omega_{nk}^2} r_{21}^p \mathbf{e}_z\mathbf{e}_z \right], \quad (4.1)$$

with $\varepsilon \equiv \varepsilon(\omega_{nk})$, $\mu \equiv \mu(\omega_{nk})$ and the reflection coefficients being given by Eq. (3.13) with $\kappa_j^\perp \mapsto k_j^\perp$, where

$$k_j^\perp(\omega) = \sqrt{\varepsilon_j(\omega)\mu_j(\omega)\frac{\omega^2}{c^2} - k^{\|2}} \qquad (4.2)$$

again denotes the wave vector perpendicular to the interface. For convenience, we write $k^\perp \equiv k_2^\perp$ with $\varepsilon_2 = 1$, $\mu_2 = 1$. Let us first briefly discuss the sign of the square root of $k_1^{\perp 2}$ for passive metamaterials with

$$\mathrm{Im}\, k_1^{\perp 2} = \frac{\omega^2}{c^2} \big(\mathrm{Re}\,\varepsilon_1 \mathrm{Im}\,\mu_1 + \mathrm{Im}\,\varepsilon_1 \mathrm{Re}\,\mu_1 \big) < 0. \qquad (4.3)$$

Such materials include ordinary materials as well as left-handed metamaterials with $\mathrm{Re}\,\varepsilon_1(\omega) < 0$ and $\mathrm{Re}\,\mu_1(\omega) < 0$ in the same frequency regime. Waves inside an absorbing medium should decay, i.e. we require $\mathrm{Im}\, k_1^\perp > 0$. This implies that $k_1^\perp$ lies in the second quadrant of the complex plane with the branch cut being along the positive real axis. See also the remarks in Sec. 4.1.2.

In the following, we will restrict our attention to the resonant CP potential since it usually dominates the nonresonant contribution if the atom is excited. We write Eq. (2.55) in the form

$$U_n(z_A)(\mathbf{r}_A) = -\mu_0 \sum_{k<n} \omega_{nk}^2 \left(\mathrm{Re}\, G_{xx}^{(1)}(z_A, z_A, \omega_{nk})|\mathbf{d}_{nk}^\||^2 + \mathrm{Re}\, G_{zz}^{(1)}(\mathbf{r}_A, \mathbf{r}_A, \omega_{nk})|\mathbf{d}_{nk}^\perp|^2 \right),$$
$$(4.4)$$

with the Green tensor being given by Eq. (4.1) and the atomic dipole moment being decomposed as $\mathbf{d}_{nk}^\| = ((d_{nk})_x, (d_{nk})_y, 0)$ and $\mathbf{d}_{nk}^\perp = (0, 0, (d_{nk})_z)$. We again study the limits of short and long atom–surface separations. In the nonretarded regime where $z_A\omega_{nk}/c \ll 1$, we approximate $k^\perp \simeq k_1^\perp \simeq ik^\|$, in which case the reflection coefficients

become independent of $k_j^\perp$,

$$r_{21}^s = \frac{\mu - 1}{\mu + 1}, \quad r_{21}^p = \frac{\varepsilon - 1}{\varepsilon + 1}. \tag{4.5}$$

Carrying out the integral in (4.1) gives, to leading order in $1/z_A$,

$$U_n(z_A) = -\sum_{k<n} \frac{|\mathbf{d}_{nk}^\parallel|^2 + 2|\mathbf{d}_{nk}^\perp|^2}{32\pi\varepsilon_0 z_A^3} \frac{|\varepsilon(\omega_{nk})|^2 - 1}{|\varepsilon(\omega_{nk}) + 1|^2} \tag{4.6}$$

unless the half space is purely magnetic, in which case the leading-order potential reads

$$U_n(z_A) = -\sum_{k<n} \frac{\mu_0 \omega_{nk}^2 |\mathbf{d}_{nk}^\parallel|^2}{16\pi z_A} \frac{|\mu(\omega_{nk})|^2 - 1}{|\mu(\omega_{nk}) + 1|^2}. \tag{4.7}$$

To obtain the full nonretarded CP potentials, Eqs. (4.6) and (4.7) should be accompanied by their nonresonant counterparts as given in Eqs. (3.24)–(3.26) with $\varepsilon_2(i\xi) = \mu_2(i\xi) = 1$ and $\alpha \mapsto 1/4(\alpha_{xx} + \alpha_{yy}) + 1/2\alpha_{zz}$ to account for a possible anisotropy of the atoms. Note that in the case of excited atoms the nonresonant interaction contains attractive as well as repulsive contributions arising from upward and downward atomic transitions, respectively. The potentials (4.6) and (4.7) reveal that close to the surface, the resonant CP potential is attractive for $|\varepsilon(\omega_{nk})| > 1$ but repulsive for metamaterials with $|\varepsilon(\omega_{nk})| < 1$. In the case of a purely magnetic metamaterial we find attraction for $|\mu(\omega_{nk})| < 1$ and repulsion for $|\mu(\omega_{nk})| > 1$. In particular, for weakly absorbing materials, the denominators get close to zero at the surface plasmon resonances where $\varepsilon(\omega_{nk}) = \mu(\omega_{nk}) \simeq -1$, leading to a strong enhancement of the associated potentials.

In the retarded regime, $z_A\omega_{nk}/c \gg 1$, the main contribution to the integral in Eq. (4.1) is due to the stationary-phase point $k^\parallel = 0$, where the reflection coefficients are approximated by

$$r_s = -r_p = \frac{\sqrt{\mu(\omega_{nk})} - \sqrt{\varepsilon(\omega_{nk})}}{\sqrt{\mu(\omega_{nk})} + \sqrt{\varepsilon(\omega_{nk})}}, \tag{4.8}$$

where the square roots $\sqrt{\mu}$ and $\sqrt{\varepsilon}$ have to be chosen such that their imaginary part is positive. After substituting Eq. (4.8) into Eq. (4.1), the integral can be carried out. Keeping only the leading order in $c/(z_A\omega_{nk})$, the retarded CP potential (4.4) takes

the form

$$U_n(z_A) = \sum_{k<n} \frac{\mu_0 \omega_{nk}^2 |\mathbf{d}_{nk}^{\parallel}|^2}{8\pi z_A} \text{Re} \left\{ e^{2iz_A\omega_{nk}/c} \frac{\sqrt{\varepsilon(\omega_{nk})} - \sqrt{\mu(\omega_{nk})}}{\sqrt{\varepsilon(\omega_{nk})} + \sqrt{\mu(\omega_{nk})}} \right\}. \qquad (4.9)$$

It can be seen that only dipole moments parallel to the surface contribute to the oscillating term in Eq. (4.9), which is due to the transverse character of the waves emitted by the atom. For a strongly electric half space we have $r_p \simeq 1$ and the potential (4.9) can be approximated by

$$U_n(z_A) = \sum_{k<n} \frac{\mu_0 \omega_{nk}^2 |\mathbf{d}_{nk}^{\parallel}|^2}{8\pi z_A} \cos(2z_A\omega_{nk}/c), \qquad (4.10)$$

which is dominated by an oscillating term of decreasing amplitude and period $\pi c/\omega_{nk}$. In contrast, for a strongly magnetic half space, the potential has the same absolute value but carries opposite sign compared to the electric case (4.10). Note that the corresponding nonresonant term (3.30) together with Eq. (3.31) is neglible due its inverse power law of $1/z_A^4$.

In Fig. 4.1 we have considered a magnetoelectric half space with different signs for $\text{Re}\,\varepsilon$ and $\text{Re}\,\mu$. The strongest oscillations are seen in the case of a metamaterial with $\text{Re}\,\varepsilon > 0$ and $\text{Re}\,\mu < 0$ such that a repulsive barrier close to the surface forms. The oscillation amplitude is very weak for a left-handed material or an ordinary one with $\text{Re}\,\varepsilon, \text{Re}\,\mu > 0$. This is due to the vanishing of the reflection coefficients (4.8) for the chosen $\text{Re}\,\varepsilon = \text{Re}\,\mu$. Note that the short-range attraction is governed by the electric medium properties.

4.1.2 Perfect lens geometry

Related to the discussion in Sec. 4.1.1, we discuss the correct choice of the refractive index n. To this end, consider Fig. 4.2. From the requirement $\text{Re}\,\varepsilon < 0$ and $\text{Re}\,\mu < 0$ for a left-handed (absorbing) material, it immediately follows that also the square of the refractive index $n^2 = \varepsilon\mu$ lies in the fourth quadrant. From the two possible choices for n (lying in the second and fourth quadrant), one has to chose the one with the positive imaginary part to account for absorption. Thus, n must lie in the second quadrant where $\text{Re}\,n < 0$.

A left-handed material refracts incident light to negative angles across the plane of incidence [82]. As was pointed out more than 10 years ago, a lossless slab of thickness
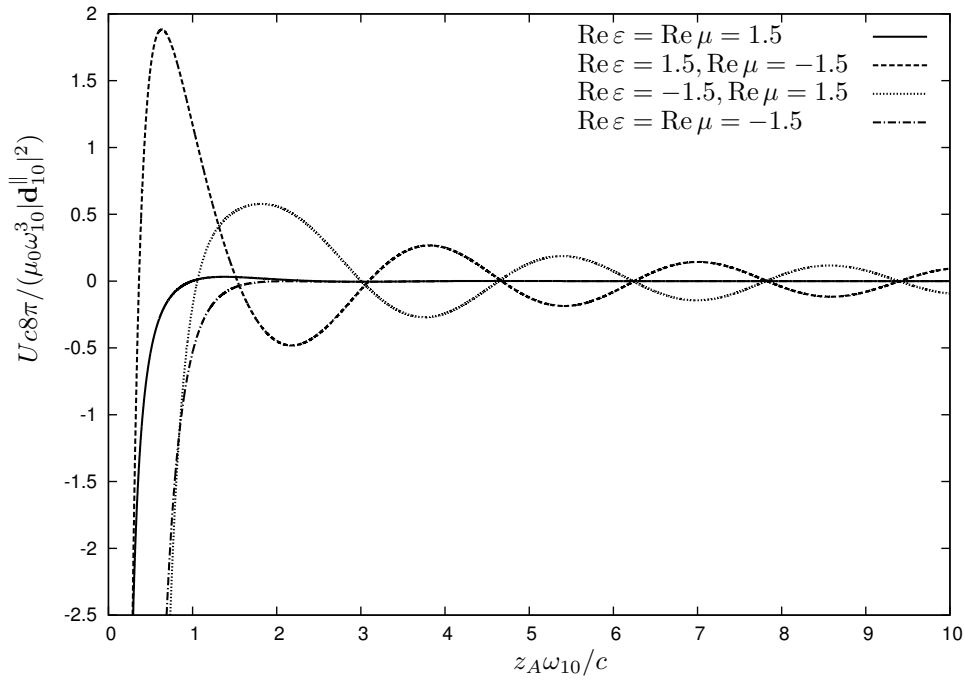
Figure 4.1: Resonant CP potential of a two-level atom in front of a weakly absorbing (Imϵ = Imμ = 10^{-3}) magnetoelectric metamaterial half space. The atomic dipole moment is aligned parallel to the surface.
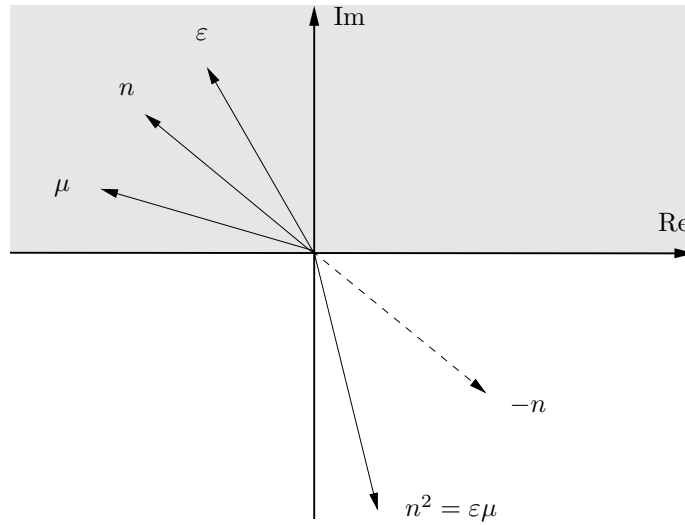
**Figure 4.2:** Refractive index for left-handed (absorbing) materials. The gray region indicates the requirement Im $n > 0$ for absorbing media.

d and unity negative refraction $n = -1$ has the peculiar feature to focus light with perfect resolution, where perfect negative refraction implies that the position of the two focal planes is a distance of $d/2$ away from the surfaces of the LHM slab [74].

The situation is sketched in Fig. 4.3 (a).

Motivated by this superlens configuration, we are interested in studying the CP potential of a single atom in an equivalent geometry. To that end, we place a perfect mirror on the far end of the LHM slab. However, two things should be kept in mind: Firstly, it is not possible to fabricate a metamaterial being left-handed for all frequencies; and secondly, every material is (at least weakly) absorbing. We will only study the resonant force component and put special emphasis to account for material absorption. Our setup as sketched in Fig. 4.3 (b) shows the layers 1,2,3 corresponding to the perfectly conducting mirror, the LHM slab of thickness d and $\varepsilon(\omega) = -1 + i\eta$, $\mu(\omega) = -1 + i\eta$, and the free-space region where the excited two-level atom is placed in, respectively.
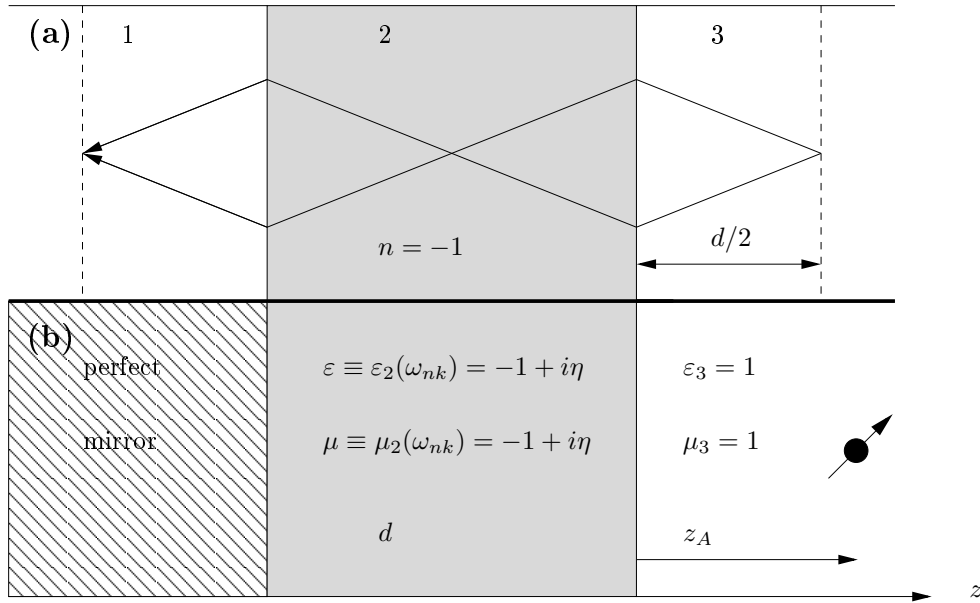
Figure 4.3: Super-lens geometries: a) A lossless LHM slab generates a complete and faithful image of an object placed in one of the focal planes a distance of $d/2$ away from the slab. b) Atom in front of an absorbing LHM slab backed by a perfect mirror.

The scattering part of the associated three-layer Green tensor at the relevant atomic transition frequency and equal positions $\mathbf{r} = \mathbf{r}' = \mathbf{r}_A$ in the free-space region is given by [132]

$$\boldsymbol{G}^{(1)}(z_A, z_A, \omega_{10}) = \frac{i}{8\pi^2} \int \mathrm{d}^2 k^{\|} \frac{1}{k^{\perp}} \sum_{\sigma=s,p} \mathbf{e}_\sigma^+ \mathbf{e}_\sigma^- r_{3-}^\sigma e^{2ik^{\perp} z_A}, \tag{4.11}$$

where the reflection coefficients read

$$r^s_{3-} = \frac{k^\perp \mu - k_2^\perp - e^{2ik_2^\perp d}(k^\perp \mu + k_2^\perp)}{k^\perp \mu + k_2^\perp - e^{2ik_2^\perp d}(k^\perp \mu - k_2^\perp)}, \quad r^p_{3-} = \frac{k^\perp \varepsilon - k_2^\perp - e^{2ik_2^\perp d}(k^\perp \varepsilon + k_2^\perp)}{k^\perp \varepsilon + k_2^\perp - e^{2ik_2^\perp d}(k^\perp \varepsilon - k_2^\perp)}, \quad (4.12)$$

with $k_j^\perp$ according to Eq. (4.2). In Eq. (4.11), we introduce polar coordinates in the $(k_x^\parallel, k_y^\parallel)$-plane,

$$\mathbf{e}_{k\parallel} = \begin{pmatrix} \cos\phi \\ \sin\phi \\ 0 \end{pmatrix}, \quad \mathbf{e}_s^\pm = \begin{pmatrix} \sin\phi \\ -\cos\phi \\ 0 \end{pmatrix}, \quad \mathbf{e}_p^\pm = \begin{pmatrix} \mp k^\perp c \cos\phi/\omega_{10} \\ \mp k^\perp c \sin\phi/\omega_{10} \\ k^\parallel c/\omega_{10} \end{pmatrix}, \quad \mathbf{e}_z = \begin{pmatrix} 0 \\ 0 \\ 1 \end{pmatrix}, \quad (4.13)$$

where $\mathrm{d}^2 k^\parallel = k^\parallel \, \mathrm{d}k^\parallel \, \mathrm{d}\phi$. By using the identities

$$\mathbf{e}_s^+ \mathbf{e}_s^- = \begin{pmatrix} \sin^2\phi & -\sin\phi\cos\phi & 0 \\ -\sin\phi\cos\phi & \cos^2\phi & 0 \\ 0 & 0 & 0 \end{pmatrix} \quad (4.14)$$

and

$$\mathbf{e}_p^+ \mathbf{e}_p^- = \frac{c^2}{\omega_{10}^2} \begin{pmatrix} -k^{\perp 2}\cos^2\phi & -k^{\perp 2}\sin\phi\cos\phi & -k^\parallel k^\perp \cos\phi \\ -k^{\perp 2}\sin\phi\cos\phi & -k^{\perp 2}\sin^2\phi & -k^\parallel k^\perp \cos\phi \\ k^\parallel k^\perp \cos\phi & k^\parallel k^\perp \sin\phi & k^{\parallel 2} \end{pmatrix}, \quad (4.15)$$

we perform the angular integration over the dyadic products,

$$\int_0^{2\pi} \mathrm{d}\phi \, \mathbf{e}_s^+ \mathbf{e}_s^- = \pi \begin{pmatrix} 1 & 0 & 0 \\ 0 & 1 & 0 \\ 0 & 0 & 0 \end{pmatrix}, \quad \int_0^{2\pi} \mathrm{d}\phi \, \mathbf{e}_p^+ \mathbf{e}_p^- = \frac{\pi c^2}{\omega_{10}^2} \begin{pmatrix} -k^{\perp 2} & 0 & 0 \\ 0 & -k^{\perp 2} & 0 \\ 0 & 0 & 2k^{\parallel 2} \end{pmatrix}, \quad (4.16)$$

and obtain for the Green tensor

$$\mathbf{G}^{(1)}(z_A, z_A, \omega_{10}) = \frac{i}{8\pi} \int_0^\infty \mathrm{d}k^\parallel \, \frac{k^\parallel}{k^\perp} \, e^{2ik^\perp z_A}$$
$$\times \begin{pmatrix} r^s_{3-} - \frac{k^{\perp 2}c^2}{\omega_{10}^2} r^p_{3-} & 0 & 0 \\ 0 & r^s_{3-} - \frac{k^{\perp 2}c^2}{\omega_{10}^2} r^p_{3-} & 0 \\ 0 & 0 & \frac{2k^{\parallel 2}c^2}{\omega_{10}^2} r^p_{3-} \end{pmatrix}. \quad (4.17)$$

From Eq. (4.17) it can be seen that an atom with a dipole moment perpendicular

to the surface is coupled to the p-polarized waves only, while an atom with a dipole moment parallel to the surface is coupled to both p- and s-polarized waves. In the following, it will be instructive to express $k^\perp$ in Eq. (4.17) in terms of $k^\parallel$ and decompose the integral into two parts,

$$\int_0^\infty \mathrm{d}k^\parallel \frac{k^\parallel}{k^\perp} e^{2ik^\perp z_A} f(k^\parallel) = \int_0^{\frac{\omega_{10}}{c}} \mathrm{d}k^\perp e^{2ik^\perp z_A} f\left(\sqrt{\frac{\omega_{10}^2}{c^2} - k^{\perp 2}}\right)$$
$$+ \frac{1}{i} \int_0^\infty \mathrm{d}\kappa e^{-2\kappa z_A} f\left(\sqrt{\frac{\omega_{10}^2}{c^2} + \kappa^2}\right), \quad (4.18)$$

where $\kappa^\perp = \kappa^\perp(\omega) = \sqrt{k^{\parallel 2} - \omega^2/c^2}$ again being the imaginary part of the wave vector component perpendicular to the surface. The first integral, which contains an oscillating factor, results from propagating waves whereas the second one, which contains an exponentially decaying factor, results from evanescent waves.

Let us first hypothetically assume that the left-handed slab is perfectly nonabsorbing with $\varepsilon = \mu = -1$. In accordance with the $\operatorname{Im} k_2^\perp > 0$ (recall the remarks in Sec. 4.1.1) the wave vector in the z-direction in the left-handed slab is then given by

$$k_2^\perp = \begin{cases} -k^\perp & \text{for } k^\parallel \leq \omega/c, \\ k^\perp & \text{for } k^\parallel \geq \omega/c, \end{cases} \quad (4.19)$$

whereas the reflection coefficients (4.12) simplify to

$$r_{3-}^s = -e^{-2ik^\perp d}, \quad r_{3-}^p = e^{-2ik^\perp d}. \quad (4.20)$$

Note that for a nonabsorbing medium, the reflection coefficients are invariant under a change $k_2^\perp \to -k_2^\perp$, and hence the final result will not depend on the sign of the square root chosen for $k_2^\perp$.

Substitution of the reflection coefficients into the Green tensor (4.17) leads to

$$\boldsymbol{G}^{(1)}(z_A, z_A, \omega_{10}) = -\frac{i}{8\pi} \int_0^{\omega_{10}/c} dk^\perp \, e^{2ik^\perp(z_A-d)}$$

$$\times \begin{pmatrix} 1 + k^{\perp 2}c^2/\omega_{10}^2 & 0 & 0 \\ 0 & 1 + k^{\perp 2}c^2/\omega_{10}^2 & 0 \\ 0 & 0 & -2(1 - k^{\perp 2}c^2/\omega_{10}^2) \end{pmatrix}$$

$$- \frac{1}{8\pi} \int_0^\infty d\kappa^\perp \, e^{-2\kappa^\perp(z_A-d)} \begin{pmatrix} 1 - \kappa^{\perp 2}c^2/\omega_{10}^2 & 0 & 0 \\ 0 & 1 - \kappa^{\perp 2}c^2/\omega_{10}^2 & 0 \\ 0 & 0 & -2(1 + c^2\kappa^{\perp 2}/\omega_{10}^2) \end{pmatrix}.$$

$$(4.21)$$

After calculating the two integrals, we obtain for $z_A > d$

$$G_{xx}^{(1)}(z_A, z_A, \omega_{10}) = G_{yy}^{(1)}(z_A, z_A, \omega_{10}) = \frac{\omega_{10}e^{i\tilde{z}}}{4\pi c\tilde{z}^3} \left(1 - i\tilde{z} - \tilde{z}^2\right), \qquad (4.22)$$

$$G_{zz}^{(1)}(z_A, z_A, \omega_{10}) = \frac{\omega_{10}e^{i\tilde{z}}}{2\pi c\tilde{z}^3} \left(1 - i\tilde{z}\right) \qquad (4.23)$$

with the abbreviation $\tilde{z} = 2\omega_{10}(z_A - d)/c$. For $z_A > d$, the resonant CP potential (4.4) for the hypothetic nonabsorbing superlens geometry then reads

$$U_1(z_A) = -\mu_0\omega_{10}^2\frac{\omega_{10}}{4\pi c\tilde{z}^3}\Big[\left(\cos(\tilde{z}) + \tilde{z}\sin(\tilde{z}) - \tilde{z}^2\cos(\tilde{z})\right)|\mathbf{d}_{10}^\parallel|^2$$
$$+ 2\left(\cos(\tilde{z}) + \tilde{z}\sin(\tilde{z})\right)|\mathbf{d}_{10}^\perp|^2\Big] \quad \text{for} \quad z_A > d. \quad (4.24)$$

The potential is divergent in the limit $z_A \to d$, despite the absence of any physical surface at $z_A = d$. Furthermore, one obtains a divergent potential for all $0 < z_A \le d$ as can be seen from the second (purely real) integral in Eq. (4.21) which tends to minus infinity in this region. As will be shown below, this unphysical result is due to the fact that absorption is neglected.

The potential (4.24) exactly coincides with the configuration in which a perfectly conducting mirror is placed at $z = d$ [158]. To illustrate this, we consider an image dipole construction for an electric dipole placed at $z_A > d$, cf. Fig. 4.4. By means of the perfect negative refraction taking place at the vacuum–LHM interface combined with the perfect reflection of the mirror we find the image dipole to be situated at $z_A^\star = d - (z_A - d)$. The same image would be obtained if a perfectly conducting mirror were placed in the focal plane, at $z = d$, thus hiding the superlens from the atom. In

this case, one would expect a strongly attractive potential as the atom approaches the mirror which diverges for $z_A \to d$.
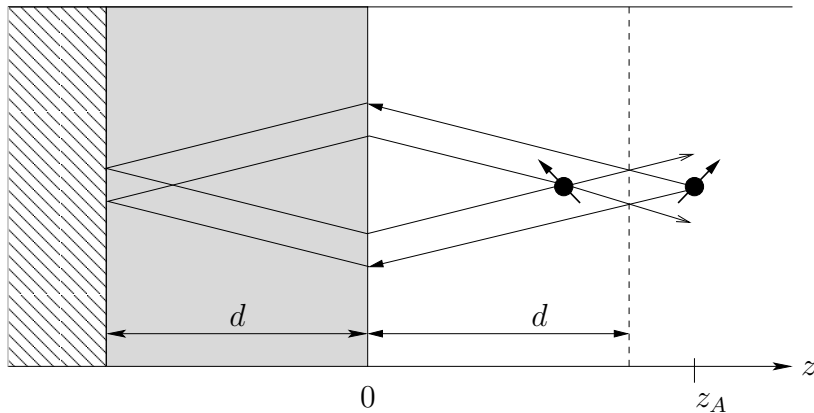
Figure 4.4: Image-dipole construction for the setup depicted in Fig. 4.3. The dashed line marks the position of a perfect mirror that would generate the same image.

To study the impact of material absorption, let us return to Eq. (4.17) for the scattering part of the Green tensor and set therein $\varepsilon(\omega_{10}) = -1 + i\eta$, $\mu(\omega_{10}) = -1 + i\eta$. Due to the positive imaginary parts of ε and μ, divergent integrals of the type of the second integral in Eq. (4.21) can never occur. In Fig. 4.5, the resulting (numerically evaluated) resonant CP potential is plotted versus the distance between atom and LHM slab, for the two cases of parallel and perpendicular alignment of the atomic dipole moment and for different values of absorption. It is seen that the potential features an attractive behavior in the nonretarded regime, which is governed by an inverse power law, while in the retarded regime an oscillating behavior with alternating sign of the potential occurs. Figure 4.5 reveals that for $z_A > d$ and extremely small absorption, the potential approaches the result from the idealized case of a left-handed slab with zero absorption, as given by Eq. (4.24). In particular, for sufficiently small absorption, the potential starts to become strongly negative around the focal plane $z_A \approx d$. This focal-plane enhancement is more noticeable in the case of perpendicular atomic dipole moment.

To clarify whether focal-plane enhancement is indeed a unique feature of the LHM slab, we have plotted the corresponding potential in Fig. 4.6. It is clearly seen, that only the superlens gives rise to the focal-plane enhancement. Instead, the highly transparent material with $\operatorname{Re}\varepsilon = \operatorname{Re}\mu = 1$ leads to a weakly oscillating potential, which is entirely due to the mirror while the materials with different signs of $\operatorname{Re}\varepsilon$ and $\operatorname{Re}\mu$ lead to near-surface potential barriers. As can be seen from Sec. 4.1.1, the latter
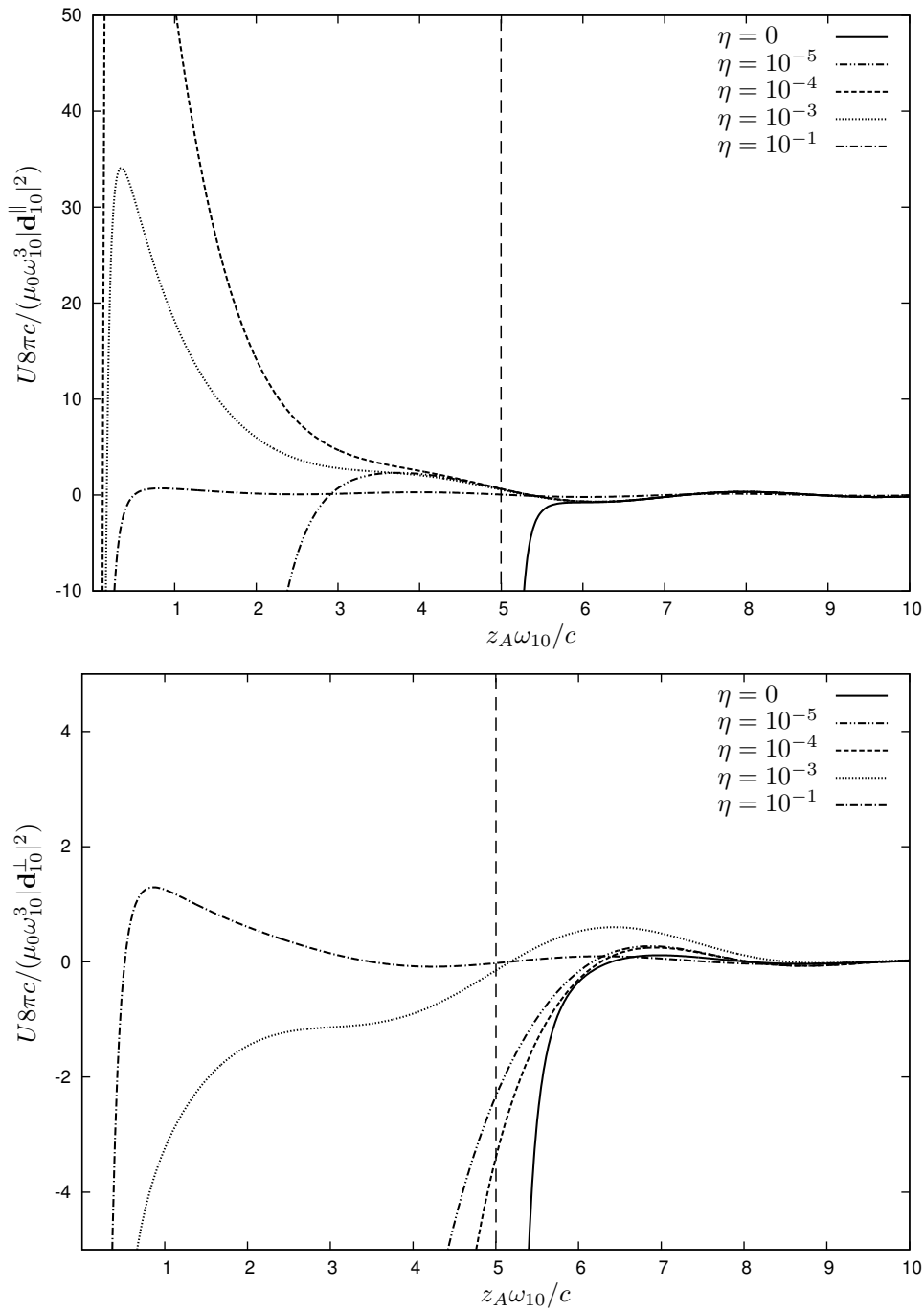
Figure 4.5: Resonant CP potential experienced by an excited two-level atom in the setup sketched in Fig. 4.3 for $d = 5c/\omega_{10}$, $\varepsilon(\omega_{10}) = \mu(\omega_{10}) = -1 + i\eta$ and dipole moment parallel (upper curve) and perpendicular (lower curve) to the surface. The vertical line indicates the position of the focal plane.

behavior is due to $\mathrm{Re}\,\varepsilon$ or $\mathrm{Re}\,\mu$ being negative.

Returning to our original LHM slab, Fig. 4.5 shows the appearance of a potential
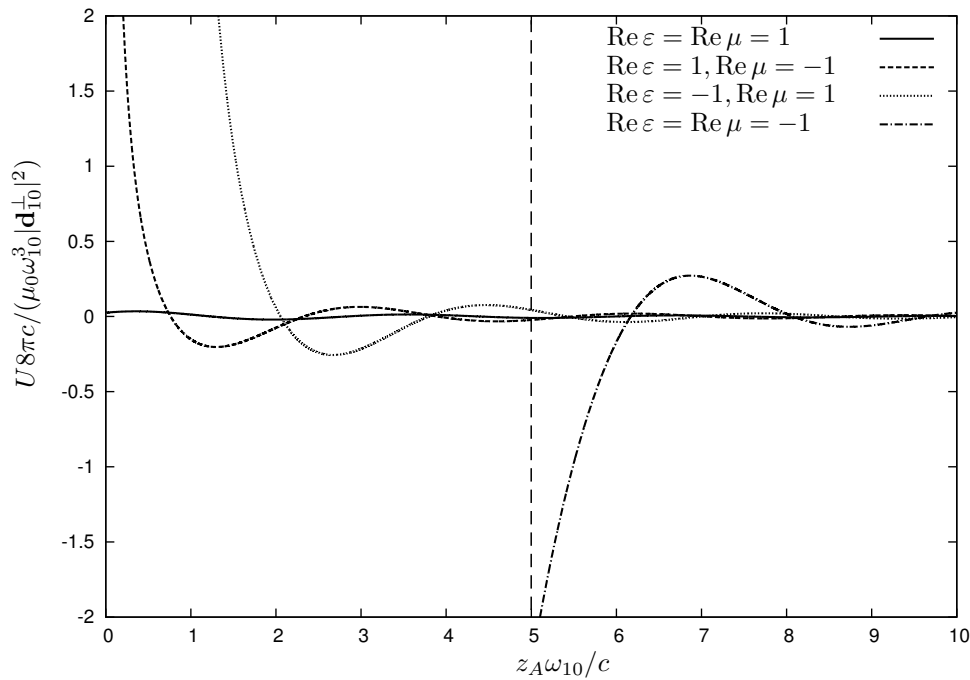
Figure 4.6: Resonant CP potential of an excited two-level atom in front of a metamaterial slab of thickness $d = 5c/\omega_{10}$ with a perfect mirror at its far end. The atomic dipole moment is oriented perpendicular to the surface and we have assumed $\text{Im}\epsilon = \text{Im}\mu = 10^{-4}$. The vertical line indicates the position of the focal plane.

barrier at distances $z_A\omega_{10}/c \lesssim 1$ as an additional feature. This arises for a transition dipole moment parallel to the surface and small (but nonvanishing) amounts of medium absorption, $10^{-4} \lesssim \eta \lesssim 10^{-3}$. The fact that barriers occur only for a transition dipole moment parallel to the surface, but not for those perpendicular to the surface, suggests that s-polarized waves, which are coupled to the first but not the latter, play an important role in their formation. In contrast, for sufficiently weak absorption [$\eta = 10^{-5}$ in Fig. 4.5 (upper) and $\eta = 10^{-3}, 10^{-4}, 10^{-5}$ in Fig. 4.5 (lower)], an attractive potential starts to appear at distances of a few wavelengths away from the surface. Atoms located within this range will get adsorbed to the surface. This behavior is more pronounced for a transition dipole moment perpendicular to the surface.

Let us now investigate the influence of the slab thickness on the CP potential as illustrated in Fig. 4.7. As the slab thickness increases, a potential barrier arises and grows in height for a dipole moment parallel to the surface. However, at some threshold value of d, the height of the barrier starts to be reduced, and the barrier eventually disappears when the slab is too thick. This can be explained as resulting
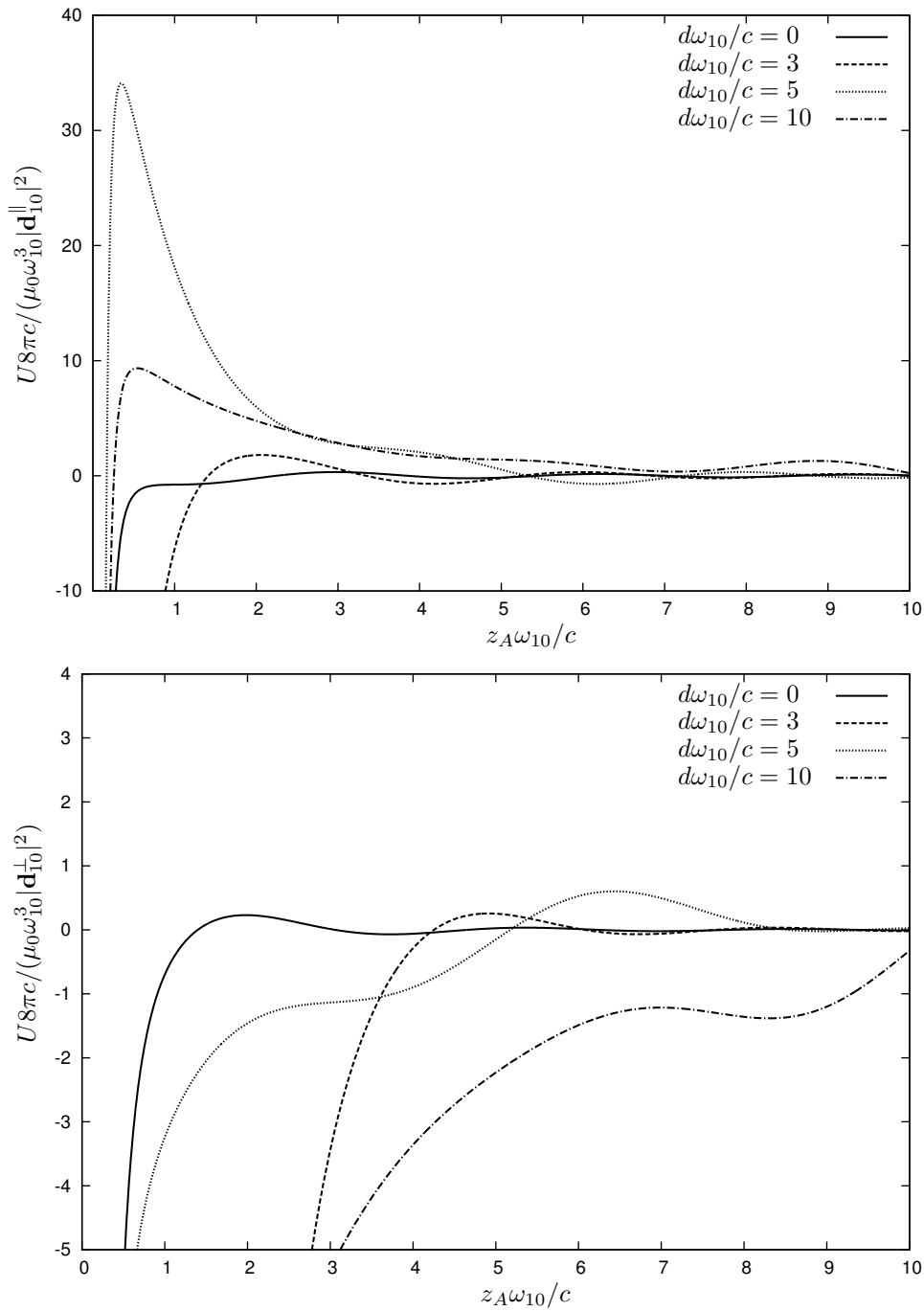
Figure 4.7: Resonant CP potential experienced by an excited atom in the setup sketched in Fig. 4.3 for $\varepsilon(\omega_{10}) = \mu(\omega_{10}) = -1 + i10^{-3}$, and dipole moment parallel (upper curve) and perpendicular (lower curve) to the surface.

from the increasing effects of material absorption. We further see, (in particular for a perpendicular atomic dipole moment) that the distances from the surface at which

a relatively strong attractive potential can occur increase with the slab thickness.

Further insight into how the appearance of the barrier depends on the amount of absorption, the orientation of the atomic dipole moment as well as the thickness of the LHM slab can be gained by examining the CP potential in the near-surface limit. Near the surface, for $z_A \omega_{10}/c \ll 1$, the evanescent waves dominate the potential, as given by the second integral in Eq. (4.18). Again, the main contribution to the $k^\parallel$-integral comes from values $k^\parallel \gg \omega_{10}/c$ and $k^\parallel \gg \sqrt{|\varepsilon\mu|}\omega_{10}/c$ in which case the nonretarded potential reads

$$U(z_A) = -\frac{\omega_{10}^2 \mu_0}{8\pi} \int_0^\infty \mathrm{d}k^\parallel \, e^{-2k^\parallel z_A} \left[\left(\mathrm{Re}\, r_{3-}^s + \frac{k^{\parallel 2} c^2}{\omega_{10}^2} \mathrm{Re}\, r_{3-}^p \right) |\mathbf{d}_{10}^\parallel|^2 + \frac{2k^{\parallel 2} c^2}{\omega_{10}^2} \mathrm{Re}\, r_{3-}^p |\mathbf{d}_{10}^\perp|^2 \right]$$

(4.25)

where

$$\mathrm{Re}\, r_{3-}^p = \frac{(|\varepsilon|^2 - 1)\left(1 + e^{-4k^\parallel d}\right) + (|\varepsilon-1|^2 + |\varepsilon+1|^2)\, e^{-2k^\parallel d}}{\left|\varepsilon + 1 + (\varepsilon - 1)e^{-2k^\parallel d}\right|^2},$$

(4.26)

$$\mathrm{Re}\, r_{3-}^s = \frac{(|\mu|^2 - 1)\left(1 + e^{-4k^\parallel d}\right) - (|\mu-1|^2 + |\mu+1|^2)\, e^{-2k^\parallel d}}{\left|\mu + 1 - (\mu - 1)e^{-2k^\parallel d}\right|^2}.$$

(4.27)

When

$$\varepsilon \simeq -1 \quad \text{and} \quad \mu \simeq -1,$$

(4.28)

the first terms in Eqs. (4.26) and (4.27) approximately vanish, thus

$$\mathrm{Re}\, r_{3-}^p \simeq \frac{(|\varepsilon - 1|^2 + |\varepsilon + 1|^2)\, e^{-2k^\parallel d}}{\left|\varepsilon + 1 + (\varepsilon - 1)e^{-2k^\parallel d}\right|^2},$$

(4.29)

$$\mathrm{Re}\, r_{3-}^s \simeq -\frac{(|\mu - 1|^2 + |\mu + 1|^2)\, e^{-2k^\parallel d}}{\left|\mu + 1 - (\mu - 1)e^{-2k^\parallel d}\right|^2},$$

(4.30)

where the opposite signs imply that the two polarizations give competing contributions to the potential. Namely, the p-polarized waves give rise to attractive contributions to the potential while the s-polarized waves lead to repulsive ones. Very close to the surface, due to the presence of the $k^{\parallel 2}$ factor [see Eq. (4.25)], the contribution to the potential of the p-polarized waves is proportional to $1/z_A^3$ while the contribution of the s-polarized waves is proportional to $1/z_A$. The contribution of the p-polarized waves hence dominates, resulting in an attractive potential (also see Figs. 4.5 and 4.7). At some distance from the surface, the contribution of the s-polarized waves can dominate under appropriate conditions, which then leads to the appearance of a potential

barrier. This also explains the absence of the barrier in the case where the dipole moment is perpendicular to the surface.

Equation (4.27) also allows us to understand the influence of the thickness of the LHM slab. It shows that the magnitude of $|\mathrm{Re}\, r_{3-}^{s}|$ is about 1 for $d \to 0$ (slab absent), and is typically determined by a $e^{2k^{\parallel}d}$ term otherwise. Therefore, the presence of the slab is crucial for the appearance of a potential barrier. When the slab is very thick, the influence of the mirror vanishes, $e^{-2k^{\parallel}d} \to 0$ [cf. Eqs. (4.26) and (4.27)], and it is not difficult to verify that Eq. (4.25) reproduces the result for the resonant part of the potential of an excited atom in front of an interface as given by Eq. 4.6.

It should be pointed out, that the appearance of the potential barrier is not a true superlens effect; it can easily be created with other, right-handed, materials [cf. Eqs. (4.6) and Eqs. (4.7)]. Further, we recall that potential barriers may also be created in planar ground-state systems as explained in Sec. 3.2, but are generally much more pronounced in the case of excited atoms. For instance, the peaks of the potentials for the superlens geometry (Fig. 4.5) are at least 4 orders of magnitude larger than those given in Sec. 3.2 concerning the potential of a ground-state atom.

Let us finally comment on the applicability of the results presented in this section. In order to observe the predicted effects, potential barriers and focal-plane enhancement, one has to ensure that both the atomic transition wavelength and the atom–surface separation are larger than the length scale of the elementary building blocks of the metamaterial. With currently available metamaterials, this may be achieved with polar molecules whose rotational and vibrational transition wavelengths can be very large. It should also be stressed that in the examples considered, metamaterials with very small absorption have been assumed. However, such metamaterials are now within the reach of today's experimental techniques [97]. Note, that our results are valid as long as the atom remains in its initial excited state, i.e., on time scales that are short compared to those of spontaneous decay. An impressive example is the first excited, metastable state of helium which has a life time of up to 8000 s [159].

4.1.3 Spontaneous decay revisited

The superlens setup has also been discussed in the context of spontaneous emission. In Refs. [160, 161], it has been reported that for an excited atom placed in the focal plane, $z_A = d$, spontaneous emission is completely suppressed for a dipole moment parallel to the surface, while the decay rate is enhanced by a factor of two for a dipole moment perpendicular to the surface. These results, however, have been obtained

under the assumption of a lossless LHM slab. In light of our findings for the CP potential, we should carefully examine whether these idealized results are an appropriate approximation to the more realistic case of a weakly absorbing LHM slab. In particular, it can be expected that absorption gives rise to nonradiative decay.

Whereas the resonant CP potential depends on the real part of the Green tensor, the rate of spontaneous decay is determined by its imaginary part. From Eq. (4.21) for the Green tensor of the completely nonabsorbing setup, it can be seen that the contributions from evanescent waves, which give rise to divergences in the region $z_A \leq d$, are purely real and thus do not contribute to the decay rate. The decay rate is thus expressed in terms of traveling-wave contributions.

For a two-level atom, we write the the decay rate $\Gamma \equiv \Gamma_1$, Eq. (2.47), in the form

$$\frac{\Gamma}{\Gamma_{\text{vac}}} = 1 + \frac{6\pi c}{\omega_{10}|\mathbf{d}_{10}|^2} \operatorname{Im} \left[G_{xx}^{(1)}|\mathbf{d}_{10}^{\parallel}|^2 + G_{zz}^{(1)}|\mathbf{d}_{10}^{\perp}|^2 \right], \tag{4.31}$$

where Γ_{vac} is the free-space decay rate,

$$\Gamma_{\text{vac}} = \frac{1}{3\pi\varepsilon_0\hbar c^3}\omega_{10}^3|\mathbf{d}_{10}|^2. \tag{4.32}$$

Let us first assume an absolutely nonabsorbing LHM having $\varepsilon(\omega_{10}) = \mu(\omega_{10}) = -1$ again. From Eqs. (4.22) and (4.23) we obtain

$$\operatorname{Im} G_{xx}^{(1)} = \frac{\omega_{10}}{4\pi c\tilde{z}^3} \left[\sin(\tilde{z}) - \tilde{z}\cos(\tilde{z}) - \tilde{z}^2\sin(\tilde{z}) \right], \tag{4.33}$$

$$\operatorname{Im} G_{zz}^{(1)} = \frac{\omega_{10}}{2\pi c\tilde{z}^3} \left[\sin(\tilde{z}) - \tilde{z}\cos(\tilde{z}) \right] \tag{4.34}$$

which formally hold for any atom–surface distance, including the region to the left of the focal plane. In particular, $\operatorname{Im} G_{xx}^{(1)}$ and $\operatorname{Im} G_{zz}^{(1)}$ are even functions of $\tilde{z} = 2(z_A - d)\omega_{10}/c$ and finite at the surface. It is not difficult to see that for $z_A = d$, Eq. (4.31) together with Eqs. (4.33) and (4.34) implies complete inhibition of spontaneous decay, $\Gamma = 0$, for a dipole moment oriented parallel to the surface, and enhancement of spontaneous decay, $\Gamma = 2\Gamma_{\text{vac}}$, for a dipole moment oriented perpendicularly to the surface [160].

To account for material absorption, we perform the calculations on the basis of the exact (scattering part of the) Green tensor as given in Eq. (4.17) together with Eqs. (4.12). Numerical examples are given in Fig. 4.8, where the case of zero absorption, in accordance with Eqs. (4.31)–(4.34), is also shown in order to facilitate

comparison. We see that in the case of strictly zero absorption, the decay rate as a function of the atomic position $z_A > 0$ is symmetric with respect to the position $z_A = d$. Any absorption destroys this symmetry. As a result, large enhancement of the spontaneous decay can be observed when the atom is near the LHM surface, which is obviously due to the absorption-assisted atomic coupling to evanescent waves. This effect implies qualitatively new distance dependences, as will be confirmed in Eq. (4.38) below. Note that the enhanced spontaneous decay near a surface is well known for ordinary materials (see e.g. Ref. [162]). Our result is also consistent with those reported in Ref. [163], where it has been pointed out that the inhibition of spontaneous decay can be weakened due to nonradiative decay at short distances and due to radiative decay at large distances.

We find that for distances $z_A \leq d$, the presence of absorption drastically changes the spontaneous decay rate such that Eq. (4.31) together with Eqs. (4.33) and (4.34) can not be regarded as an acceptable approximation to the spontaneous decay rate in the case of small absorption. As similar failure of the zero-absorption limit has been found for the CP potential.

To further elucidate the influence of the evanescent waves, let us examine the near-surface limit of the rate of spontaneous decay. By using approximations similar to those in Sec. 4.1.2, it can be shown that for $z_A \omega_{10}/c \ll 1$,

$$
\frac{\Gamma}{\Gamma_{\text{vac}}} = 1 + \frac{3c}{4\omega_{10}|\mathbf{d}_{10}|^2} \int_0^\infty \mathrm{d}k^\| \, e^{-2k^\| z_A}
$$
$$
\times \left[\left(\operatorname{Im} r_{3-}^s + \frac{k^{\|2}c^2}{\omega_{10}^2} \operatorname{Im} r_{3-}^p \right) |\mathbf{d}_{10}^\||^2 + \frac{2k^{\|2}c^2}{\omega_{10}^2} \operatorname{Im} r_{3-}^p |\mathbf{d}_{10}^\perp|^2 \right], \quad (4.35)
$$

where

$$
\operatorname{Im} r_{3-}^s = \frac{2\operatorname{Im}\mu(1 - e^{-4k^\| d})}{|\mu + 1 - (\mu - 1)e^{-2k^\| d}|^2}, \quad (4.36)
$$

$$
\operatorname{Im} r_{3-}^p = \frac{2\operatorname{Im}\varepsilon\left(1 - e^{-4k^\| d}\right)}{|\varepsilon + 1 - (\varepsilon - 1)e^{-2k^\| d}|^2}. \quad (4.37)
$$

Unlike the real parts [cf. Eqs. (4.26) and (4.27)], the imaginary parts of r_{3-}^s and r_{3-}^p have the same (positive) sign. The two polarizations therefore contribute constructively to the spontaneous decay rate. If the slab becomes sufficiently thick, Eq. (4.35)
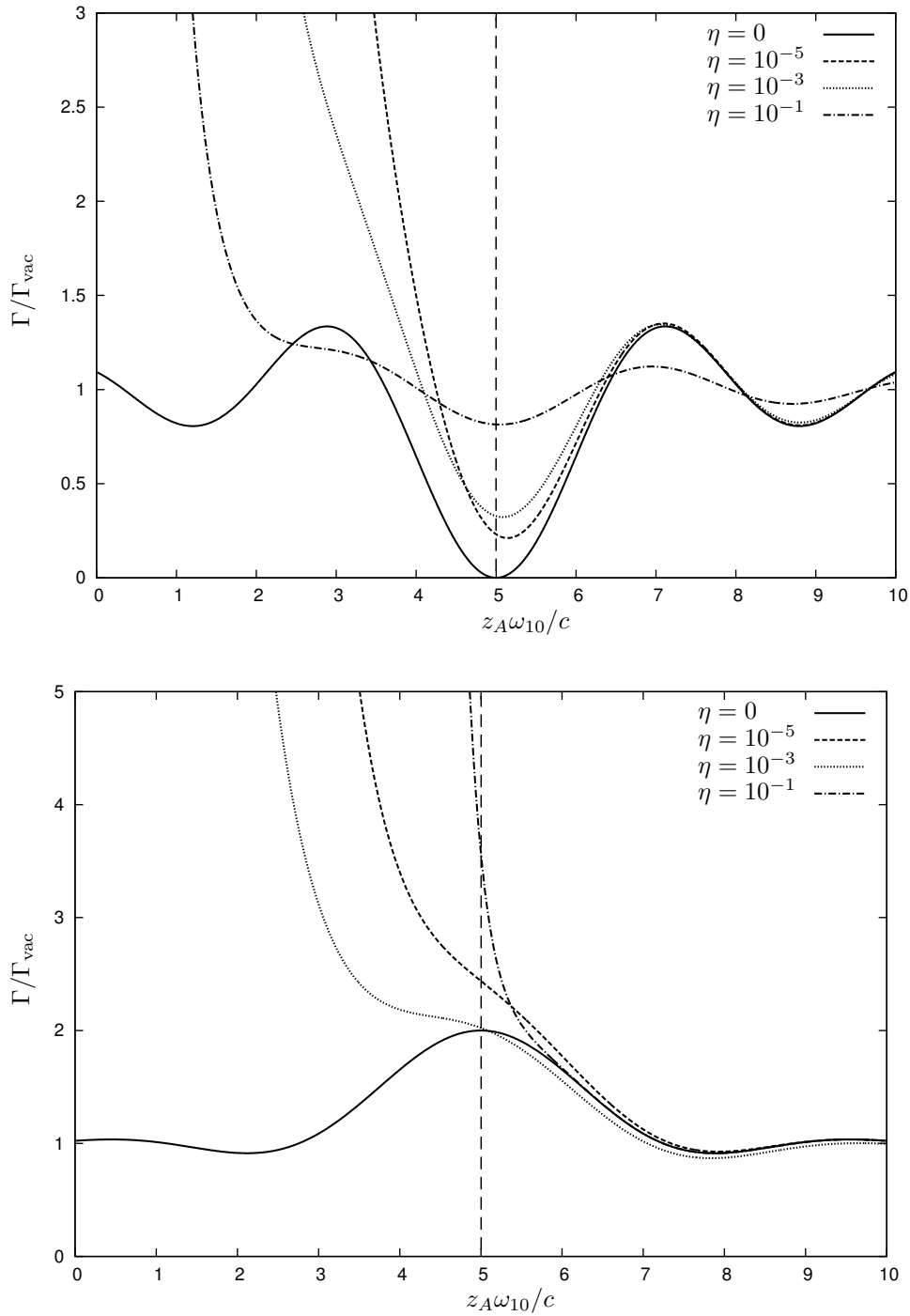
Figure 4.8: Atom–surface distance dependence of the decay rate of an excited two-level atom in the setup in Fig. 4.3 for $\varepsilon = \mu = -1 + i\eta$, $d = 5c/\omega_{10}$ and dipole moment parallel (upper curve) and perpendicular (lower) to the surface. The vertical line indicates the position of the focal plane.

reduces to leading order to

$$\frac{\Gamma}{\Gamma_{\text{vac}}} = 1 + \frac{3c^3\big(|\mathbf{d}_{10}^{\parallel}|^2 + 2|\mathbf{d}_{10}^{\perp}|^2\big)}{8\omega_{10}^3|\mathbf{d}_{10}|^2 z_A^3}\frac{\operatorname{Im}\varepsilon}{|\varepsilon + 1|^2}. \tag{4.38}$$

Equation (4.38) shows that the decay rate takes on large values as $z_A \to 0$, which is a consequence of the direct energy transfer from the atom to the constituents of the medium (see e.g., Ref. [162]).

4.2 Casimir force on an amplifying body

So far we have studied the nonresonant and resonant CP interaction in planar and spherical systems. In this section, we focus on Casimir forces between bodies where amplification in the sense of Eq. (2.1) is present in limited space and frequency regions. In Sec. 4.2.1, we will introduce the Casimir force, in close analogy to the CP force, as the quantum-average Lorentz force acting on the internal charge and current densities. Firstly, we will study an arbitrary system without specifying the Green tensor of the geometry. Secondly, we will investigate the Casimir force between a partially amplifying plate and an electric half space (Sec. 4.2.2). The results in this section are based on Refs. [AS5, AS6].

4.2.1 Arbitrary geometry

Let us consider an arbitrary arrangement of linearly responding magnetoelectric bodies described by the permittivity $\varepsilon(\mathbf{r}, \omega)$ and permeability $\mu(\mathbf{r}, \omega)$.

Volume-force formulation

The (zero-temperature) Casimir force on one of these bodies with volume V can be found by calculating the quantum-average Lorentz force with respect to the quasi-stationary state $|\{0\}\rangle$ as introduced in Chap. 2,

$$\mathbf{F} = \int_V \mathrm{d}^3 r \int_0^\infty \langle\{0\}|\hat{\rho}(\mathbf{r})\hat{\mathbf{E}}(\mathbf{r}') + \hat{\mathbf{j}}(\mathbf{r}) \times \hat{\mathbf{B}}(\mathbf{r}')|\{0\}\rangle_{\mathbf{r}' \to \mathbf{r}}. \tag{4.39}$$

The coincidence limit $\mathbf{r}' \to \mathbf{r}$ has to be performed in such a way that divergent self-forces are discarded. We will return to this point later.

As a first step, we recall the expression of the noise current density (2.26) together with the conductivity tensor (2.12) and the commutation relations (2.27) and verify

that

$$\langle \underline{\hat{\mathbf{j}}}_N(\mathbf{r},\omega)\underline{\hat{\mathbf{j}}}_N(\mathbf{r}',\omega')\rangle = \mathbf{0} = \langle \underline{\hat{\mathbf{j}}}_N^\dagger(\mathbf{r},\omega)\underline{\hat{\mathbf{j}}}_N^\dagger(\mathbf{r}',\omega')\rangle, \tag{4.40}$$

$$\langle \underline{\hat{\mathbf{j}}}_N(\mathbf{r},\omega)\underline{\hat{\mathbf{j}}}_N^\dagger(\mathbf{r}',\omega')\rangle = \frac{\hbar\omega}{\pi}\delta(\omega-\omega')\sum_{\lambda=e,m}\operatorname{Re}\boldsymbol{Q}_\lambda(\mathbf{r},\mathbf{r}',\omega)\Theta[\kappa_\lambda(\mathbf{r},\omega)], \tag{4.41}$$

$$\langle \underline{\hat{\mathbf{j}}}_N^\dagger(\mathbf{r},\omega)\underline{\hat{\mathbf{j}}}_N(\mathbf{r}',\omega')\rangle = -\frac{\hbar\omega}{\pi}\delta(\omega-\omega')\sum_{\lambda=e,m}\operatorname{Re}\boldsymbol{Q}_\lambda(\mathbf{r},\mathbf{r}',\omega)\Theta[-\kappa_\lambda(\mathbf{r},\omega)]. \tag{4.42}$$

Note that, if no intervening symbol between two vectors is given, the dyadic product is meant. Combining these results with the field expansion (2.16) as well as Eq. (2.31), together with Eq. (2.8), we find the expressions

$$\langle \hat{\rho}(\mathbf{r},\omega)\underline{\hat{\mathbf{E}}}(\mathbf{r}',\omega')\rangle = \mathbf{0} = \langle \hat{\rho}^\dagger(\mathbf{r},\omega)\underline{\hat{\mathbf{E}}}^\dagger(\mathbf{r}',\omega')\rangle, \tag{4.43}$$

$$\langle \underline{\hat{\rho}}(\mathbf{r},\omega)\underline{\hat{\mathbf{E}}}^\dagger(\mathbf{r}',\omega')\rangle = \frac{\hbar}{\pi}\frac{\omega^2}{c^2}\delta(\omega-\omega')\mu_0\omega\sum_{\lambda=e,m}\int \mathrm{d}^3s\int \mathrm{d}^3s'\Theta[\kappa_\lambda(\mathbf{s},\omega)]$$

$$\times \boldsymbol{\nabla}\cdot\boldsymbol{G}(\mathbf{r},\mathbf{s},\omega)\cdot\operatorname{Re}\boldsymbol{Q}_\lambda(\mathbf{s},\mathbf{s}',\omega)\cdot\boldsymbol{G}^*(\mathbf{s}',\mathbf{r}',\omega), \tag{4.44}$$

$$\langle \underline{\hat{\rho}}^\dagger(\mathbf{r},\omega)\underline{\hat{\mathbf{E}}}(\mathbf{r}',\omega')\rangle = -\frac{\hbar}{\pi}\frac{\omega^2}{c^2}\delta(\omega-\omega')\mu_0\omega\sum_{\lambda=e,m}\int \mathrm{d}^3s\int \mathrm{d}^3s'\Theta[-\kappa_\lambda(\mathbf{s},\omega)]$$

$$\times \boldsymbol{\nabla}\cdot\boldsymbol{G}^*(\mathbf{r},\mathbf{s},\omega)\cdot\operatorname{Re}\boldsymbol{Q}_\lambda(\mathbf{s},\mathbf{s}',\omega)\cdot\boldsymbol{G}(\mathbf{s}',\mathbf{r}',\omega). \tag{4.45}$$

To calculate the second term in Eq. (4.39), we recall Eqs. (2.17) and (2.30) together with Eq. (2.8) and use the vector identity,

$$\mathbf{a}\times\mathbf{b} = -\operatorname{tr}(\boldsymbol{I}\times\mathbf{ab}), \tag{4.46}$$

where we have introduced the notation $[\operatorname{tr}\boldsymbol{T}]_i = T_{kik}$. We eventually arrive at the expressions

$$\langle \underline{\hat{\mathbf{j}}}(\mathbf{r},\omega)\times\underline{\hat{\mathbf{B}}}(\mathbf{r}',\omega')\rangle = \mathbf{0} = \langle \underline{\hat{\mathbf{j}}}^\dagger(\mathbf{r},\omega)\times\underline{\hat{\mathbf{B}}}^\dagger(\mathbf{r}',\omega')\rangle, \tag{4.47}$$

$$\langle \underline{\hat{\mathbf{j}}}(\mathbf{r},\omega)\times\underline{\hat{\mathbf{B}}}^\dagger(\mathbf{r}',\omega')\rangle = \frac{\hbar}{\pi}\delta(\omega-\omega')\mu_0\omega\sum_{\lambda=e,m}\int \mathrm{d}^3s\int \mathrm{d}^3s'\Theta[\kappa_\lambda(\mathbf{s},\omega)]$$

$$\times \operatorname{tr}\left[\boldsymbol{I}\times\left(\boldsymbol{\nabla}\times\boldsymbol{\nabla}\times-\frac{\omega^2}{c^2}\right)\boldsymbol{G}(\mathbf{r},\mathbf{s},\omega)\cdot\operatorname{Re}\boldsymbol{Q}_\lambda(\mathbf{s},\mathbf{s}',\omega)\cdot\boldsymbol{G}^*(\mathbf{s}',\mathbf{r}',\omega)\times\overleftarrow{\boldsymbol{\nabla}}'\right] \tag{4.48}$$

and

$$\langle \hat{\underline{\mathbf{j}}}^\dagger(\mathbf{r},\omega) \times \hat{\underline{\mathbf{B}}}(\mathbf{r}',\omega') \rangle = -\frac{\hbar}{\pi}\delta(\omega - \omega')\mu_0\omega \sum_{\lambda=e,m} \int d^3s \int d^3s' \Theta[-\kappa_\lambda(\mathbf{s},\omega)]$$

$$\times \mathrm{tr}\left[\mathbf{I} \times \left(\boldsymbol{\nabla} \times \boldsymbol{\nabla} \times -\frac{\omega^2}{c^2} \right) \boldsymbol{G}^*(\mathbf{r},\mathbf{s},\omega) \cdot \mathrm{Re}\,\boldsymbol{Q}_\lambda(\mathbf{s},\mathbf{s}',\omega) \cdot \boldsymbol{G}(\mathbf{s}',\mathbf{r}',\omega) \times \overleftarrow{\boldsymbol{\nabla}}' \right]. \quad (4.49)$$

We now apply the identity

$$\Theta[\kappa_\lambda(\mathbf{s},\omega)] = 1 - \Theta[-\kappa_\lambda(\mathbf{s},\omega)] \quad (4.50)$$

to Eqs. (4.44) and (4.48) and combine the terms proportional to $\Theta[-\kappa_\lambda(\mathbf{s},\omega)]$ with Eqs. (4.45) and (4.49). For the parts including the whole frequency integration, we use the integral relation (2.24). As a result, we obtain the Casimir force in the form [AS6]

$$\mathbf{F} = \mathbf{F}^{\mathrm{res}} + \mathbf{F}^{\mathrm{nres}} \quad (4.51)$$

with

$$\mathbf{F}^{\mathrm{nres}} = \frac{\hbar}{\pi} \int_V d^3r \int_0^\infty d\omega \left\{ \frac{\omega^2}{c^2}\boldsymbol{\nabla} \cdot \mathrm{Im}\boldsymbol{G}(\mathbf{r},\mathbf{r}',\omega) \right.$$

$$\left. + \mathrm{tr}\left[\mathbf{I} \times \left(\boldsymbol{\nabla} \times \boldsymbol{\nabla} \times -\frac{\omega^2}{c^2} \right) \mathrm{Im}\boldsymbol{G}(\mathbf{r},\mathbf{r}',\omega) \times \overleftarrow{\boldsymbol{\nabla}}' \right] \right\}_{\mathbf{r}' \to \mathbf{r}} \quad (4.52)$$

and

$$\mathbf{F}^{\mathrm{res}} = -\frac{2\hbar\mu_0}{\pi} \int_V d^3r \int_0^\infty d\omega\,\omega \sum_{\lambda=e,m} \int d^3s \int d^3s' \Theta[-\kappa_\lambda(\mathbf{s},\omega)]$$

$$\times \mathrm{Re}\left\{ \frac{\omega^2}{c^2}\boldsymbol{\nabla} \cdot \boldsymbol{G}(\mathbf{r},\mathbf{s},\omega) \cdot \mathrm{Re}\,\boldsymbol{Q}_\lambda(\mathbf{s},\mathbf{s}',\omega) \cdot \boldsymbol{G}^*(\mathbf{s}',\mathbf{r}',\omega) \right.$$

$$\left. + \mathrm{tr}\left[\mathbf{I} \times \left(\boldsymbol{\nabla} \times \boldsymbol{\nabla} \times -\frac{\omega^2}{c^2} \right) \boldsymbol{G}(\mathbf{r},\mathbf{s},\omega) \cdot \mathrm{Re}\,\boldsymbol{Q}_\lambda(\mathbf{s},\mathbf{s}',\omega) \cdot \boldsymbol{G}^*(\mathbf{s}',\mathbf{r}',\omega) \times \overleftarrow{\boldsymbol{\nabla}}' \right] \right\}_{\mathbf{r}' \to \mathbf{r}}.$$
$$(4.53)$$

Recall that in Eq. (4.52), we have to remove self-forces before taking the coincidence limit $\mathbf{r}' \to \mathbf{r}$. These unphysical divergent self-forces arise from the fact that the electric field at $\mathbf{r}$ inside the body, originating from a source point $\mathbf{r}'$ inside the same volume element, contains back-reactions onto itself in the coincidence limit, as expressed via $\boldsymbol{G}(\mathbf{r},\mathbf{r},\omega)$. For a homogeneous body we can remove such terms by simply replacing

$\boldsymbol{G}$ with its scattering counter part $\boldsymbol{G}^{(1)}(\mathbf{r}, \mathbf{r}', \omega)$ and discarding the bulk contribution [105]. Similarly, if the body is inhomogeneous we can remove the corresponding bulk tensor for each small homogeneous region inside the inhomogeneous body. The identification of self forces in the resonant force term (4.53) is not so straightforward since the arguments of the appearing Green tensors $\boldsymbol{G}(\mathbf{r}, \mathbf{s}, \omega)$ and $\boldsymbol{G}^*(\mathbf{s}', \mathbf{r}', \omega)$ do not lie in the same layer. If self-forces are present they can, however, be found by calculating the force on the body in the absence of any other matter. A physically reasonable Casimir force should vanish in this situation, any terms that survive can be regarded as self-forces and should therefore be discarded.

Equations (4.52) and (4.53) represent general expressions for the Casimir force acting on a linearly polarizable and magnetizable body of arbitrary shape in an arbitrary environment (of additional bodies or media), where the body under consideration or those forming the environment, or both may be amplifying. The term $\mathbf{F}^{\mathrm{nres}}$ is a purely nonresonant contribution to the force. However, although looking formally like the Casimir force for purely absorbing bodies [105], the frequency response is different if amplification is present. The resonant term $\mathbf{F}^{\mathrm{res}}$ is a new term which, as evident from the factors $\Theta[-\varepsilon_I(\mathbf{s}, \omega)]$, $\Theta[-\mu_I(\mathbf{s}, \omega)]$, only arises in the presence of amplification. It depends on the amplification-assisted frequencies inside the body which indicates that it is connected to spontaneous decay and real-photon emission processes.

For convenience, we express the nonresonant force (4.52) in terms of the conductivity tensor. To that end, we apply the identities

$$\left(\boldsymbol{\nabla} \times \boldsymbol{\nabla} \times - \frac{\omega^2}{c^2}\right) \mathrm{Im}\, \boldsymbol{G}^{(1)}(\mathbf{r}, \mathbf{r}', \omega) \;=\; \mu_0 \omega \mathrm{Re} \int \mathrm{d}^3 s \boldsymbol{Q}(\mathbf{r}, \mathbf{s}, \omega) \cdot \boldsymbol{G}(\mathbf{s}, \mathbf{r}', \omega) \quad (4.54)$$

and

$$\boldsymbol{\nabla} \cdot \mathrm{Im}\, \boldsymbol{G}^{(1)}(\mathbf{r}, \mathbf{r}', \omega) = -\frac{1}{\varepsilon_0 \omega} \mathrm{Re}\, \boldsymbol{\nabla} \cdot \int \mathrm{d}^3 s \boldsymbol{Q}(\mathbf{r}, \mathbf{s}, \omega) \cdot \boldsymbol{G}(\mathbf{s}, \mathbf{r}', \omega), \quad (4.55)$$

where the first identity follows directly from the differential equation (2.20), and for the second one, we have also used the fact that the divergence of a curl vanishes. Hence we write the nonresonant force in the form

$$\mathbf{F}^{\mathrm{nres}} = \frac{\hbar \mu_0}{\pi} \int_V \mathrm{d}^3 r \mathrm{Re} \int_0^\infty \mathrm{d}\omega \omega \Big[\boldsymbol{\nabla}' \mathrm{tr} \int \mathrm{d}^3 s \boldsymbol{Q}(\mathbf{r}, \mathbf{s}, \omega) \cdot \boldsymbol{G}(\mathbf{s}, \mathbf{r}', \omega)$$
$$- (\boldsymbol{\nabla} + \boldsymbol{\nabla}') \cdot \int \mathrm{d}^3 s \boldsymbol{Q}(\mathbf{r}, \mathbf{s}, \omega) \cdot \boldsymbol{G}(\mathbf{s}, \mathbf{r}', \omega) \Big]_{\mathbf{r}' \to \mathbf{r}}, \quad (4.56)$$

where we have applied the general tensor identity

$$\text{tr}\big[\boldsymbol{I} \times \boldsymbol{T}(\mathbf{r},\mathbf{r}',\omega) \times \overleftarrow{\boldsymbol{\nabla}}'\big] = \boldsymbol{\nabla}'\text{tr}\,\boldsymbol{T}(\mathbf{r},\mathbf{r}',\omega) - \boldsymbol{\nabla}' \cdot \boldsymbol{T}(\mathbf{r},\mathbf{r}',\omega). \qquad (4.57)$$

The second term in Eq. (4.56) can be converted to a vanishing surface integral for a body in free space. It is instructive to write out the conductivity tensor in terms of the electric and magnetic susceptibilities of the body, $\varepsilon(\mathbf{r},\omega) - 1$ and $1 - 1/\mu(\mathbf{r},\omega)$, with $\mathbf{r} \in V$ [recall Eqs. (2.12)–(2.14)],

$$\begin{aligned}
\mathbf{F}^{\text{nres}} = \frac{\hbar}{2\pi} \int_V \mathrm{d}^3r \text{Im} \int_0^\infty \mathrm{d}\omega \bigg(&\frac{\omega^2}{c^2}[\varepsilon(\mathbf{r},\omega) - 1]\boldsymbol{\nabla}\text{tr}\,\boldsymbol{G}^{(1)}(\mathbf{r},\mathbf{r},\omega) \\
&- \boldsymbol{\nabla}\Big\{\Big[1 - \frac{1}{\mu(\mathbf{r},\omega)}\Big]\text{tr}\Big[\boldsymbol{\nabla} \times \boldsymbol{G}^{(1)}(\mathbf{r},\mathbf{r}',\omega) \times \overleftarrow{\boldsymbol{\nabla}}'\Big]_{\mathbf{r}'\to\mathbf{r}}\Big\}\bigg),
\end{aligned} \qquad (4.58)$$

where we have used the symmetry property of the Green tensor (2.23), which implies

$$\Big[\boldsymbol{\nabla}'\text{tr}\,\boldsymbol{G}^{(1)}(\mathbf{r},\mathbf{r}',\omega)\Big]_{\mathbf{r}'\to\mathbf{r}} = \frac{1}{2}\boldsymbol{\nabla}\text{tr}\Big[\boldsymbol{G}^{(1)}(\mathbf{r},\mathbf{r}',\omega)\Big]_{\mathbf{r}'\to\mathbf{r}}. \qquad (4.59)$$

Equation (4.58) can be more conveniently written as an integral over imaginary frequencies. To that end, we write $\text{Im}\,\boldsymbol{G}^{(1)} = (\boldsymbol{G}^{(1)} - \boldsymbol{G}^{(1)*})/(2i)$ and use the Schwartz reflection principle (2.22),

$$\int_0^\infty \mathrm{d}\omega \text{Im}\,f(\omega) = \frac{1}{2i}\int_0^\infty \mathrm{d}\omega\,f(\omega) - \frac{1}{2i}\int_{-\infty}^0 \mathrm{d}\omega\,f(\omega), \qquad (4.60)$$

where $f(\omega)$ denotes the integrand in Eq. (4.52). Recall the analyticity of the Green tensor as well as that of the permittivity and the permeability in the upper half of the complex frequency plane (including the real axis). On exploiting the small-frequency behavior of the Green tensor, Eq. (2.25), we can apply Cauchy's theorem. It implies that any closed-contour integral in the upper ω half-plane must vanish. Thus, the two integrals over the real frequency axis in Eq. (4.60) can be rewritten in terms of an integral over the positive imaginary axis and an integral over an infinite quarter-circle in the first [first integral in Eq. (4.60)] or second quadrant [second integral in Eq. (4.60)]. Since the integrals over the quarter-circles vanish due to the high-frequency limit of $\boldsymbol{G}^{(1)}$, Eq. (2.25), the force (4.52) can finally be transformed to an

integral over purely imaginary frequencies,

$$\mathbf{F}^{\mathrm{nres}} = -\frac{\hbar}{2\pi} \int_V \mathrm{d}^3 r \int_0^\infty \mathrm{d}\xi \left(\frac{\xi^2}{c^2} [\varepsilon(\mathbf{r}, i\xi) - 1] \boldsymbol{\nabla} \mathrm{tr} \boldsymbol{G}^{(1)}(\mathbf{r}, \mathbf{r}, i\xi) \right.$$
$$\left. - \boldsymbol{\nabla} \left\{ \left[1 - \frac{1}{\mu(\mathbf{r}, i\xi)} \right] \mathrm{tr} \left[\boldsymbol{\nabla} \times \boldsymbol{G}^{(1)}(\mathbf{r}, \mathbf{r}', i\xi) \times \overleftarrow{\boldsymbol{\nabla}}' \right]_{\mathbf{r}' \to \mathbf{r}} \right\} \right). \quad (4.61)$$

Contact to Casimir–Polder forces

To get more insight, we establish a relation between the Casimir force on an amplifying body according to (4.51), (4.61) and (4.53) and the CP force on an excited atom. To that end, we consider the Casimir force on an optically dilute amplifying body of volume V placed in a free-space region in an environment of purely absorbing bodies.

We consider first the nonresonant contribution and make use of the fact that the amplifying body is assumed to be optically dilute by expanding the result (4.61) to leading, linear order in the susceptibilities $\varepsilon(\mathbf{r}, \omega) - 1$ and $1 - 1/\mu(\mathbf{r}, \omega)$ where $\mathbf{r} \in V$. Since these susceptibilities already explicitly appear as factors in the above expression, the Green tensors have to be expanded to zeroth order in these functions. In other words, we have to replace $\boldsymbol{G}^{(1)}$ with the Green tensor $\overline{\boldsymbol{G}}^{(1)}$ of the system in the absence of the amplifying body, which is the solution to the Helmholtz equation (2.20) with

$$\overline{\varepsilon}(\mathbf{r}, \omega), \overline{\mu}(\mathbf{r}, \omega) = \begin{cases} \varepsilon(\mathbf{r}, \omega), \mu(\mathbf{r}, \omega) & \text{for } \mathbf{r} \notin V, \\ 1 & \text{for } \mathbf{r} \in V \end{cases} \quad (4.62)$$

in place of $\varepsilon(\mathbf{r}, \omega)$ and $\mu(\mathbf{r}, \omega)$.

Let us assume that the amplifying body consists of a dilute medium of isotropic atoms in an excited state $|n\rangle$, transition frequencies ω_{nk}, polarizability α_n and magnetizability β_n [recall Eqs. (2.54), (2.62)]. The electric and magnetic susceptibilities of the body are related to the atomic polarizability and magnetizability via the linearized Clausius–Mossotti laws

$$\varepsilon(\omega) - 1 = \frac{\eta \alpha_n(\omega)}{\varepsilon_0}, \qquad 1 - \frac{1}{\mu(\omega)} = \mu_0 \eta \beta_n(\omega), \quad (4.63)$$

where η denotes the atomic number density. Thus we finally obtain

$$\mathbf{F}^{\mathrm{nres}} = -\int \mathrm{d}^3 r \eta \boldsymbol{\nabla} U_n^{\mathrm{nres}}(\mathbf{r}) \quad (4.64)$$

where U_n^{nres} is the combination of electric and the magnetic CP potential as given by

Eqs. (2.53) and (2.63):

$$
\begin{aligned}
U_n^{\mathrm{nres}}(\mathbf{r}) = & \frac{\hbar\mu_0}{2\pi} \int_0^\infty \mathrm{d}\xi \Big\{ \xi^2 \alpha_n(i\xi) \mathrm{tr}\overline{\mathbf{G}}^{(1)}(\mathbf{r},\mathbf{r},i\xi) \\
& + \beta_n(i\xi) \mathrm{tr}\big[\boldsymbol{\nabla} \times \overline{\mathbf{G}}^{(1)}(\mathbf{r},\mathbf{r},i\xi) \times \overleftarrow{\boldsymbol{\nabla}}' \big]_{\mathbf{r}'\to\mathbf{r}} \Big\}.
\end{aligned}
\tag{4.65}
$$

The nonresonant Casimir force on an optically dilute amplifying body is hence a summation over the respective nonresonant CP forces on the excited atoms the body consists of. However, there is one important difference to the case of the force on an absorbing object which consists of ground-state atoms: While for ground-state atoms the frequencies ω_{kn} in Eqs. (2.54) and (2.62) are positive so that all (virtual) transitions contribute to the nonresonant CP potential with the same sign, upward as well as downward transitions are possible for excited atoms, so that positive and negative ω_{kn} occur. In particular for a two-level atom, the nonresonant CP force for the atom in its excited state is exactly opposite to the respective ground-state force.

Let us next consider the resonant Casimir force $\mathbf{F}^{\mathrm{res}}$, which is only present for an amplifying body, by following essentially the same steps as for the nonresonant force. We first recall that the real parts of the conductivity tensor contributions read

$$
\mathrm{Re}\,\boldsymbol{Q}_e(\mathbf{r},\mathbf{r}',\omega) = \varepsilon_0 \omega \varepsilon_I(\mathbf{r},\omega) \delta(\mathbf{r}-\mathbf{r}')\boldsymbol{I},
\tag{4.66}
$$

$$
\mathrm{Re}\,\boldsymbol{Q}_m(\mathbf{r},\mathbf{r}',\omega) = -\frac{1}{\mu_0\omega}\boldsymbol{\nabla} \times \frac{\mu_I(\mathbf{r},\omega)}{|\mu_I(\mathbf{r},\omega)|^2}\delta(\mathbf{r}-\mathbf{r}')\boldsymbol{I} \times \overleftarrow{\boldsymbol{\nabla}}',
\tag{4.67}
$$

where the (imaginary parts of the) susceptibilities of the amplifying body are already explicitly present at this stage. A linear approximation in these susceptibilities in Eq. (4.53) can hence be obtained by using the zeroth-order identities

$$
\left(\boldsymbol{\nabla} \times \boldsymbol{\nabla} \times -\frac{\omega^2}{c^2} \right) \boldsymbol{G}(\mathbf{r},\mathbf{r}',\omega) = \boldsymbol{I}\delta(\mathbf{r}-\mathbf{r}'),
\tag{4.68}
$$

$$
\frac{\omega^2}{c^2}\boldsymbol{\nabla} \cdot \boldsymbol{G}(\mathbf{r},\mathbf{r}',\omega) = -\boldsymbol{\nabla}\delta(\mathbf{r}-\mathbf{r}'),
\tag{4.69}
$$

as following from Eq. (2.20), and replacing $\boldsymbol{G}^*$ with $\overline{\boldsymbol{G}}^*$. Expanding the result with the aid of Eqs. (4.57) and discarding terms involving total divergences for a body in

free space, we find

$$
\mathbf{F}^{\mathrm{res}} = -\frac{\hbar}{\pi} \int_V \mathrm{d}^3 r \int_0^\infty \mathrm{d}\omega \bigg\{ \Theta[-\varepsilon_I(\mathbf{r},\omega)] \frac{\omega^2}{c^2} \varepsilon_I(\mathbf{r},\omega) \boldsymbol{\nabla} \operatorname{tr} \operatorname{Re} \boldsymbol{G}^{(1)}(\mathbf{r},\mathbf{r},\omega)
$$
$$
- \Theta[-\mu_I(\mathbf{r},\omega)] \frac{\mu_I(\mathbf{r},\omega)}{|\mu(\mathbf{r},\omega)|^2} \boldsymbol{\nabla} \operatorname{tr}\big[\boldsymbol{\nabla} \times \operatorname{Re} \boldsymbol{G}^{(1)}(\mathbf{r},\mathbf{r}',\omega) \times \overleftarrow{\boldsymbol{\nabla}}'\big]_{\mathbf{r}' \to \mathbf{r}} \bigg\} \quad (4.70)
$$

where we again have performed the coincidence limit by replacing the Green tensor with its scattering part.

Relating ε_I and μ_I to the polarizability and magnetizability of the atoms by means of the Clausius–Mossotti relation (4.63), we finally obtain

$$
\mathbf{F}^{\mathrm{res}} = -\int \mathrm{d}^3 r \eta \boldsymbol{\nabla} U_n^{\mathrm{res}}(\mathbf{r}), \qquad (4.71)
$$

where

$$
U_n^{\mathrm{res}}(\mathbf{r}) = \frac{\hbar\mu_0}{\pi} \int_0^\infty \mathrm{d}\omega \bigg\{ \Theta[-\operatorname{Im}\alpha_n(\omega)] \operatorname{Im}\alpha_n(\omega) \omega^2 \operatorname{tr} \operatorname{Re} \boldsymbol{G}^{(1)}(\mathbf{r},\mathbf{r},\omega)
$$
$$
- \Theta[-\operatorname{Im}\beta_n(\omega)] \operatorname{Im}\beta_n(\omega) \operatorname{tr}\big[\boldsymbol{\nabla} \times \operatorname{Re} \boldsymbol{G}^{(1)}(\mathbf{r},\mathbf{r}',\omega) \times \overleftarrow{\boldsymbol{\nabla}}'\big]_{\mathbf{r}' \to \mathbf{r}} \bigg\} \quad (4.72)
$$

is the resonant part of the CP potential of the excited atoms contained in the body. By means of the identity

$$
\lim_{\epsilon \to 0} 1/(x + i\epsilon) = \mathcal{P}/x - i\pi\delta(x), \qquad (4.73)
$$

where $\mathcal{P}$ denotes the principal value, the imaginary parts of polarizability and magnetizability, as given by Eqs. (2.54) and (2.62), can be written in the form

$$
\alpha_I(\omega) = \frac{\pi}{3\hbar} \sum_k |\mathbf{d}_{nk}|^2 [\delta(\omega + \omega_{nk}) - \delta(\omega - \omega_{nk})], \qquad (4.74)
$$
$$
\beta_I(\omega) = \frac{\pi}{3\hbar} \sum_k |\mathbf{m}_{nk}|^2 [\delta(\omega + \omega_{nk}) - \delta(\omega - \omega_{nk})]. \qquad (4.75)
$$

Hence, the resonant CP potential can be derived to be

$$
U_n^{\mathrm{res}}(\mathbf{r}) = -\frac{\mu_0}{3} \sum_k \Theta(\omega_{nk}) \Big\{ \omega_{nk}^2 |\mathbf{d}_{nk}|^2 \operatorname{tr} \operatorname{Re} \boldsymbol{G}^{(1)}(\mathbf{r},\mathbf{r},\omega_{nk})
$$
$$
- |\mathbf{m}_{nk}|^2 \operatorname{tr}\big[\boldsymbol{\nabla} \times \operatorname{Re} \boldsymbol{G}^{(1)}(\mathbf{r},\mathbf{r},\omega) \times \overleftarrow{\boldsymbol{\nabla}}'\big]_{\mathbf{r}' \to \mathbf{r}} \Big\}. \qquad (4.76)
$$

The potential (4.76) generalizes previous results for purely electric atoms [113], as given in Eq. (2.55), to the magnetoelectric case. The resonant part of the CP potential is associated with real, energy-conserving transitions of the excited atom to lower states. As expected, the resonant part of the CP potential of an excited atom in free space is duality-invariant, just like the nonresonant part [136].

Combining our results (4.64) and (4.71), in accordance with Eq. (4.51), we have shown that the Casimir force on an optically dilute, homogeneous, amplifying magnetoelectric body is the sum of the CP forces on the excited atoms contained in it,

$$\mathbf{F} = -\int \mathrm{d}^3 r \eta \boldsymbol{\nabla} U_n(\mathbf{r}). \tag{4.77}$$

This result generalizes similar findings for purely absorbing bodies (consisting of ground-state atoms) [9, 10, 154, 164] to the amplifying case. In addition, our calculation has rendered explicit expressions for the free-space CP potential of excited magnetoelectric atoms in the presence of an arbitrary arrangement of absorbing bodies,

$$U_n(\mathbf{r}) = U_n^{\mathrm{nres}}(\mathbf{r}) + U_n^{\mathrm{res}}(\mathbf{r}), \tag{4.78}$$

with U_n^{nres} and U_n^{res} being given by Eqs. (4.65) and (4.76), respectively. In this dilute-medium limit, the nonresonant and resonant components of the Casimir force (4.52) and (4.53) are directly related to the respective CP potential components which in turn are associated with virtual and real transitions of the atoms. The most important difference between forces on ground-state versus excited atoms is the contribution from possible real transitions only present for excited atoms, which manifests itself as the resonant contribution (4.53) of the Casimir force. Note that the established direct relation between Casimir forces and single-atom CP forces is only valid for dilute media, while for bodies with stronger magnetoelectric properties, many-atom interactions begin to play a role and lead to a breakdown of additivity (see e.g., Refs. [9, 154]).

Stress tensor approach

For bodies with simple surfaces, it is convenient to transform the volume integral (4.39) into a surface integral over the outer boundaries of the bodies. We rewrite the Lorentz force density in the form [105]

$$\mathbf{f}(\mathbf{r}) = \hat{\rho}(\mathbf{r})\hat{\mathbf{E}}(\mathbf{r}) + \hat{\mathbf{j}}(\mathbf{r}) \times \hat{\mathbf{B}}(\mathbf{r}) = \boldsymbol{\nabla}\boldsymbol{T}(\mathbf{r}) - \varepsilon_0 \frac{\partial}{\partial t}\left[\hat{\mathbf{E}}(\mathbf{r}) \times \hat{\mathbf{B}}(\mathbf{r})\right], \tag{4.79}$$

where we have introduced the symmetric Maxwell's stress tensor

$$\boldsymbol{T}(\mathbf{r}) = \lim_{\mathbf{r'} \to \mathbf{r}} \boldsymbol{T}(\mathbf{r}, \mathbf{r'}) = \varepsilon_0 \langle\{0\}| \hat{\mathbf{E}}(\mathbf{r})\hat{\mathbf{E}}(\mathbf{r'}) |\{0\}\rangle + \mu_0^{-1} \langle\{0\}| \hat{\mathbf{B}}(\mathbf{r})\hat{\mathbf{B}}(\mathbf{r'}) |\{0\}\rangle$$
$$- \frac{1}{2}\big(\varepsilon_0 \langle\{0\}| \hat{\mathbf{E}}(\mathbf{r}) \cdot \hat{\mathbf{E}}(\mathbf{r'}) |\{0\}\rangle + \mu_0^{-1} \langle\{0\}| \hat{\mathbf{B}}(\mathbf{r}) \cdot \hat{\mathbf{B}}(\mathbf{r'}) |\{0\}\rangle\big)\boldsymbol{I}. \quad (4.80)$$

Note that in other references the Abraham–Minkowski's stress tensor is used [106–108], which is not consistent with the Lorentz-force formulation [165]. The two proposed approaches, however, Maxwell versus Abraham-Minkowski's stress tensor, coincide if the body under consideration is placed in a free-space region [105]. For velocity-independent systems, the Casimir force reduces to a surface integral over the stress tensor

$$\mathbf{F} = \int_{\partial V} \mathrm{d}\mathbf{a} \cdot \boldsymbol{T}(\mathbf{r}). \quad (4.81)$$

Let us now calculate the field correlation functions appearing in the stress tensor. The correlation functions of the electric field can be obtained by combining Eqs. (2.16) and (4.41)–(4.42),

$$\langle 0|\hat{\mathbf{E}}(\mathbf{r})\hat{\mathbf{E}}(\mathbf{r'})|0\rangle = \frac{\hbar}{\pi\varepsilon_0} \int_0^\infty \mathrm{d}\omega \frac{\omega^2}{c^2} \mathrm{Im}\boldsymbol{G}(\mathbf{r},\mathbf{r'},\omega) - 2\frac{\hbar}{\pi\varepsilon_0} \int \mathrm{d}^3 s \int_0^\infty \mathrm{d}\omega \frac{\omega^2}{c^2}\mu_0\omega$$
$$\times \sum_{\lambda=e,m} \int \mathrm{d}^3 s' \mathrm{Re}\big[\boldsymbol{G}(\mathbf{r},\mathbf{s},\omega) \cdot \mathrm{Re}\,\boldsymbol{Q}_\lambda(\mathbf{s},\mathbf{s'},\omega) \cdot \boldsymbol{G}^*(\mathbf{s},\mathbf{r'},\omega)\big]\Theta[-\mathrm{Im}\,\kappa_\lambda(\mathbf{s},\omega)], \quad (4.82)$$

where we have again used the identity $\Theta(x) + \Theta(-x) = 1$ together with the integral relation (2.24). For a purely electric system, Eq. (4.82) takes the form

$$\langle 0|\hat{\mathbf{E}}(\mathbf{r})\hat{\mathbf{E}}(\mathbf{r'})|0\rangle = -\frac{\hbar}{\pi\varepsilon_0} \int_0^\infty \mathrm{d}\xi \frac{\xi^2}{c^2}\boldsymbol{G}(\mathbf{r},\mathbf{r'},i\xi) - 2\frac{\hbar}{\pi\varepsilon_0} \int \mathrm{d}^3 s \int_0^\infty \mathrm{d}\omega \frac{\omega^4}{c^4}\mathrm{Im}\,\varepsilon(\mathbf{s},\omega)$$
$$\times \mathrm{Re}[\boldsymbol{G}(\mathbf{r},\mathbf{s},\omega) \cdot \boldsymbol{G}^*(\mathbf{s},\mathbf{r'},\omega)]\Theta[-\varepsilon_I(\mathbf{s},\omega)], \quad (4.83)$$

where we have already expressed the first term as an integral over imaginary frequencies in the familiar manner. In a similar way, by means of Eqs. (2.17), (4.41)–(4.42)

and (2.24), we obtain

$$
\langle 0|\hat{\mathbf{B}}(\mathbf{r})\hat{\mathbf{B}}(\mathbf{r}')|0\rangle = -\frac{\hbar}{\pi\varepsilon_0}\int_0^\infty \mathrm{d}\omega \frac{1}{c^2}\boldsymbol{\nabla}\times\mathrm{Im}\,\boldsymbol{G}(\mathbf{r},\mathbf{r}',\omega)\times\overleftarrow{\boldsymbol{\nabla}}' - 2\frac{\hbar}{\pi\varepsilon_0}\int \mathrm{d}^3 s\int_0^\infty \mathrm{d}\omega\frac{\mu_0\omega}{c^2}
$$
$$
\times\sum_{\lambda=e,m}\int \mathrm{d}^3 s'\mathrm{Re}[\boldsymbol{\nabla}\times\boldsymbol{G}(\mathbf{r},\mathbf{s},\omega)\cdot\mathrm{Re}\,\boldsymbol{Q}_\lambda(\mathbf{s},\mathbf{s}',\omega)\cdot\boldsymbol{G}^*(\mathbf{s}',\mathbf{r}',\omega)\times\overleftarrow{\boldsymbol{\nabla}}']\Theta[-\mathrm{Im}\,\kappa_\lambda(\mathbf{s},\omega)],
$$
$$
(4.84)
$$

which for a purely electric system reduces to

$$
\langle 0|\hat{\mathbf{B}}(\mathbf{r})\hat{\mathbf{B}}(\mathbf{r}')|0\rangle = -\frac{\hbar\mu_0}{\pi}\int_0^\infty \mathrm{d}\xi\boldsymbol{\nabla}\times\boldsymbol{G}(\mathbf{r},\mathbf{r}',i\xi)\times\overleftarrow{\boldsymbol{\nabla}}' - 2\frac{\hbar\mu_0}{\pi}\int \mathrm{d}^3 s\int_0^\infty \mathrm{d}\omega\frac{\omega^2}{c^2}\varepsilon_I(\mathbf{s},\omega)
$$
$$
\times\mathrm{Re}[\boldsymbol{\nabla}\times\boldsymbol{G}(\mathbf{r},\mathbf{s},\omega)\cdot\boldsymbol{G}^*(\mathbf{s}',\mathbf{r}',\omega)\times\overleftarrow{\boldsymbol{\nabla}}']\Theta[-\varepsilon_I(\mathbf{s},\omega)]. \quad (4.85)
$$

It should be emphasized that the terms proportional to $\Theta[-\varepsilon_I]$, $\Theta[-\mu_I]$ cannot be expressed in terms of imaginary frequencies since the integrand is not an analytic function. Note that the space integral runs over a finite region such that the integral relation (2.24) cannot be applied.

4.2.2 Planar geometry

As an example, let us calculate the Casimir force on an amplifying, purely electric slab of thickness d_3 and permittivity ε_3, where $\mathrm{Im}\,\varepsilon_3 < 0$ for a limited frequency interval, and an electric (absorbing) half space of permittivity ε_1 is placed at a distance of d_2 from the slab. The setup is sketched in Fig. 4.9. Note that this is one of the simplest
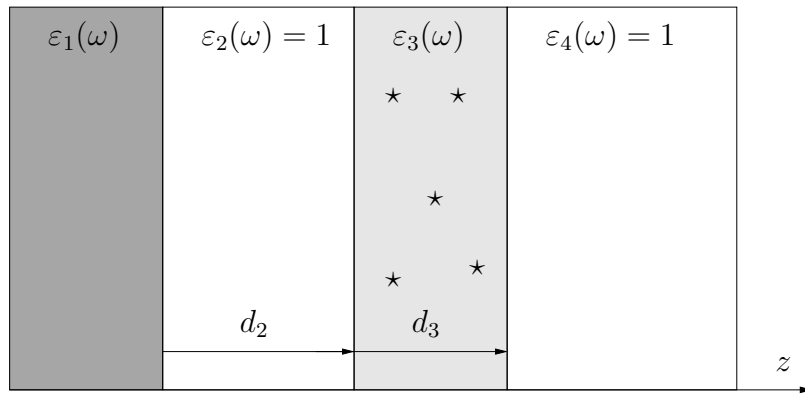
Figure 4.9: 4-layer structure electric half space − vacuum − amplifying slab− vacuum

possible planar geometries that can be studied in the presence of amplification. The

seemingly simpler case of an amplifying semi-infinite half space would immediately lead to unphysical results since the amplitudes of the propagating waves would become arbitrarily large.

Dilute-medium approximation

Let us first study the case where the slab is optically dilute and consists of excited, purely electric, isotropic (two-level) atoms. Here, we will only consider the dominant resonant component of the Casimir force, $\mathbf{F} \approx \mathbf{F}^{\mathrm{res}}$, as given by Eq. (4.71) together with Eq. (4.76). As a simple example, we assume the half space in region 1 to be a perfect mirror. In that case, the associated Green tensor is given in Eqs. (4.22) and (4.23), and the Casimir force per unit area on the weakly polarizable slab is given by

$$
\begin{aligned}
\mathbf{F}(d_2) &= \frac{\mu_0}{3}\eta\omega_{10}^2|\mathbf{d}_{10}|^2 \int_{d_2}^{d_2+d_3} \mathrm{d}z_A \frac{\partial}{\partial z_A}\mathrm{Re}\, G_{ii}^{(1)}(\mathbf{r}_A,\mathbf{r}_A,\omega)\mathbf{e}_z \\
&= \frac{\mu_0}{12\pi c}\eta\omega_{10}^3\frac{|\mathbf{d}_{10}|^2}{\tilde{z}^3}\left[(2-\tilde{z}^2)\cos(\tilde{z})+2\tilde{z}\sin(\tilde{z})\right]_{z_A=d_2}^{z_A=d_2+d_3}\mathbf{e}_z,
\end{aligned} \qquad (4.86)
$$

where here $\tilde{z}=2z_A\omega_{10}/c$, and η denotes the density of atoms in the slab. On recalling our results from Sec. 4.1.1, Eq. (4.6) in the limit $\varepsilon_1 \to \infty$, we find an attractive Casimir force in the nonretarded limit,

$$
\mathbf{F}(d_2) = -\frac{|\mathbf{d}_{10}|^2}{24\pi\varepsilon_0}\left[\frac{1}{d_2^3}-\frac{1}{(d_2+d_3)^3}\right], \qquad (4.87)
$$

where we have used that for isotropic atoms $|\mathbf{d}^{\parallel}|^2 = 2|\mathbf{d}^{\perp}|^2 = 2/3|\mathbf{d}|^2$. Accordingly, on recalling Eq. (4.10), we find the force in the retarded limit,

$$
\mathbf{F}(d_2) = -\frac{\eta\mu_0\omega_{10}^2|\mathbf{d}_{10}|^2}{12\pi}\left[\frac{\cos(2(d_2+d_3)\omega_{10}/c)}{d_2+d_3}-\frac{\cos(2d_2\omega_{10}/c)}{d_2}\right]. \qquad (4.88)
$$

Figure (4.10) shows the (dimensionless) Casimir force per thickness d_3 of the slab as a function of the slab–mirror separation. For reference, we have also displayed the resonant part of the CP force on the individual atoms contained in the slab. It can be seen that the Casimir force on the amplifying slab near a perfect mirror shows an attractive behavior in the short-distance regime while for large slab–mirror separations an oscillating behavior is observed. This is a direct consequence of the respective behavior of the CP forces on the atoms contained in the slab. The amplitude
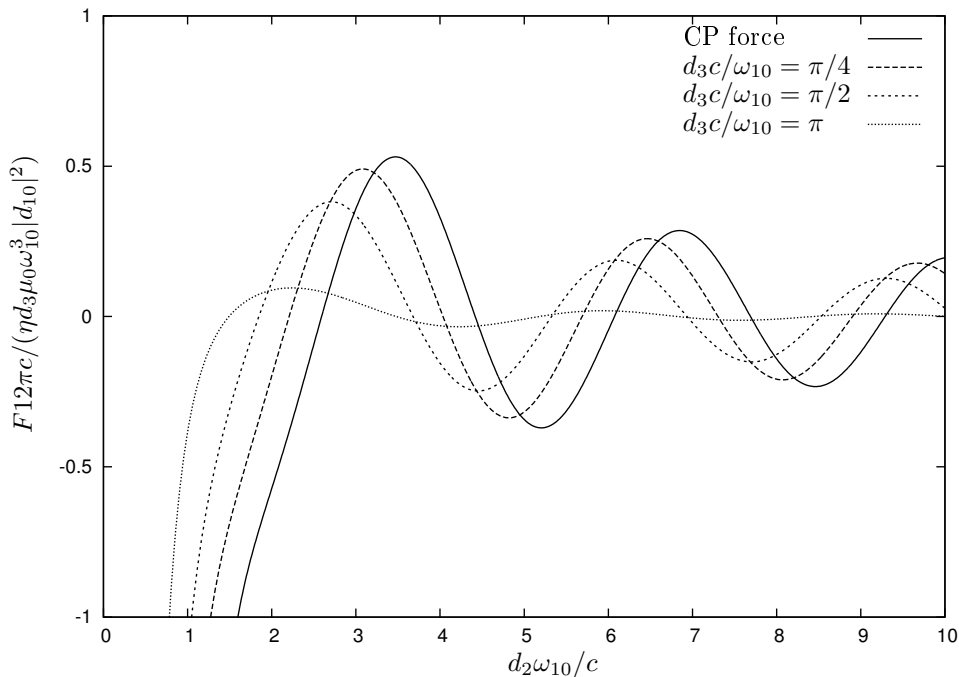
Figure 4.10: Resonant Casimir force (per thickness d_3) between a planar, optically dilute sample of excited atoms and a perfect mirror plotted vs. the slab–mirror distance. The atomic dipole moments are oriented parallel to the surface. The solid line shows the resonant CP force on each excited atom.

of the oscillations decreases with increasing thickness of the slab, since the integrated Casimir force per slab thickness is a spatial average of the oscillating CP forces over the slab thickness. The occurrence of oscillations can be regarded as a typical impact of amplification on the Casimir force.

It should be pointed out that the Casimir force can also be repulsive in the non-retarded limit when the perfect mirror is replaced by a dielectric half space. As can be seen from the excited-atom potential (4.6), the nonretarded Casimir force is then given by Eq. (4.87) multiplied by $(|\varepsilon_1(\omega_{10})|^2 - 1)/(|\varepsilon_1(\omega_{10}) + 1|^2)$. Thus, we find repulsion if $|\varepsilon_1(\omega_{10})| < 1$.

Casimir force on a non-dilute slab

In the following, we investigate whether the results from the dilute-medium approximation qualitatively also hold beyond this limit. For the planar 4-layer geometry under consideration (recall Fig. 4.9), it is convenient to calculate the Casimir force in the stress tensor formulation, i.e., substituting the correlation functions (4.83) and (4.85) into Eq. (4.80) together with Eq. (4.81). The Casimir force per unit area is thus

given by the sum of the stress tensor elements T_{zz} on the two boundaries of the slab,

$$\mathbf{f} = \mathbf{f}^r - \mathbf{f}^l = \left[\boldsymbol{T}^r_{zz}(\mathbf{r})|_{z=0} - \boldsymbol{T}^l_{zz}(\mathbf{r})|_{z=d_2} \right] \mathbf{e}_z. \qquad (4.89)$$

Here, the index r denotes the force component acting on the right boundary of the slab, i.e., $\mathbf{r}, \mathbf{r}'$ are located in layer 4. To calculate the force acting on the left boundary, $\mathbf{f}^l$, we have to take the relevant stress tensor element with $\mathbf{r}, \mathbf{r}'$ pointing into layer 2. The minus sign in Eq. (4.89) arises from the fact that the surface vector points in the negative z direction for the force acting on the left boundary of the slab. Note that for realistic systems with finite lateral extension, our results can still provide an approximation by integrating the force density over the finite area of the slab. Such an approximation is reasonable as long as the lateral extensions of the system are large compared to the separation between the slabs. In this case effects arising from the edges of the slabs can be neglected. We have explicitly checked that Eq. (4.89) ensures that the Casimir force on the amplifying slab vanishes in the absence of the half space.

The correlation functions (4.83) and (4.85) contain two terms each; one that involves the full frequency integral leading to a nonresonant force contribution as can be expected from our results in Sec. 4.2.1, and a second term being proportional to $\Theta[-\varepsilon_I(\mathbf{s}, \omega)]$ which genuinely arises from the presence of amplification and leads to a resonant force component. Thus, we decompose the Casimir force per unit area according to Eq. (4.51),

$$\mathbf{f} = \mathbf{f}^{\mathrm{nres}} + \mathbf{f}^{\mathrm{res}}. \qquad (4.90)$$

We first study the nonresonant contribution to the Casimir force in which case the stress tensor can be written in the form

$$\boldsymbol{T}(\mathbf{r}) = -\frac{\hbar}{\pi} \int_0^\infty \mathrm{d}\xi \left\{ \frac{\xi^2}{c^2} \boldsymbol{G}^{(1)}(\mathbf{r}, \mathbf{r}, i\xi) + \boldsymbol{\nabla} \times \boldsymbol{G}^{(1)}(\mathbf{r}, \mathbf{r}', i\xi) \times \overset{\leftarrow}{\boldsymbol{\nabla}}'|_{\mathbf{r}'=\mathbf{r}} \right.$$
$$\left. -\frac{1}{2} \mathrm{tr} \left[\frac{\xi^2}{c^2} \boldsymbol{G}^{(1)}(\mathbf{r}, \mathbf{r}, i\xi) + \boldsymbol{\nabla} \times \boldsymbol{G}^{(1)}(\mathbf{r}, \mathbf{r}', i\xi) \times \overset{\leftarrow}{\boldsymbol{\nabla}}'|_{\mathbf{r}'=\mathbf{r}} \right] \boldsymbol{I} \right\}, \quad (4.91)$$

where the scattering Green tensor (with $\mathbf{r}$ and $\mathbf{r}'$ in the same layer 2) can be found e.g., in Ref. [132]. The nonresonant Casimir force found formally looks like the corre-

sponding ground-state result [1],

$$\mathbf{f}^{\mathrm{nres}} = -\frac{\hbar}{2\pi^2} \int_0^\infty \mathrm{d}\xi \int_0^\infty \mathrm{d}k^\| k^\| \kappa^\perp \sum_{\sigma=s,p} \frac{r_{2+}^\sigma r_{21}^\sigma e^{-2\kappa^\perp d_2}}{1 - r_{21}^\sigma r_{2+}^\sigma e^{-2\kappa^\perp d_2}} \mathbf{e}_z, \qquad (4.92)$$

where

$$r_{2+}^\sigma = \frac{r_{23}^\sigma\left(1 - e^{-2\kappa_3^\perp d_3}\right)}{1 - r_{23}^{\sigma 2} e^{-2\kappa_3^\perp d_3}} \qquad (4.93)$$

together with the single-layer reflection coefficients (3.13), and $\kappa_1^\perp \equiv \kappa^\perp$ as defined in Eq. (3.14). It should be emphasized that the imaginary part of the wave vector component in the z-direction is always real for positive $\varepsilon_3(i\xi)$ and thus unambiguously given as $\kappa_3^\perp = \sqrt{\varepsilon_3(i\xi)\omega^2/c^2 + k^{\|2}}$.

The nonretarded and retarded limits can be obtained in analogy to the same asymptotic limits of the ground-state force between two half spaces. For simplicity we restrict our attention to a sufficiently thick slab, $d_3 \gg d_2$. Note that the nonresonant force remains finite in this limit ($d_3 \to \infty$), and we approximate $r_{2+}^\sigma = r_{23}^\sigma$. We find for the nonretarded force

$$\mathbf{f}^{\mathrm{nres}}\big|_{d_3\to\infty} = \frac{\hbar}{8\pi^2 d_2^3} \int_0^\infty \mathrm{d}\xi \mathrm{Li}_3\left[\frac{1-\varepsilon_3(i\xi)}{\varepsilon_3(i\xi)+1}\frac{\varepsilon_1(i\xi)-1}{\varepsilon_1(i\xi)+1}\right]\mathbf{e}_z, \qquad (4.94)$$

where $\mathrm{Li}_n(z) = \sum_{k=1}^\infty z^k/k^n$ defines the polylogarithm function. In particular, we have $\mathrm{Li}_3(x) \approx 1.2x$ for $0 \le x \le 1$. Similarly, we obtain the Casimir force in the retarded limit,

$$\mathbf{f}_{\mathrm{ret}} = \frac{3\hbar c}{16\pi^2 d_2^4} \int_1^\infty \frac{\mathrm{d}v}{v^2}\left\{\mathrm{Li}_4\left[\frac{v-\sqrt{\varepsilon_1-1+v^2}}{v+\sqrt{\varepsilon_1-1+v^2}}\frac{\sqrt{\varepsilon_3-1+v^2}-v}{v+\sqrt{\varepsilon_3-1+v^2}}\right]\right.$$
$$\left. + \mathrm{Li}_4\left[\frac{\varepsilon_1 v-\sqrt{\varepsilon_1-1+v^2}}{\varepsilon_1 v+\sqrt{\varepsilon_1-1+v^2}}\frac{\sqrt{\varepsilon_3-1+v^2}-\varepsilon_3 v}{\varepsilon_3 v+\sqrt{\varepsilon_3-1+v^2}}\right]\right\}\mathbf{e}_z, \quad (4.95)$$

where $\mathrm{Li}_4(x) \approx x\pi^4/90$ for $0 \le x \le 1$. If amplification is present in a sufficiently large frequency regime where

$$0 < \varepsilon_3(i\xi) = 1 - \frac{\omega_P^2}{\xi^2 + \omega_t^2 + \xi\gamma} < 1, \qquad (4.96)$$

---

[1]Note that the most simple absorbing geometry typically consists of two half spaces separated by a free-space region, see e.g., Ref. [105].

we immediately see from the nonretarded and retarded results that the nonresonant Casimir force is repulsive. Note that the case of $\varepsilon_3(i\xi) < 0$ would correspond to a very large amount of amplification which cannot be considered by means of linear QED (see also the example below).

In Ref. [70], the total Casimir force is identified with the purely nonresonant term and it is suggested that it may be repulsive. However, the presence of amplification is not taken into account in the quantization scheme used. On using a path-integral approach, a planar system consisting of two perfect mirrors enclosing an amplifying slab is studied in Ref. [166] . The proposed (attractive) Casimir force is again purely nonresonant. In my opinion, resonant force components can crucially contribute to the total Casimir force and should be carefully investigated, as we will do in the following.

To calculate $\mathbf{f}^{\mathrm{res}}$, we basically have to calculate the product $\boldsymbol{G}(\mathbf{r}, \mathbf{s}) \cdot \boldsymbol{G}^*(\mathbf{s}, \mathbf{r}')$ as can be seen from the correlation functions (4.83) and (4.85) together with Eqs. (4.80) and (4.89). To that end, we have to study the relevant 4-layer Green tensor. However, in the presence of amplification, the correct choice of the wave vector perpendicular to the slab must be chosen with care. To elucidate (and solve) the problem, we first study the corresponding bulk Green tensor of an amplifying, right-handed medium in the planar-wave expansion (Weyl expansion) for the special choice of $\mathbf{r} = \mathbf{0}$ and $\mathbf{r}' = (0, 0, z)$ [151],

$$
\boldsymbol{G}^{(0)}(\mathbf{r}, \mathbf{r}', \omega) = \frac{i}{8\pi} \int_0^\infty \frac{\mathrm{d}k^\| k^\|}{k^\perp} e^{ik^\perp z}
\begin{pmatrix}
1 + \frac{k^{\perp 2}}{k^2} & 0 & 0 \\
0 & 1 + \frac{k^{\perp 2}}{k^2} & 0 \\
0 & 0 & 2\frac{k^{\| 2}}{k^2}
\end{pmatrix},
\tag{4.97}
$$

where here the wave vector $\mathbf{k}$ is decomposed as in a planar system according to $\mathbf{k}^\perp = (0, 0, k_z)$ and $\mathbf{k}^\| = (k_x, k_y, 0)$. The imaginary part of the permittivity of an amplifying (right-handed) medium is negative, $\mathrm{Im}\,\varepsilon < 0$, which implies that also $\mathrm{Im}\,k^{\perp 2} < 0$, as can be seen from $k^{\perp 2} = \varepsilon\omega^2/c - k^{\| 2}$. Thus, $k^{\perp 2}$ lies in the third (evanescent waves) and fourth (propagating waves) quadrant of the complex plane. While propagating waves are amplified when traveling through an amplifying medium, manifesting in $\mathrm{Im}\,k^\perp < 0$, the situation for the evanescent contributions, where $\mathrm{Re}\,k^{\perp 2} < 0$, has been controversially discussed in the literature [90, 167, 168].

To proceed, we change the integration variable according to $\mathrm{d}k^\| = -k^\perp \mathrm{d}k^\perp/k^\|$. The basic physical requirement that the amplitude of the propagating modes should be amplified implies that for $k^\| = 0$ the new lower bound uniquely reads $k^\perp = \sqrt{\varepsilon}\omega/c = k$

with $\text{Im}\sqrt{\varepsilon} < 0$. For the new upper bound, corresponding to arbitrarily large values of $k^{\parallel}$, we have $k^{\perp} = \pm i\infty$, where the sign is yet to be determined. Hence, we have

$$\boldsymbol{G}^{(0)}(\mathbf{r}, \mathbf{r}', \omega) = -\frac{i}{8\pi} \int_{k}^{\pm i\infty} \mathrm{d}k^{\perp} e^{ik^{\perp}z} \begin{pmatrix} 1 + \frac{k^{\perp 2}}{k^2} & 0 & 0 \\ 0 & 1 + \frac{k^{\perp 2}}{k^2} & 0 \\ 0 & 0 & 2 - 2\frac{k^{\perp 2}}{k^2} \end{pmatrix}. \qquad (4.98)$$

To determine the correct choice of the square root in $k^{\perp}$, we require Eq. (4.98) to agree with the explicit expression of the bulk Green tensor, Eq. (3.66),

$$\boldsymbol{G}^{(0)}(\mathbf{r}, \mathbf{r}', \omega) = -\frac{e^{ikz}}{4\pi k^2 z^3} \begin{pmatrix} 1 - ikz - (kz)^2 & 0 & 0 \\ 0 & 1 - ikz - (kz)^2 & 0 \\ 0 & 0 & -2(1 - ikz) \end{pmatrix} \qquad (4.99)$$

which is finite for finite z, despite the boundary condition at infinity for an infinitely extended amplifying medium, $\boldsymbol{G}(\mathbf{r}, \mathbf{r}', \omega) \to \infty$ as $|\mathbf{r}-\mathbf{r}'| \to \infty$. We see that Eqs. (4.98) and (4.99) coincide if we choose $k^{\perp} = +i\infty$ for the upper bound and if $k^{\perp}$ is continuous along the integration path. Thus, we are left with the following requirements to determine the correct square root,

$$k^{\perp}(\omega, k^{\parallel} = 0) = \sqrt{\varepsilon}\omega/c \quad \text{with} \quad \text{Im}\, k^{\perp} < 0 \quad \text{(propagating)} \qquad (4.100)$$

$$k^{\perp}(\omega, k^{\parallel} \to \infty) \to +i\infty \quad \text{(evanescent)}, \qquad (4.101)$$

which implies that the branch cut in the $k^{\perp 2}$ plane should be conveniently chosen along the negative imaginary axis. Our result is in agreement with Ref. [168]. We thus have the first Riemann sheet for $-\pi/2 < \theta < 3/2\pi$ and the second Riemann sheet for angles $3/2\pi < \theta < 7/2\pi$. As indicated in Fig. 4.11 the physically correct square root is given by

$$k^{\perp} = |k^{\perp}|e^{i\phi}, \quad -\pi/4 < \phi < 3/4\pi. \qquad (4.102)$$

In practice, we have to ensure that the integration path starts from $k^{\perp} = \sqrt{\varepsilon}\omega/c$ in the fourth quadrant and goes to $k^{\perp} \to i\infty$ but avoids the branch cut such that the choice of the branch of the square root is preserved and the integrand is continuous. A possible integration path is sketched in Fig. 4.11. In particular, $k^{\parallel}$ must be allowed to take complex values.

Let us now return to the problem at hand and consider the relevant Green tensors
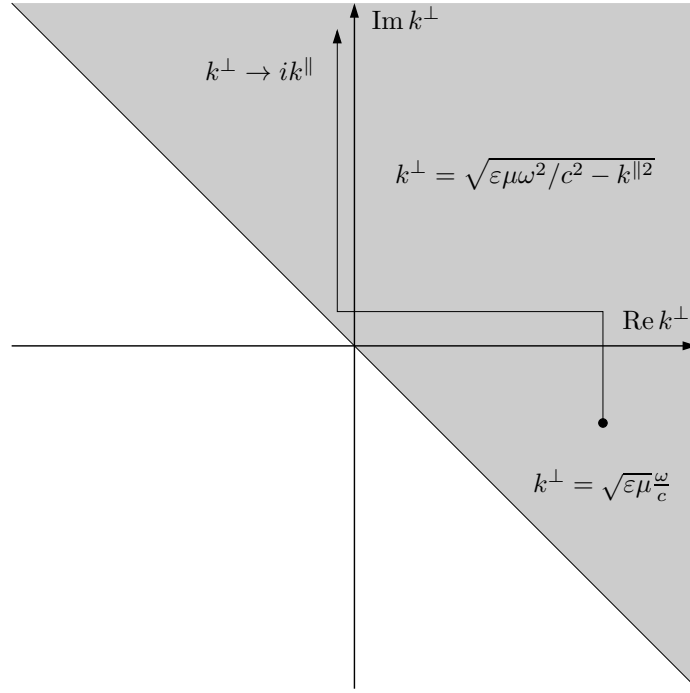
Figure 4.11: Correct choice of the wave vector in a right-handed amplifying medium (gray region). A possible integration path is indicated.

for the 4-layer geometry. In this case, we have three different values of ε_j, and hence $k_j^\perp$. For $k_3^\perp$ inside the amplifying slab, we recall our conditions (4.100) and (4.101). The common integration path for $k^\parallel$ must then be chosen such that the branch cut is avoided inside the amplifying slab.

For the force acting on the left boundary of the slab we need the Green tensor with $\mathbf{r}$ in layer 2 and $\mathbf{s}$ in layer 3, as given by [132],

$$
\boldsymbol{G}(\mathbf{r}, \mathbf{s}, \omega) = \frac{i}{8\pi^2} \int \mathrm{d}^2 k^\parallel \frac{e^{i\mathbf{k}^\parallel \cdot (\mathbf{r}-\mathbf{s})}}{k^\perp} \sum_{\sigma=s,p} \frac{t_{23}^\sigma e^{ik^\perp d_2}}{(1 - r_{34}^\sigma r_{3-}^\sigma e^{2ik_3^\perp d_3})(1 - r_{21}^\sigma r_{23}^\sigma e^{2ik^\perp d_2})}
$$
$$
\times \left(e^{-ik^\perp z} e^{ik_3^\perp s_z} \mathbf{e}_{2\sigma}^- \mathbf{e}_{3\sigma}^- + r_{34}^\sigma e^{-ik^\perp z} e^{-ik_3^\perp s_z} e^{2ik_3^\perp d_3} \mathbf{e}_{2\sigma}^- \mathbf{e}_{3\sigma}^+ \right.
$$
$$
\left. + r_{21}^\sigma e^{ik^\perp z} e^{ik_3^\perp s_z} \mathbf{e}_{2\sigma}^+ \mathbf{e}_{3\sigma}^- + r_{21}^\sigma r_{34}^\sigma e^{ik^\perp z} e^{-ik_3^\perp s_z} e^{2ik_3^\perp d_3} \mathbf{e}_{2\sigma}^+ \mathbf{e}_{3\sigma}^+ \right), \quad (4.103)
$$

and, by using $\boldsymbol{G}(\mathbf{s}, \mathbf{r}') = \boldsymbol{G}^\top(\mathbf{r}', \mathbf{s})$, we also find

$$
\boldsymbol{G}^*(\mathbf{s}, \mathbf{r}', \omega) = \frac{-i}{8\pi^2} \int \mathrm{d}^2 k^{\parallel} \frac{e^{-i\mathbf{k}^{\parallel} \cdot (\mathbf{r}'-\mathbf{s})}}{k^{\perp *}} \sum_{\sigma=s,p} \frac{t_{23}^{*\sigma} e^{-ik^{\perp *} d_2}}{\left(1 - r_{34}^{*\sigma} r_{3-}^{*\sigma} e^{-2ik_3^{\perp *} d_3}\right)\left(1 - r_{21}^{*\sigma} r_{23}^{*\sigma} e^{-2ik^{\perp *} d_2}\right)}
$$
$$
\times \left(e^{ik^{\perp *} z'} e^{-ik_3^{\perp *} s_z} \mathbf{e}_{3\sigma}^{*-} \mathbf{e}_{2\sigma}^{*-} + r_{34}^{*\sigma} e^{ik^{\perp *} z'} e^{ik_3^{\perp *} s_z} e^{-2ik_3^{\perp *} d_3} \mathbf{e}_{3\sigma}^{*+} \mathbf{e}_{2\sigma}^{*-} \right.
$$
$$
\left. + r_{21}^{*\sigma} e^{-ik^{\perp *} z'} e^{-ik_3^{\perp *} s_z} \mathbf{e}_{3\sigma}^{*-} \mathbf{e}_{2\sigma}^{*+} + r_{21}^{*\sigma} r_{34}^{*\sigma} e^{-ik^{\perp *} z'} e^{ik_3^{\perp *} s_z} e^{-2ik_3^{\perp *} d_3} \mathbf{e}_{3\sigma}^{*+} \mathbf{e}_{2\sigma}^{*+} \right). \quad (4.104)
$$

The relevant reflection and transmission coefficients read

$$
r_{3-}^\sigma = \frac{r_{32}^\sigma + e^{2ik^{\perp} d_2} r_{21}^\sigma}{1 + r_{32}^\sigma r_{21}^\sigma e^{2ik^{\perp} d_2}}, \quad t_{43}^s = t_{23}^s = 1 + r_{23}^s, \quad t_{43}^p = t_{23}^p = (1 + r_{23}^p)\frac{1}{\sqrt{\varepsilon_3}} \quad (4.105)
$$

with the familiar single-interface coefficients

$$
r_{ij}^s = \frac{k_i^{\perp} - k_j^{\perp}}{k_i^{\perp} + k_j^{\perp}}, \quad r_{ij}^p = \frac{\varepsilon_j k_i^{\perp} - \varepsilon_i k_j^{\perp}}{\varepsilon_j k_i^{\perp} + \varepsilon_i k_j^{\perp}}. \quad (4.106)
$$

In particular, we have $r_{34}^\sigma = r_{32}^\sigma = -r_{23}^\sigma$. The polarization unit-vectors are given by Eq. (3.15). Recall also the notation for the wave vectors, Eq. (4.2). In contrast, to calculate the force density on the right boundary of the slab we need the Green tensor with $\mathbf{r}, \mathbf{r}'$ in layer 4 and $\mathbf{s}$ in layer 3 [132]

$$
\boldsymbol{G}(\mathbf{r}, \mathbf{s}, \omega) = \frac{i}{8\pi^2} \int \mathrm{d}^2 k^{\parallel} \frac{e^{i\mathbf{k}^{\parallel} \cdot (\mathbf{r}-\mathbf{s})}}{k^{\perp}} \sum_{\sigma=s,p} \frac{t_{43}^\sigma e^{ik_3^{\perp} d_3} e^{ik^{\perp} z}}{\left(1 - r_{34}^\sigma r_{3-}^\sigma e^{2ik_3^{\perp} d_3}\right)}
$$
$$
\times \left(e^{-ik_3^{\perp} s_z} \mathbf{e}_4^+ \mathbf{e}_3^+ + r_{3-}^\sigma e^{ik_3^{\perp} s_z} \mathbf{e}_4^+ \mathbf{e}_3^- \right) \quad (4.107)
$$

and accordingly,

$$
\boldsymbol{G}^*(\mathbf{s}, \mathbf{r}', \omega) = \frac{-i}{8\pi^2} \int \mathrm{d}^2 k^{\parallel} \frac{e^{-i\mathbf{k}^{\parallel} \cdot (\mathbf{r}'-\mathbf{s})}}{k^{\perp *}} \sum_{\sigma=s,p} \frac{t_{43}^{\sigma *} e^{-ik_3^{\perp *} d_3} e^{-ik^{\perp *} z'}}{\left(1 - r_{34}^{\sigma *} r_{3-}^{\sigma *} e^{-2ik_3^{\perp *} d_3}\right)}
$$
$$
\times \left(e^{ik_3^{\perp *} s_z} \mathbf{e}_3^{+*} \mathbf{e}_4^{+*} + r_{3-}^{\sigma *} e^{-ik_3^{\perp *} s_z} \mathbf{e}_3^{-*} \mathbf{e}_4^{+*} \right). \quad (4.108)
$$

As already pointed out, the analyticity of the Green tensors in the upper ω half-plane is a basic requirement to justify the quantization scheme. In the following, we illustrate the relation between poles in the upper ω half-plane and the strength of the amplification. As an example consider the Green tensor (4.107). Although the permittivity, the reflection and transmission coefficients and the numerator are

analytic functions in the upper half of the complex ω plane including the real axis, this is not necessarily the case for the Green tensor itself. That is to say, we have to check under which conditions the poles of the Green tensor are located in the upper ω half-plane. Similar considerations can be found in Ref. [116]. The poles are the roots of the denominator in (4.107). As an approximation, we assume that $r_{3-}^{\sigma} \approx r_{32}^{\sigma} = r_{34}^{\sigma} \equiv r(\omega) = |r(\omega)|e^{i\phi_r}$ and consider only propagating waves of normal incidence $(k^{\|} = 0)$ in the denominator. The condition for the poles is thus given by

$$1 - g(\omega) = 1 - |g(\omega)|e^{i\phi_g} \equiv 1 - r^2(\omega)e^{2i\sqrt{\varepsilon_3}d_3\omega/c} = 0, \qquad (4.109)$$

where $\mathrm{Im}\,\sqrt{\varepsilon_3} < 0$. Condition (4.109), for complex ω, is fulfilled for

$$|g(\omega)| = |r(\omega)|^2 e^{-2(\mathrm{Re}\,\omega\mathrm{Im}\,\sqrt{\varepsilon_3}+\mathrm{Im}\,\omega\mathrm{Re}\,\sqrt{\varepsilon_3})d_3/c} = 1 \quad \text{and} \qquad (4.110)$$

$$\cos\phi_g = \cos[2\phi_r + 2(\mathrm{Re}\,\omega\mathrm{Re}\,\sqrt{\varepsilon_3} - \mathrm{Im}\,\omega\mathrm{Im}\,\sqrt{\varepsilon_3})d_3/c] = 1. \qquad (4.111)$$

The function $g(\omega)$ is analytic in the upper ω half-plane and can be identified with the gain (or loss) of the electric field emitted from one point in the slab, traveling to each of the two surfaces where it is reflected and finally comes back to the same point. Hence, the condition (4.110) implies that the loss via transmission through the surfaces is equal to the gain in the medium while condition (4.111) enforces phase matching after a round-trip.

The Green tensor is analytic if $g(\omega) \neq 1$ in the entire upper ω half-plane. According to the maximum modulus principle, $|g(\omega)|$ takes its maximum at the boundary of this region. Since for $\mathrm{Im}\,\omega \to \infty$ the modulus of the gain function $|g(\omega)|$ goes to zero on the infinite semicircle, the maximum must be located on the real axis which is consistent with Eq. (4.111). It is hence sufficient to require that

$$|g(\omega)| = |r(\omega)|^2 e^{-2\mathrm{Im}\,\sqrt{\varepsilon_3}d_3\omega/c} < 1 \quad \text{for real } \omega. \qquad (4.112)$$

For absorption-assisted frequencies where $\mathrm{Im}\,\sqrt{\varepsilon_3} > 0$, this condition is always fulfilled. For amplification-assisted frequencies Eq. (4.112) yields the condition

$$|r(\omega)| = \frac{|1 - \sqrt{\varepsilon_3}|}{|1 + \sqrt{\varepsilon_3}|} < e^{-|\mathrm{Im}\,\sqrt{\varepsilon_3}|d_3\omega/c} \quad \text{for real } \omega. \qquad (4.113)$$

Thus, Eq. (4.113) implicitly holds conditions for the medium parameters in $\varepsilon_3(\omega)$. If the amplification in the body (over)compensates the transmission losses, $|g(\omega)| > 1$,

the poles may approach the real axis and migrate into the upper half-plane. In this case, instabilities may arise and the electromagnetic field will blow up with time [90], which implies that the slab starts lasing action. Clearly, for such medium parameters, the concept of *linear* macroscopic QED breaks down.

Keeping these considerations in mind, the resonant Casimir force can now be obtained by evaluating Eq. (4.89) together with Eq. (4.80), where the Green tensors (4.103), (4.104), (4.107) and (4.108) enter via the correlation functions (4.83) and (4.85). This result can be regarded as a generalization of the Lifshitz-theory [2] to excited bodies. The appearing integrals must (in general) be solved numerically by choosing the integration path according to our considerations above.

Nonretarded limit

In order to answer the question whether the Casimir force can be repulsive, let us investigate the nonretarded limit more closely. In this limit, evanescent waves dominate and we can approximate $k_j^\perp = ik^\parallel$ for every layer, where $k^\parallel$ is real. In this case, the Green tensors (4.103) and (4.104) can be combined by using

$$
\int \mathrm{d}^2 k^\parallel \int \mathrm{d}^2 k'^\parallel \int_{-\infty}^{\infty} \mathrm{d}s_x \int_{-\infty}^{\infty} \mathrm{d}s_y \, e^{-is_x(k_x^\parallel - k_x'^\parallel)} e^{-is_y(k_y^\parallel - k_y'^\parallel)} f(s_z)
$$

$$
= 4\pi^2 \int \mathrm{d}^2 k^\parallel \int \mathrm{d}^2 k'^\parallel \delta(k_x^\parallel - k_x'^\parallel)\delta(k_y^\parallel - k_y'^\parallel) f(s_z) = 4\pi^2 \int \mathrm{d}^2 k^\parallel f(s_z). \quad (4.114)
$$

In the nonretarded limit, all *s*-polarized reflection coefficients vanish and the force is dominated by *p*-polarized contributions. Thus we calculate the relevant inner (scalar) products between the polarization unit-vectors appearing in the Green tensors (4.103) and (4.104),

$$
\mathbf{e}_{3p}^\pm \cdot \mathbf{e}_{3p}^{\pm *} = 2\frac{c^2}{|\varepsilon_3|\omega^2} k^{\parallel 2}, \quad \mathbf{e}_{3p}^\pm \cdot \mathbf{e}_{3p}^{\mp *} = 0. \quad (4.115)
$$

In the next step, we determine the outer (dyadic) products between the polarization vectors, where the relevant element [recall that we need T_{zz} together with Eq. (4.83)] is given by

$$
\frac{1}{2}[\mathbf{e}_{2p}^M \mathbf{e}_{2p}^N]_{zz-xx-yy} = \frac{1}{2}\big(k^{\parallel 2} - MNk^{\parallel 2}\big) = k^{\parallel 2}, \quad (4.116)
$$

where the last equality holds for $M, N = +1, -1$ or $-1, +1$. As expected from the fact that only *p*-polarized terms appear in the force, magnetic terms involving curls acting on the product of the Green tensors [recall (4.85)] do not contribute in the

nonretarded limit,

$$\frac{1}{2}[\boldsymbol{\nabla} \times e^{i\mathbf{k}^{\|}(\mathbf{r}-\mathbf{r}')}e^{Mik^{\perp}z}e^{-Nik^{\perp*}z'}\mathbf{e}_{2p}^{M}\mathbf{e}_{2p}^{N} \times \overleftarrow{\boldsymbol{\nabla}}']_{zz-xx-yy} = 0. \qquad (4.117)$$

From the scalar and dyadic products we see that only two terms, together with their complex conjugate counterparts, contribute to T_{zz} at the left boundary of the slab,

$$T_{zz}^{l}(z=d_2) = -\frac{\hbar}{\pi^2}\int d\omega\Theta[-\text{Im}\,\varepsilon_3(\omega)]\frac{|\text{Im}\,\varepsilon_3(\omega)|}{|\varepsilon_3(\omega)|}\int_0^{\infty}dk^{\|}k^{\|3}e^{-2k^{\|}d_2}\int_0^{d_3}ds_z$$

$$\times \frac{\text{Re}\,r_{21}^{p}|t_{23}^{p}|^2}{|1+r_{3-}^{p}r_{23}^{p}e^{-2k^{\|}d_3}|^2|1-r_{21}^{p}r_{23}^{p}e^{-2k^{\|}d_2}|^2}\Big[e^{-2k^{\|}s_z} + |r_{23}^{p}|^2e^{-4k^{\|}d_3}e^{2k^{\|}s_z}\Big]\mathbf{e}_z \quad (4.118)$$

where we have already performed the angular integration by using $d^2k^{\|} = k^{\|}d\phi dk^{\|}$. It should be pointed out that the single-layer reflection coefficients do not depend on $k_j^{\perp}$ when $k_j^{\perp} = ik^{\|}$. The integration over s_z can now be carried out. Hence, the resonant (nonretarded) Casimir force density reads

$$\mathbf{f}^{\text{res}} = T_{zz}(z=d_2) = -\frac{\hbar}{2\pi^2}\int d\omega\Theta[-\text{Im}\,\varepsilon_3(\omega)]\frac{|\text{Im}\,\varepsilon_3|}{|\varepsilon_3|}\int_0^{\infty}dk^{\|}k^{\|2}e^{-2k^{\|}d_2}$$

$$\times \frac{\text{Re}\,r_{21}^{p}|t_{23}^{p}|^2}{|1+r_{3-}^{p}r_{23}^{p}e^{-2k^{\|}d_3}|^2|1-r_{21}^{p}r_{23}^{p}e^{-2k^{\|}d_2}|^2}\Big[(1-e^{-2k^{\|}d_3}) + |r_{23}^{p}|^2(e^{-2k^{\|}d_3}-e^{-4k^{\|}d_3})\Big]\mathbf{e}_z.$$

$$(4.119)$$

Note that in the nonretarded limit, force contributions on the right boundary of the slab vanish as can be seen by applying Eqs. (4.115) and (4.116) (which also hold for the vacuum layer 4) to the product of Green tensors (4.103) and (4.104). The nonretarded resonant force remains finite in the limit $d_3 \to \infty$. In this case, the force is approximated by

$$\mathbf{f}^{\text{res}} = -\frac{\hbar}{2\pi^2}\int d\omega\Theta[-\text{Im}\,\varepsilon_3(\omega)]\frac{|\text{Im}\,\varepsilon_3|}{|\varepsilon_3|}\int_0^{\infty}dk^{\|}k^{\|2}e^{-2k^{\|}d_2}\frac{\text{Re}\,r_{21}^{p}|t_{23}^{p}|^2}{|1-r_{21}^{p}r_{23}^{p}e^{-2k^{\|}d_2}|^2}\mathbf{e}_z.$$

$$(4.120)$$

Two approximations can be applied to evaluate the $k^{\|}$ integral in Eq. (4.120). Firstly, we consider the case of weakly reflecting interfaces such that the multiple reflections in the denominator can be neglected and the denominator is approximated by 1. In this case, we can read off a d_2^{-3} power law,

$$\mathbf{f}^{\text{res}} = -\frac{\hbar}{2\pi^2d_2^3}\int d\omega\,\Theta[-\text{Im}\,\varepsilon_3(\omega)]|\text{Im}\,\varepsilon_3|\frac{|\varepsilon_1|^2-1}{|\varepsilon_1+1|^2|\varepsilon_3+1|^2}\mathbf{e}_z \qquad (4.121)$$

where we have used that

$$|t_{23}^p|^2 = \frac{4|\varepsilon_3|}{|\varepsilon_3 + 1|^2}, \quad \operatorname{Re} r_{21}^p = \frac{|\varepsilon_1|^2 - 1}{|\varepsilon_1 + 1|^2}. \tag{4.122}$$

Equation (4.121) is consistent with the resonant CP potential of an excited atom in front of a dielectric half space (4.6). As a second approximation to Eq. (4.120), we assume the reflection coefficients in the denominator to be close to one, which corresponds to a maximal impact of multiple reflections. In this case we find

$$\mathbf{f}^{\mathrm{res}} = -\frac{2\hbar}{\pi^2} \int d\omega \, \Theta[-\operatorname{Im}\varepsilon_3(\omega)]|\operatorname{Im}\varepsilon_3| \frac{|\varepsilon_1| - 1}{|\varepsilon_1 + 1|^2 |\varepsilon_3 + 1|^2} \int_0^\infty dk^{\parallel} \frac{k^{\parallel 2} e^{-2k^{\parallel} d_2}}{(1 - e^{-2k^{\parallel} d_2})^2} \mathbf{e}_z$$

$$= -\frac{\hbar}{12 d_2^3} \int d\omega \Theta[-\operatorname{Im}\varepsilon_3(\omega)]|\operatorname{Im}\varepsilon_3| \frac{|\varepsilon_1|^2 - 1}{|\varepsilon_1 + 1|^2 |\varepsilon_3 + 1|^2} \mathbf{e}_z. \tag{4.123}$$

In general, it can be expected that the nonretarded force will take values between the extreme cases Eqs. (4.121) and (4.123). In particular, these results reveal that the Casimir force on an amplifying slab can indeed be repulsive, provided that the half space consists of a metamaterial with $|\varepsilon_1| < 1$ for the frequencies where the slab is amplifying.

5 Summary and prospective work

In this thesis, we have used macroscopic quantum electrodynamics to extend the concept of dispersion forces to objects in media and on excited systems. In particular, we have shown that forces in media can be modified considerably by local-field effects, and that excited systems can be subject to strongly enhanced or repulsive dispersion forces.

In the first part, we have investigated the Casimir–Polder potential of a ground-state atom embedded in a medium environment. The ground-state Casimir–Polder interaction contains the Green tensor of the body and the atomic polarizability in an integral form. To account for the local-field correction we have applied the Onsager real cavity model and decomposed the Green tensor into the Green tensor of the system without the cavity combined with a local-field-correction factor, and a position-independent part accounting for scattering processes inside the cavity.

We have first studied the ground-state atom in front of a planar interface between two magnetodielectric media. This generalizes earlier studies of an atom in free space interacting with a magnetodielectric plate. Our theory is applicable to a larger range of realistic situations, for example in cell biology. As we have shown, the Casimir–Polder interaction tends to move the atom towards the medium with the higher permittivity while it is repelled from the medium with the larger permeability. We have extended the well known asymptotic power laws beyond the free-space case. Numerical evaluation elucidates the potential at intermediate distances. In particular, we have investigated how competing effects of electric and magnetic properties may lead to the appearance of potential walls and wells. The impact of the local-field correction factor has been studied as a function of distance and as a function of the static permittivity of the local medium environment. In particular, we have shown that under certain circumstances (e.g., for purely electric half-spaces) the local-field corrections to the CP potential can be very significant, up to 30% of the uncorrected values. In addition, we have for the first time studied the layer-dependent, constant part of the Casimir–Polder potential. This has allowed us to propose an estimate of the on-surface value of the potential. Our considerations may easily be extended to

other geometries, such as spherically or cylindrically layered host media.

Secondly, we have examined the Casimir–Polder interaction of a ground-state atom and a small magnetodielectric sphere in the presence of arbitrary magnetodielectric background media and bodies. Employing a similar (point-scattering) technique, we have expressed the Green tensor in the presence of the sphere as a simple function of the Green tensor of the environment. Using this result, we have found closed general expressions for the CP potential of a magnetoelectric atom interacting with a small magnetodielectric sphere which depend on the sphere's polarizability and magnetizability. A comparison with the van der Waals potential between two ground-state atoms in the presence of the background medium has revealed how the different microscopic/macroscopic natures of atom versus sphere manifest themselves in the dispersion potentials. For the first time, we have proposed a model that is able to describe molecular systems of arbitrary size: It consists of a sphere of variable radius located inside an Onsager cavity and is able to interpolate continuously between the two limiting cases of a microscopic atom and macroscopic sphere. In particular, our result provides the correct polarizability of such a medium-sized spherical molecular system and explicitly accounts for local-field effects. The implemented point-scattering method may also be used to calculate the Casimir force on a small sphere in an arbitrary environment and, in particular, the Casimir force between two small spheres.

In the second part of the thesis, we have studied the impact of excitation on dispersion forces. We have first considered the resonant Casimir–Polder potential of an excited atom in front of a magnetoelectric metamaterial half space. As we have shown, the atom exhibits attenuated oscillations in the retarded regime, while close to the surface the potential becomes attractive or repulsive depending on the medium response at the atomic transitions frequencies.

To demonstrate the impact of negative refraction on the Casimir–Polder potential, we have studied the more complex superlens scenario: It consists of an excited atom placed in a free-space region in front of a left-handed metamaterial slab mounted on a perfect mirror. In the idealized case of a nonabsorbing superlens, we have found that the atom is strongly attracted towards the focal plane of the superlens. In the more realistic case of a weakly absorbing lens, focal-plane attraction becomes a less distinct feature. Instead, potential barriers may form that are typically several orders of magnitude higher than those observed in ground-state Casimir–Polder potentials. Provided that metamaterials with very small absorption can be fabricated, such barriers might be of interest to levitate particles or for use in trapping or (evaporate)

cooling mechanisms.

We have also investigated another quantum vacuum effect, the spontaneous decay of an excited atom in the superlens geometry. As previously shown, an idealized, non-absorbing superlens can allow for complete inhibition or strong enhancement of the spontaneous decay if the atom is placed in the focal plane, depending on its dipole orientation. We have shown that an arbitrarily small but finite amount of material absorption drastically changes the decay rate compared to the ideal scenario with vanishing absorption. In particular, nonradiative coupling leads to a strong enhancement of the decay rate in the region close to the superlens. We may easily combine our studies of the Casimir–Polder interaction and the decay rate to obtain a full picture of the dynamical Casimir–Polder force of an excited atom in a a superlens geometry.

As another example for dispersion forces on excited systems, we have calculated the Casimir force on an amplifying but linearly responding, magnetoelectric body. The resulting force contains a nonresonant contribution that formally looks like its ground-state counterpart but is influenced by the frequency window where amplification is present. We have shown that amplification also leads to resonant force components which have been neglected in all previous approaches but which often dominate the total force. We have proven that the Casimir force on an optically dilute amplifying body can be calculated as a sum over the Casimir–Polder forces on the excited atoms inside the body.

As an application of the general theory, we have explicitly calculated the Casimir force between an amplifying slab and a dielectric half space. Calculations in the dilute-slab limit show that the force is oscillating at large inter-plate separations, and can be be attractive or repulsive at small separations. To go beyond the dilute-slab limit, we have carefully examined the correct choice of the wave vector inside the amplifying medium, and have given an upper limit for the possible strength of amplification such that our linear theory remains valid. The derived force formula extends Lifshitz theory to the amplifying case and lay the foundation for thorough numerical evaluation. We have explicitly answered the question whether Casimir repulsion can be realized. As shown, the nonretarded force is proportional to the third power of the inter-plate separation and can be repulsive if the permittivity of the absorbing half space is smaller than unity in the frequency window of amplification.

The results of this thesis facilitate a deeper understanding of dispersion interactions in the context of biological systems and colloid science. They stress the potential of amplification and left-handed metamaterials for manipulating dispersion forces on atoms and bodies in nanotechnologies.

List of Publications

[AS1] A. Sambale, S. Y. Buhmann, D.-G. Welsch, and M.-S. Tomaš. *Local-field correction to one- and two-atom van der Waals interactions.* Phys. Rev. A, 75:042109 (2007). The content of the paper was also part of my diploma thesis.

[AS2] A. Sambale, D.-G. Welsch, D. T. Ho, and S. Y. Buhmann. *Van der Waals interaction and spontaneous decay of an excited atom in a superlens-type geometry.* Phys. Rev. A, 78(5):053828 (2008).

[AS3] A. Sambale, S. Y. Buhmann, H. T. Dung, and D.-G. Welsch. *Resonant Casimir–Polder forces in planar meta-materials.* Phys. Scripta T, 135:014019 (2009).

[AS4] A. Sambale, D.-G. Welsch, H. T. Dung, and S. Y. Buhmann. *Local-field corrected van der Waals potentials in magnetodielectric multilayer systems.* Phys. Rev. A, 79(2):022903 (2009).

[AS5] A. Sambale, D.-G. Welsch, S. Y. Buhmann, and H. T. Dung. *Impact of amplifying media on the Casimir force.* Phys. Rev. A, 80(5):051801(R) (2010).

[AS6] A. Sambale, D.-G. Welsch, S. Y. Buhmann, and H. T. Dung. *Casimir force on amplifying bodies.* Opt. and Spec., 108(3):391 (2010).

[AS7] A. Sambale, S. Y. Buhmann, and S. Scheel. *Casimir–Polder interaction between an atom and a small magnetoelectric sphere.* Phys. Rev. A, 81(1):012509 (2010).

List of Presentations

[P1] A. SAMBALE. *Interaction of an atom with absorbing left-handed media.* 15th Central European Workshop on Quantum Optics, Belgrade (2008). Talk.

[P2] A. SAMBALE. *Resonant Casimir-Polder interaction in planar meta-materials.* XIIth International Conference on Quantum Optics, Vilnius (2008). Talk.

[P3] A. SAMBALE. *Casimir force on amplifying bodies.* DPG spring meeting in Hannover (2010). Short talk.

[P4] A. SAMBALE and S. Y. BUHMANN. *Casimir force on amplifying metamaterials.* 3rd International Topical Meeting on Nanophotonics and Metamaterials, Seefeld (2011). Poster.

[P5] A. SAMBALE. *Lifshitz-theory for amplifying systems.* Quantum field theory under the influence of external conditions, Benasque (2011).

Bibliography

[1] H. B. G. CASIMIR. *On the attraction between two perfectly conducting plates.* Proc. K. Ned. Akad. Wet., 51: 793 (1948)

[2] E. LIFSHITZ. *The theory of molecular attractive forces between solids.* J. Exper. Theoret. Phys. USSR, 29: 94 (1955)

[3] S. K. LAMOREAUX. *The Casimir force: background, experiments, and applications.* Rep. Prog. Phys., 68 (1): 201 (2005)

[4] J. E. LENNARD-JONES. *Processes of absorption and diffusion on solid surfaces.* Trans. Faraday Society, 28: 333 (1932)

[5] H. B. G. CASIMIR and D. POLDER. *The influence of retardation on the London–van der Waals forces.* Phys. Rev., 73 (4): 360 (1948)

[6] S. Y. BUHMANN and D.-G. WELSCH. *Dispersion forces in macroscopic quantum electrodynamics.* Progr. in Quant. Electr., 31 (2) (2007)

[7] F. LONDON. *The general theory of molecular forces.* Trans. Faraday Society, 33: 8 (1937)

[8] P. W. MILONNI. The Quantum Vacuum. Academic Press, New York (1994)

[9] S. Y. BUHMANN, H. SAFARI, D.-G. WELSCH, *et al.* *Microscopic origin of Casimir–Polder forces.* Open Sys. & Information Dyn., 13 (4): 427 (2006)

[10] C. RAABE and D.-G. WELSCH. *Dispersive forces on bodies and atoms: A unified approach.* Phys. Rev. A, 73 (6): 063822 (2006). Note erratum Phys. Rev. A 74 (1) (2006) 019901(E) .

[11] E. POWER and T. THIRUNAMACHANDRAN. *Casimir–Polder potential as an interaction between induced dipoles.* Phys. Rev. A, 48 (6): 4761 (1993)

[12] E. A. POWER and T. THIRUNAMACHANDRAN. *Dispersion forces between molecules with one or both molecules excited.* Phys. Rev. A, 51 (5): 3660 (1995)

[13] Y. SHERKUNOV. *Van der Waals interaction of excited media.* Phys. Rev. A, 72: 052703 (2005)

[14] Y. SHERKUNOV. *Casimir interaction between gas media of excited atoms.* J. Phys. D: App. Phys., 40: 86 (2007)

[15] M. BORDAG, U. MOHIDEEN, and V. M. MOSTEPANENKO. *New developments in the Casimir effect.* Phys. Rep., 353: 1 (2001)

[16] A. D. MCLACHLAN. *Van der Waals forces between an atom and a surface.* Mol. Phys., 7 (4): 381 (1964)

[17] G. S. AGARWAL. *Quantum electrodynamics in the presence of dielectrics and conductors. II. Theory of dispersion forces.* Phys. Rev. A, 11 (1): 243 (1975)

[18] B. HUTTNER and S. M. BARNETT. *Quantization of the electromagnetic field in dielectrics.* Phys. Rev. A, 46 (7): 4306 (1992)

[19] S. SCHEEL and S. Y. BUHMANN. *Macroscopic quantum electrodynamics - concepts and applications.* Acta Physica Slovaca, 58 (5): 675 (2008)

[20] A. BECHLER. *Quantum electrodynamics of the dispersive dielectric medium—a path intergral approach.* J. of Mod. Opt., 46 (5): 901 (1999)

[21] S. Y. BUHMANN, D. T. HO, and D.-G. WELSCH. *The van der Waals energy of atomic systems near absorbing and dispersing bodies.* J. Opt. B: Quantum and Semiclassical Optics, 6: 127 (2004)

[22] V. A. PARSEGIAN. *Long-range physical forces in the biological milieu.* A. Rev. Biophys. Bioeng., 2: 221 (1973)

[23] J. N. ISRAELACHVILI. Intermolecular and surface forces. Academic Press (1992)

[24] M. V. VOLKENSTEIN. Molecular Biophysics. Academic Press, New York (1977)

[25] J. N. ISRAELACHVILI. *Van der Waals forces in biological systems.* Q. Rev. Biophys., 6 (4): 341 (1974)

[26] S. NIR. *Van der Waals interactions between surfaces of biological interest.* Prog. Surf. Sci., 8 (1): 1 (1977)

[27] L. BOESEL, C. GREINER, E. ARZT, *et al. Gecko-inspired surfaces: A path to strong and reversible dry adhesives.* Adv. Mat., 22 (19): 2125 (2010)

[28] K. AUTUMN, M. SITTI, Y. A. LIANG, *et al. Evidence for van der Waals adhesion in gecko setae.* PNAS, 99 (19): 12252 (2002)

[29] H. M. GERRIT HUBER AND, R. SPOLENAK, K. MECKE, *et al. Evidence for capillarity contributions to gecko adhesion from single spatula nanomechanical measurements.* PNAS, 102: 16293 (2005)

[30] G. HUBER, S. N. GORB, N. HOSODA, *et al. Influence of surface roughness on gecko adhesion.* Acta Biomaterialia, 3 (4): 607 (2007)

[31] P. Y. HSU, L. GE, X. LI, *et al. Direct evidence of phospholipids in gecko footprints and spatula–substrate contact interface detected using surface-sensitive spectroscopy.* J. R. Soc. Interface (2011)

[32] S. M. GATICA, M. W. COLE, and D. VELEGOL. *Designing van der Waals forces between nanocolloids.* Nano Lett., 5 (1): 169 (2005)

[33] H.-Y. KIM, J. O. SOFO, D. VELEGOL, *et al. Van der Waals dispersion forces between dielectric nanoclusters.* Langmuir, 23 (4): 1735 (2007)

[34] D. N. THOMAS, S. J. JUDD, and N. FAWCETT. *Flocculation modelling: A review.* Water Res., 33: 1579 (1999)

[35] J. W. LIU and E. LUIJTEN. *Stabilization of colloidal suspensions by means of highly charged nanoparticles.* Phys. Rev. Lett., 92 (24): 247802 (2004)

[36] J. GREGORY. *The role of colloid interactions in solid-liquid separation.* Water Sci. Technol., 27: 1 (1993)

[37] Y. LIANG, N. HILAL, P. LANGSTON, *et al. Interaction forces between colloidal particles in liquid: Theory and experiment.* Adv. colloid and interface science, 134–35: 151 (2007). ISSN 0001-8686

[38] M. FUCHS and K. SCHWEIZER. *Structure of colloid-polymer suspensions.* J.Phys.Cond. Matter, 14 (12): R239 (2002)

[39] T. POPPE, J. BLUM, and T. HENNING. *New experiments on collisions of solid grains related to the preplanetary dust aggregation.* Adv. Space Res., 23 (7): 1197 (1999)

[40] K. A. MILTON. *The Casimir effect: Recent controversies and progress.* J. Phys. A: Math. Gen., 37: R209 (2004)

[41] S. K. LAMOREAUX. *Demonstration of the Casimir force in the 0.6 to 6 μm range.* Phys. Rev. Lett., 78 (5): 5475 (1997)

[42] U. MOHIDEEN and A. ROY. *Precision measurement of the Casimir force from 0.1 to 0.9 μm.* Phys. Rev. Lett., 81: 4549 (1998)

[43] R. S. DECCA, D. LÓPEZ, E. FISCHBACH, *et al. Precise comparison of theory and new experiment for the Casimir force loads to stronger constraints on thermal quantum effects and long-range interactions.* Ann. Phys. NY, 318: 37 (2005)

[44] G. L. KLIMCHITSKAYA, U. MOHIDEEN, and V. M. MOSTEPANENKO. *The Casimir force between real materials: Experiment and theory.* Rev. Mod. Phys., 81 (4): 1827 (2009)

[45] A. CANAGUIER-DURAND, P. A. M. NETO, A. LAMBRECHT, *et al. Thermal Casimir effect in the plane–sphere geometry.* Phys. Rev. Lett., 104 (4): 040403 (2010)

[46] S. K. LAMOREAUX. *Reanalysis of Casimir force measurements in the 0.6-to-6-μm range.* Phys. Rev. A, 82: 024102 (2010)

[47] A. SUSHKOV, W. KIM, D. DALVIT, *et al. Observation of the thermal Casimir force.* Nat. Phys., 7 (3): 230 (2011)

[48] V. M. MOSTEPANENKO, V. B. BEZERRA, R. S. DECCA, *et al. Present status of controversies regarding the thermal Casimir force.* J. of Phys. A: Mathematical and General, 39: 6589 (2006)

[49] R. ZANDI, T. EMIG, and U. MOHIDEEN. *Quantum and thermal Casimir interaction between a sphere and a plate: Comparison of Drude and plasma models.* Phys. Rev. B, 81 (19): 195423 (2009)

[50] G.-L. INGOLD, A. LAMBRECHT, and S. REYNAUD. *Quantum dissipative Brownian motion and the Casimir effect.* Phys. Rev. E, 80: 041113 (2009)

[51] G. L. KLIMCHITSKAYA, M. BORDAG, E. FISCHBACH, *et al. Observation of the thermal Casimir force is open to question.* Int. J. Mod. Phys. A, 26 (22): 3918 (2011)

[52] V. SANDOGHDAR, C. I. SUKENIK, E. A. HINDS, *et al. Direct measurement of the van der Waals interaction between an atom and its image in a micron-sized cavity.* Phys. Rev. Lett., 68 (23): 3432 (1992)

[53] M. CHEVROLLIER, M. ORIA, J. G. DE SOUZA, *et al. Selective reflection spectroscopy of a resonant vapor at the interface with a metallic layer.* Phys. Rev. E, 63: 046610 (2001)

[54] H. FAILACHE, S. ALTIEL, M. FICHET, *et al. Resonant coupling in the van der Waals interaction between excited alkali atom and a dielectric surface: An experimental study via stepwise selective reflection spectroscopy.* Eur. Phys. J. D, 23: 237 (2003)

[55] C. I. SUKENIK, M. G. BOSHIER, D. CHO, *et al. Measurement for Casimir–Polder force.* Phys. Rev. Lett., 70: 5 (1993)

[56] H. GIES and K. KLINGMÜLLER. *Casimir effect for curved geometries: Proximity-force-approximation validity limits.* Phys. Rev. Lett., 96 (22): 220401 (2006)

[57] D. A. R. DALVIT, P. A. MAIA NETO, A. LAMBRECHT, *et al. Lateral Casimir–Polder force with corrugated surfaces.* J. Phys. A: Math. Theoret., 41 (16): 164028 (2008)

[58] R. MESSINA, D. A. R. DALVIT, P. A. M. NETO, *et al. Dispersive interactions between atoms and non planar surfaces.* Phys. Rev. A, 80 (2): 022119 (2009)

[59] A. CONTRERAS-REYES, R. GUEROUT, P. A. MAIA NETO, *et al. Casimir–Polder interaction between an atom and a dielectric grating.* Phys. Rev. A, 82 (5): 052517 (2010)

[60] A. A. FEILER, L. BERGSTRÖM, and M. W. RUTLAND. *Superlubricity using repulsive van der Waals forces.* Langmuir, 24: 2274 (2008)

[61] J. N. MUNDAY, F. CAPASSO, and V. A. PARSEGIAN. *Measured long-range repulsive casimir–lifshitz forces.* Nat., 457: 170 (2009)

[62] E. BUKS and M. L. ROUKES. *Stiction, adhesion energy, and the casimir effect in micromechanical systems.* Phys. Rev. B, 63: 033402 (2001)

[63] Y. P. ZHAO. *Stiction and anti-stiction in MEMS and NEMS.* Acta Mechanica Sinica, 19 (1): 1 (2003)

[64] Y. P. ZHAO, L. S. WANG, and T. X. YU. *Mechanics of adhesion in MEMS - a review.* J. Adh. Sci Tech., 17 (4): 519 (2003)

[65] L. W. BRUCH. *Evaluation of the van der Waals force for atomic force microscopy.* Phys. Rev. B, 72 (3): 033410 (2005)

[66] Y.-J. LIN, I. TEPER, C. CHIN, *et al. Impact of the Casimir–Polder potential and Johnson noise on Bose–Einstein condensate stability near surfaces.* Phys.

Rev. Lett., 92 (5): 050404 (2004)

[67] P. BUSHEV, A. WILSON, J. ESCHNER, *et al. Forces between a single atom and its distant mirror image.* Phys. Rev. Lett., 92 (22): 223602 (2004)

[68] M. AL-AMRI and M. BABIKER. *Atomic reflection off conductor walls as a tool in cold atom traps.* Europ. Phys. J. D, 48 (3): 417 (2008)

[69] V. DRUZHININA and M. DEKIEVIET. *Experimental observation of quantum reflection far from treshold.* Phys. Rev. Lett., 91: 193202 (2003)

[70] U. LEONHARDT and T. G. PHILBIN. *Quantum levitation by left-handed materials.* N. J. of Phys., 9: 254 (2007)

[71] S. SCHEEL and S. Y. BUHMANN. *Casimir–Polder forces on moving atoms.* Phys. Rev. A, 80 (4): 042902 (2009)

[72] C. ROCKSTUHL, F. LEDERER, C. ETRICH, *et al. Design of an artificial three-dimensional composite metamaterial with magnetic resonances in the visible range of the electromagnetic spectrum.* Phys. Rev. Lett., 99 (1): 017401 (2007)

[73] N. LIU, H. GUO, L. FU, *et al. Three-dimensional photonic metamaterials at optical frequencies.* Nature Mat., 7: 31 (2008)

[74] J. B. PENDRY. *Negative refraction makes a perfect lens.* Phys. Rev. Lett., 85 (18): 3966 (2000)

[75] A. P. VINOGRADOV, A. V. DOROFEENKO, and S. ZOUHDI. *On the problem of the effective parameters of metamaterials.* Phys. Usp., 51 (5): 485 (2008)

[76] O. PAUL, C. IMHOF, B. REINHARD, *et al. Negative index bulk metamaterial at terahertz frequencies.* Opt. Expr., 16 (9): 6736 (2008)

[77] S. RAMAKRISHNA. *Physics of negative refractive index materials.* Rep. Progr. Phys., 68 (2): 449 (2005)

[78] A. BOLTASSEVA and V. M. SHALAEV. *Fabrication of optical negative-index metamaterials: Recent advances and outlook.* Metamat., 2: 1 (2008)

[79] D. R. SMITH, W. J. PADILLA, D. C. VIER, *et al. Composite medium with simultaneously negative permeability and permittivity.* Phys. Rev. Lett., 84: 4184 (2000)

[80] R. A. SHELBY, D. R. SMITH, S. C. NEMAT-NASSER, *et al. Microwave transmission through a two-dimensional, isotropic, left-handed metamaterial.* App. Phys. Lett., 78 (4): 489 (2001)

[81] H. J. LEZEC, J. A. DIONNE, and H. A. ATWATER. *Negative refraction at visible frequencies.* Sci., 316: 430 (2007)

[82] V. G. VESELAGO. *The electrodynamics of substances with simultaneously negative values of ε and μ.* Sov. Phys. Usp., 10 (4): 509 (1968)

[83] S. V. H. C. VESELAGO V, BRAGINSKY L. *Negative refractive index materials.* J. Comp and Theor. Nanosci., 2 (2): 189 (2006)

[84] U. LEONHARDT. *Optical conformal mapping.* Sci., 312 (5781): 1777 (2006)

[85] D. SCHURIG, J. J. MOCK, B. J. JUSTICE, *et al. Metamaterial electromagnetic cloak at microwave frequencies.* Sci., 314: 977 (2006)

[86] P. G. KIK, S. A. MAIER, and H. A. ATWATER. *Image resolution of surface-plasmon-mediated near-field focusing with planar metal films in three dimensions using finite-linewidth dipole sources.* Phys. Rev. B., 69 (4): 045418 (2004)

[87] S. A. RAMAKRISHNA and J. B. PENDRY. *Removal of absorption and increase in resolution in a near-field lens via optical gain.* Phys. Rev. B, 67: 201101 (2003)

[88] J. J. CHEN, T. M. GRZEGORCZYK, B.-I. WU, *et al. Imaging properties of finite-size left-handed material slabs.* Phys. Rev. E, 74: 046615 (2006)

[89] D. R. SMITH, D. SCHURIG, M. ROSENBLUTH, *et al. Limitations on subdiffraction imaging with a negative refractive index slab.* App. Phys. Lett., 82 (10): 1506 (2003)

[90] B. NISTAD and J. SKAAR. *Causality and electromagnetic properties of active media.* Phys. Rev. E, 78: 036603 (2008)

[91] S. Y. BUHMANN, D.-G. WELSCH, and T. KAMPF. *Ground-state van der Waals forces in planar multilayer magnetodielectrics.* Phys. Rev. A, 72 (3): 032112 (2005)

[92] C. HENKEL and K. JOULAIN. *Casimir force between designed materials: What is possible and what not.* Europhys. Lett., 72 (6): 929 (2005)

[93] S. SPAGNOLO, D. A. R. DALVIT, and P. W. MILONNI. *Van der Waals interactions in a magneto-dielectric medium.* Phys. Rev. A, 75: 052117 (2007)

[94] M. STOCKMANN. *Criterion for negative refraction with low optical losses from a fundamental principle of causality.* Phys. Rev. Lett., 98 (17): 177404 (2007)

[95] M. RICCI, N. ORLOFF, and S. M. ANLAGE. *Superconducting metamaterials.* App. Phys. Lett., 87: 034102 (2005)

[96] A. K. POPOV and V. M. SHALAEV. *Compensating losses in negative-index metamaterials by optical parametric amplification.* Opt. Lett., 31 (14): 2169 (2006)

[97] S. XIAO, V. DRACHEV, A. V. KILDISHEV, *et al. Loss-free and active optical negative-index metamaterials.* Nature, 466 (2010)

[98] T. H. BOYER. *Van der waals forces and zero-point energy for dielectric and permeable materials.* Phys. Rev. A, 9: 2078 (1974)

[99] M. S. TOMAŠ. *Casimir force between dispersive magnetodielectrics.* Phys. Lett. A, 342: 381 (2005)

[100] F. S. S. ROSA, D. A. R. DALVIT, and P. W. MILONNI. *Casimir-Lifshitz theory and metamaterials.* Phys. Rev. Lett., 100: 183602 (2008)

[101] I. DZYALOSHINSKII, E. M. LIFSHITZ, and L. PITALEVSKII. *The general theory of van der Waals forces.* Adv. Phys., 10 (38): 165 (1961)

[102] A. W. RODRIGUEZ, J. N. MUNDAY, J. D. JOANNOPOULOS, *et al. Stable suspension and dispersion-induced transitions from repulsive Casimir forces between fluid-separated eccentric cylinders.* Phys. Rev. Lett., 101 (19): 190404 (2008)

[103] A. D. MCLACHLAN. *Effect of the medium on dispersion forces in liquids.* Discussion of the Faraday Soc., 40: 239 (1965)

[104] L. ONSAGER. *Electric moments of molecules in liquids.* J. Am. Chem. Soc., 58: 1486 (1936)

[105] C. RAABE and D.-G. WELSCH. *Casimir force acting on magnetodielectric bodies embedded in media.* Phys. Rev. A, 71: 013814 (2005)

[106] L. P. PITAEVSKII. *Comment on "Casimir force acting on magnetodielectric bodies embedded in media".* Phys. Rev. A, 73: 047801 (2006)

[107] R. N. C. PFEIFER, N. T. A., H. N. R., *et al. Colloquium: Momentum of an electromagnetic wave in dielectric media.* Rev. Mod. Phys., 79 (4): 1197 (2007)

[108] I. BREVIK and S. A. ELLINGSEN. *Comment on "Casimir force acting on magnetodielectric bodies embedded in media".* Phys. Rev. A, 79 (2): 027801 (2009)

[109] E. POWER and T. THIRUNAMACHANDRAN. *Two- and three-body dispersion forces with one excited molecule.* Chem. Phys., 198: 5 (1995)

[110] L. RIZZUTO, R. PASSANTE, and F. PERSICO. *Dynamical Casimir–Polder energy between an excited- and a ground-state atom.* Phys. Rev. A, 70: 012107 (2004)

[111] R. PASSANTE, F. PERSICO, and L. RIZZUTO. *Vacuum field correlations and three-body Casimir-Polder potential with one excited atom.* J. Mod. Opt., 52 (14): 1957 (2005)

[112] J. M. WYLIE and J. E. SIPE. *Quantum electrodynamics near an interface.* Phys. Rev. A, 30 (3): 185 (1984)

[113] S. Y. BUHMANN, L. KNÖLL, D.-G. WELSCH, *et al. Casimir–Polder forces: A nonperturbative approach.* Phys. Rev. A, 70: 052117 (2004)

[114] Y. SHERKUNOV. *Casimir–Polder interaction between an excited atom and a gas dielectric medium.* Phy. Rev. A, 75: 012705 (2007)

[115] J. JEFFERS, S. M. BARNETT, R. LOUDON, *et al. Canonical quantum theory of light propagation in amplifying media.* Opt. Commun., 131: 66 (1996)

[116] R. MATLOOB, R. LOUDON, M. ARTONI, *et al. Electromagnetic field quantization in amplifying dielectrics.* Phys. Rev. A, 55 (3): 1623 (1997)

[117] C. RAABE and D.-G. WELSCH. *QED in arbitrary linear media: Amplifying media.* Eur. Phys. J. - Special Topics, 160: 371 (2008)

[118] S. Y. BUHMANN and S. SCHEEL. *Thermal Casimir vs Casimir–Polder forces: Equilibrium and non-equilibrium forces.* Phys. Rev. Lett., 100: 253201 (2008)

[119] M. ANTEZZA, L. P. PITAEVSKII, and S. STRINGARI. *New asymptotic behavior of the surface-atom force out of thermal equilibrium.* Phys. Rev. Lett., 95: 113202

(2005)

[120] M. Antezza, L. P. Pitaevskii, S. Stringari, *et al. Casimir–Lifshitz force out of thermal equilibrium.* Phys. Rev. A, 77: 022901 (2008)

[121] D. M. Harber, J. M. Obrecht, J. M. McGuirk, *et al. Measurement of the Casimir-Polder force through center-of-mass oscillations of a Bose-Einstein condensate.* Phys. Rev. A, 72: 033610 (2005)

[122] J. M. Obrecht, R. J. Wild, M. Antezza, *et al. Measurement of the temperature dependence of the Casimir–Polder force.* Phys. Rev. Lett., 98: 063201 (2007)

[123] S. J. Rahi, M. Kardar, and T. Emig. *Constraints on stable equilibria with fluctuation-induced (Casimir) forces.* Phys. Rev. Lett., 105: 070404 (2010)

[124] C. Raabe. Macroscopic QED in linearly responding media and a Lorentz-force approach to dispersion forces. Ph.D. thesis, F.-Schiller-University Jena (2008)

[125] R. Kubo, M. Toda, and N. Hashitsume. Statistical Physics II: Nonequilibrium Statistical Mechanics. Springer Verlag Berlin (1998)

[126] D. B. Melrose and R. C. McPhedran. Electromagnetic processes in dispersive media : A treatment based on the dielectric tensor. Cambridge Univ. Press, (2003)

[127] S. Y. Buhmann, D. T. Butcher, and S. Scheel. *Macroscopic quantum electrodynamics and duality in non-local and onsager-violating media.* arxiv: 1109.6193 (2011)

[128] R. Kubo. *The fluctuation–dissipation theorem.* Rep. Prog. Phys., 29: 255 (1966)

[129] L. Knöll, S. Scheel, and D.-G. Welsch. *QED in dispersing and absorbing dielectric media.* J. Peřina (Ed.), Coherence and Statistics of Photons and Atoms. Wiley, New York (2001)

[130] S. Scheel, L. Knöll, and D.-G. Welsch. *QED commutation relations for inhomogenous Kramers–Kronig dielectrics.* Phys. Rev. A, 58: 700 (1998)

[131] L.-W. Li, P.-S. Kooi, M.-S. Leong, *et al. Electromagnetc dyadic Green's function in spherically multilayered media.* TEEE Trans.on Microwave Theory and Tech., 42 (12): 2302 (1994)

[132] M. S. Tomaš. *Green function for multilayers: Light scattering in planar cavities.* Phys. Rev. A, 51 (3): 2545 (1995)

[133] M. Scully and M. S. Zubairy. Quantum optics. Cambr. Univ. Press (1997)

[134] S. Y. Buhmann. Casimir–Polder forces on atoms in the presence of magneto-electric bodies. Ph.D. thesis, F.-Schiller-Universität Jena (2007)

[135] V. M. Fain and Y. I. Khanin. Quantum Electronics. Cambridge, Mass., MIT Press (1969)

[136] S. Y. BUHMANN and S. SCHEEL. *Macroscopic quantum electrodynamics and duality.* Phys. Rev. Lett., 102: 140404 (2009)

[137] S. BUHMANN and S. SCHEEL. Int. J. Mod. Phys. A, 24: 1796 (2009)

[138] A. SAMBALE. Local-field corrected van der Waals interaction of ground-state atoms. Master's thesis, Friedrich–Schiller university Jena (2007)

[139] D. T. HO, S. Y. BUHMANN, and D.-G. WELSCH. *Local-field correction to the spontaneous decay rate of atoms embedded in bodies of finite size.* Phys. Rev. A, 74: 023803 (2006)

[140] H. SAFARI, D.-G. WELSCH, S. Y. BUHMANN, *et al. Van-der-waals potentials of paramagnetic atoms.* Phys. Rev. A, 78: 069201 (2008)

[141] I. BREVIK and H. KOLBENSTVEDT. *The Casimir force in a solid ball wenn* $\varepsilon\mu = 1$. Ann. Phys., 143: 179 (1982)

[142] E. ZAREMBA and W. KOHN. *Van der Waals interaction between an atom and a solid surface.* Phys. Rev. B, 13 (6): 2270 (1976)

[143] G. MUKHOPADHYAY and J. MAHANTY. *Van der Waals interaction between molecule and metal surface.* Solid State Commun., 16 (5): 597 (1975)

[144] C. HOLMBERG and P. APELL. *Improved description of the vdW interaction in physisorption.* Solid State Commun., 49: 513 (1984)

[145] C. HOLMBERG and P. APELL. *Van der Waals interaction in atom–surface scattering.* Phys. Rev. B, 30 (10): 5721 (1984)

[146] J. MAHANTY and B. W. NINHAM. Dispersion Forces. Academic Press, London (1976)

[147] J. N. ISRAELACHVILI. *Van der Waals forces in biological systems.* Quart. Rev. of Biophys., 6 (4): 341 (1974)

[148] M. BOUSTIMI, J. BAUDON, J. ROBERT, *et al. Single atom inside or outside a dielectric or metallic bubble.* Phys. Rev. B, 62 (11): 7593 (2000)

[149] M. M. TADDEI, T. N. C. MENDES, and C. FARINA. *Dispersive interaction between an atom and a conduction sphere.* arxiv 0903.2091 (2009)

[150] M. ABRAMOWITZ and I. STEGUN (Eds.). Handbook of Mathematical Functions. Dover, New York (1973)

[151] W. C. CHEW. Waves and Fields in Inhomogeneous Media. IEEE, New York (1995)

[152] L. LANDAU and E. LIFSHITZ. Electrodynamics of Continuous Media, vol. 8 of *2nd edition.* Pergamon Press, Oxford (1984)

[153] M. XU and M. J. DIGNAM. *A new approach to the surface plasma resonance of small metal particles.* J. Chem. Phys., 96 (5): 3370 (1992)

[154] S. Y. BUHMANN and D.-G. WELSCH. *Born expansion of the Casimir–Polder*

interaction of a ground-state atom with dielectric bodies. Appl. Phys. B, 82 (2): 189 (2006)

[155] H. SAFARI, S. Y. BUHMANN, D.-G. WELSCH, *et al. Body-assisted van der Waals interaction between two atoms.* Phys. Rev. A, 74: 042101 (2006)

[156] D. F. PARSONS and B. W. NINHAM. *Surface charge reversal and hydration forces explained by ionic dispersion forces and surface hydration.* Colloids and Surfaces A: Physicochem. Eng. Aspects, 383: 2 (2011)

[157] J. D. JACKSON. Classical Electrodynamics. Wiley, New York, 3rd ed. (1998)

[158] G. BARTON. *Frequency shifts near an interface: inadequacy of two-level atomic models.* J. Phys. B: At. Mol. Opt. Phys., 7: 2134 (1974)

[159] S. S. HODGMAN, R. G. DALL, L. J. BYRON, *et al. Metastable helium: A new determination of the longest atomic excited-state lifetime.* Phys. Rev. Lett., 103: 053002 (2009)

[160] J. KÄSTEL and M. FLEISCHHAUER. *Quantum electrodynamics in media with negative refraction.* Laser Phys., 15 (1): 135 (2005)

[161] J. KÄSTEL and M. FLEISCHHAUER. *Suppression of spontaneous emission and superradiance over macroscopic distances in media with negative refraction.* Phys. Rev. A, 71 (1): 011804(R) (2005)

[162] W. VOGEL and D.-G. WELSCH. Quantum Optics, 3rd edition. Wiley-VCH, Weinheim, auflage: 3rd rev&ex ed. (2006)

[163] J. ping XU, Y. ping YANG, H. CHEN, *et al. Spontaneous decay process of a two-level atom embedded in a one-dimensional structure containing left-handed material.* Phys. Rev. A, 76 (6): 063813 (2007)

[164] M. TOMAŠ. *Screened Casimir forces.* Phys. Rev. A, 71: 060101(R) (2005)

[165] Y. N. OBUKHOV and F. W. HEHL. *Electromagnetic energy–momentum and forces in matter.* Phys. Rev. Lett. A, 311: 277 (2003)

[166] E. AMOOGHORBAN, M. WUBS, N. A. MORTENSEN, *et al. Casimir forces in multilayer magnetodielectrics with both gain and losses.* Phys. Rev. A, 84: 013806 (2011)

[167] A. LAKHTAKIA and J. B. G. I. T. G. MACKAY. *When does the choice of the refractive index of a linear, homogeneous, isotropic, active, dielectric medium matter?* Opt. Expr., 15 (26): 17714 (2007)

[168] S. A. RAMAKRISHNA and O. J. F. MARTIN. *Resolving the wave vector in negative refractive index media.* Opt. Lett., 30 (19): 2626 (2005)

Notation

$\underline{O}$	Fourier component of O
H.c.	hermitian conjugate
C.c.	complex conjugate
$\boldsymbol{G}$	second-rank tensor
$\boldsymbol{I}$	second-rank unit tensor
$\hat{O}$	operator O
$\mathrm{tr}\boldsymbol{M}$	trace of matrix M
$\mathbf{v}$	vector
$\boldsymbol{\nabla}$	gradient
$\overleftarrow{\boldsymbol{\nabla}}$	gradient acting to the left
$\circledast$	duality transformation
$\times$	vector product
$\cdot$	scalar product
$[\mathbf{ab}]_{ij} = a_i b_j$	dyadic product: no intervening symbol
$\Theta(x)$	Theta function with $\Theta(0) \equiv 1$
$P_1^m(x)$	associated Legendre polynomials
$j_l(x)$	lth spherical Bessel function of the first kind
$h_l^{(1)}(x)$	lth spherical Hankel function of the first kind
$[\mathrm{tr}\,\boldsymbol{T}]_i = T_{kik}$	notation for the trace of a tensor

Acknowledgements

Ehrenwörtliche Erklärung

Ich erkläre hiermit ehrenwörtlich, dass ich die vorliegende Arbeit selbständig, ohne unzulässige Hilfe Dritter und ohne Benutzung anderer als der angegebenen Hilfsmittel und Literatur angefertigt habe. Die aus anderen Quellen direkt oder indirekt übernommenen Daten und Konzepte sind unter Angabe der Quelle gekennzeichnet.

Bei der Auswahl und Auswertung haben mir die nachstehend aufgeführten Personen in der jeweils beschriebenen Weise unentgeltlich geholfen:

1. Dr. Stefan Yoshi Buhmann — beratend,

2. Prof. Dirk-Gunnar Welsch — beratend,

3. Prof. Holger Gies — beratend.

Weitere Personen waren an der inhaltlich-materiellen Erstellung der vorliegenden Arbeit nicht beteiligt. Insbesondere habe ich hierfür nicht die entgeltliche Hilfe von Vermittlungs- bzw. Beratungsdiensten (Promotionsberater oder andere Personen) in Anspruch genommen. Niemand hat von mir unmittelbar oder mittelbar geldwerte Leistungen für Arbeiten erhalten, die im Zusammenhang mit dem Inhalt der vorgelegten Dissertation stehen.

Die Arbeit wurde bisher weder im In- noch im Ausland in gleicher oder ähnlicher Form einer anderen Prüfungsbehörde vorgelegt.

Die geltende Promotionsordnung der Physikalisch-Astronomischen Fakultät ist mir bekannt.

Ich versichere ehrenwörtlich, dass ich nach bestem Wissen die reine Wahrheit gesagt und nichts verschwiegen habe.

Jena, den 08.12.2011   Agnes Sambale

Zusammenfassung

Im Rahmen der makroskopischen Quantenelektrodynamik in linearen Medien wurde in den letzten Jahren eine Theorie der Dispersionskräfte entwickelt, die Casimirkräfte (zwischen Körpern), Casimir–Polder–Kräfte (zwischen Atom und Körper) und van–der–Waals–Kräfte (zwischen Atomen) einbezieht und Rechnungen erlaubt, die für beliebige Geometrien anwendbar sind. Dabei werden Körper durch komplexwertige, orts- und frequenzabhängige elektische Permittivitäts- und magnetische Permeabilitätsfunktionen beschrieben, welche Eingang in den klassischen Greentensor finden. Anwesende Atome werden durch ihre Übergangsfrequenz, die entsprechenden Dipolmatrixelemente sowie ihre Polarisierbarkeit und gegebenenfalls Magnetisierbarkeit charakterisiert. Das elektromagnetische Feld wird durch bosonische dynamische Feldvariablen quantisiert, so dass die fundamentalen Vertauschungsregeln für elektrisches Feld und Induktionsfeld erfüllt werden und der zugehörige Hamiltonoperator des Systems im Einklang mit den Maxwellgleichungen ist. Die Casimir- und Casimir–Polder–Kräfte werden als Lorentzkräfte beschrieben.

Während Dispersionskräfte zwischen Grundzustandsobjekten im freien Raum experimentell gut nachgewiesen sind, sind sowohl Dispersionskräfte auf Objekte in Medien als auch die Wechselwirkung angeregter Systeme bislang viel weniger experimentell untersucht, vor allem weil die praktische Umsetzung wie z.B. die Berücksichtigung von Reibungskräften und die Erzeugung verstärkender Metamaterialien schwierig ist. Insbesondere ist auch die Möglichkeit, abstoßende Dispersionkräfte zu erzeugen und nachzuweisen, entscheidend für Fortschritte in den Nanowissenschaften. Die theoretischen Grundlagen hierzu sind weitestgehend unerforscht. Ein Schwerpunkt dieser Arbeit ist daher die Erweiterung der bestehenden Theorie der Grundzustandswechselwirkung zwischen Atom und Körper, wobei das Atom in ein beliebiges Medium eingebettet ist und das zugehörige Potenzial entsprechend lokalfeldkorrigiert wird. Dies trägt der Tatsache Rechnung, dass sich das makroskopische Feld vom lokalen Feld am Ort des Atoms unterscheidet. Dabei wird am Beispiel zweier magnetoelektrischer Halbräume

- der Effekt der Lokalfeldkorrektur unter Verwendung des Onsager (real cavity) Modells analysiert und mit den unkorrigierten Potenzialen verglichen,

- untersucht unter welchen Bedingungen abstoßende Kräfte auftreten und

- die Größe des Potenzials an einer Grenzfläche abgeschätzt.

Bei der Lokalfeldkorrektur mittels des Onsager Modells wird das Atom in die Mitte einer kleinen leeren Kugel (Kavität) platziert. Der Radius der Kugel kann mit dem interatomaren Abstand identifiziert werden und sollte kleiner sein als die relevanten Wellenlängen der atomaren Übergänge sowie kleiner als die Abstände zwischen Atom und Körper, um die Anwendbarkeit des Modells zu gewährleisten. Durch Punktstreutechniken kann gezeigt werden, dass der lokale Greentensor sich als Funktion des Greentensors des Systems ohne die Kavität darstellen lässt. Als Lokalfeldkorrektur ergibt sich für kleine Kavitätsradien ein einfacher frequenzabhängiger Faktor, der nur von den magnetoelektrischen Eigenschaften am Ort des Atoms abhängt. Dazu kommt ein nicht explizit vom Ort abhängiger Summand, der vom Radius der Kugel abhängt. Die Zerlegung des Greentensors wird auf das Casimir–Polder–Potenzial eines Grundzustandsatoms in einem magnetoelektrischen Zweischichtsystem angewendet. Die bekannten Abstandsgesetze werden unter Berücksichtigung von Lokalfeldeffekten erweitert. Insbesondere zeigt sich auch hier, dass das Atom zum anderen Halbraum gezogen wird, falls dieser stärkere elektrische Eigenschaften aufweist. Im nichtretardierten Fall gilt für magnetisch dominierte Systeme ein schwächeres Abstandsgesetz. Das Atom wird von einer Platte mit stärkeren magnetischen Eigenschaften (als am Ort des Atoms) abgestoßen. Numerische Berechnungen beleuchten insbesondere das Verhalten für mittlere Abstände zwischen Atom und Grenzschicht und zeigen, dass ein Zusammenspiel von elektrischen und magnetischen Eigenschaften zur Ausprägung von Potenzialtöpfen und -barrieren führt. Besonderes Augenmerk wird auch auf die Untersuchung des konstanten, schichtabhängigen Anteils des Potenzials gelegt, der zwar nicht zu einer Kraftwirkung führt, wohl aber zum Verständnis der Bewegung eines Atoms in der Nähe einer Schichtgrenze beiträgt und ausschlaggebend für die vorgeschlagene Abschätzung des Potenzials an der Grenzfläche ist.

Für Anwendungen ist es besonders wichtig die lokalfeldkorrigierten Potenziale für (sphärische) Mikroobjekte beliebiger Größe zu kennen. Daher wird in dieser Dissertation

- eine geschlossene Formel für die Casimir–Polder–Wechselwirkung zwischen

Grundzustandsatom und kleiner Kugel in beliebiger absorptiver Mediumumgebung hergeleitet,

- gezeigt wie die verschiedenen mikroskopischen und makroskopischen Charakteristiken von Atom bzw. Kugel sich in den Dispersionspotenzialen manifestieren und

- dargestellt wie die Lokalfeldkorrektur kontinuierlich zwischen den Extremfällen Atom und Kugel interpoliert werden kann.

Dazu wird zunächst der Greentensor einer Kugel in Anwesenheit eines beliebigen umgebenden Mediums als Funktion des Greentensors der Umgebung ohne die Kugel dargestellt. Daraus wird das Casimir–Polder–Potenzial zwischen Atom und Kugel berechnet und mit der van-der-Waals–Kraft zwischen zwei Atomen verglichen: Der direkte Kontakt zwischen makroskopischer Kugel und umgebenden Medium führt zum expliziten Auftreten der Permittivität und inversen Permeabilität des Mediums, während die Kopplung des lokalen elektromagnetischen Feldes mit dem Atom zu Lokalfeldfaktoren führt. Um den kontinuierlichen Übergang zwischen diesen Extremfällen deutlich zu machen, wird der Greentensor einer Kugel mit variablem Radius, eingebettet in eine zweite, leere Kugel studiert. Das entsprechende Potenzial enthält die Polarisierbarkeit eines kugelförmigen Moleküls variabler Größe und berücksichtigt Lokalfeldkorrekturen.

Als zweiter Schwerpunkt der Dissertation werden Dispersionskräfte auf angeregte Systeme untersucht. Die durch die Anregung zu erwartenden resonanten Kraftkomponenten eignen sich um Kräfte zu manipulieren. Grundsätzlich sind zwei Möglichkeiten vorstellbar, wie der Einfluss von bestimmten Metamaterialieneigenschaften wie zum Beispiel Linkshändigkeit erhöht werden kann. Zum einen können Potenziale angeregter Atome untersucht werden, insbesondere werden

- die resonante Casimir–Polder–Wechselwirkung zwischen angeregtem Atom und planarem Metamaterial berechnet und

- das Szenario der Superlinse unter Berücksichtigung von Absorption beleuchtet.

Die Rechnung zeigt, dass das resonante Casimir–Polder–Potenzial eine angeregten Atoms for einer magnetoelektrischen Platte für große Atom–Platten–Abstände oszilliert. Nahe an der Grenzfläche ist das Potenzial anziehend, wenn die Absolutbeträge von Permittivität und Permeabilität größer als eins sind, andernfalls ist es abstoßend. Um den Effekt negativer Brechung näher zu untersuchen, wird das Potenzial eines

Atoms in einer Superlinsengeometrie diskutiert. Die Anordnung der Superlinse ist effektiv ein Dreischichtsystem bestehend aus perfektem Spiegel, daran angrenzend eine Platte mit gleichzeitig negativem Realteil von Permittivität und Permeabilität, sowie einer Freiraumregion, in der das angeregte Atom sitzt. Im Falle einer idealisierten, absorptionsfreien linkshändigen Schicht ist das Potential stark anziehend, divergiert aber für Atom–Platten–Abstände, die kleiner als die Plattendicke sind. Es wird gezeigt, dass dieses unphysikalische Verhalten nicht auftritt, wenn eine schwache Absorption des linkshändigen Materials zugelassen wird. Für größere Atom–Platten–Abstände kann der absorptionsfreie Fall jedoch als gute Näherung zum Resultat mit hinreichend kleiner Absorption angesehen werden. Insbesondere findet man auch im absorptiven Fall eine starke Anziehung für Abstände in der Größe der Plattendicke – ein Phänomen, das charakteristisch für die Superlinsenanordnung ist. Die Anordnung der Superlinse kann weiterhin dafür genutzt werden um Potenzialbarrieren zu erzeugen, die um mehrere Größenordnungen höher sind als die im Fall von Grundzustandsatomen erzeugbaren. Daran anschließend wird der spontane Zerfall eines angeregten Atoms in der selben (schwach absorbierenden) Superlinsengeometrie untersucht. Es werden ebenfalls große Abweichungen vom entsprechenden absorptionsfreien Fall festgestellt, die vom strahlungslosen Anteil des spontanen Zerfalls herrühren.

Im Zusammenhang mit Casimirkräften zwischen Körpern treten verstärkende Medien an die Stelle der angeregten Atome. Das sind Materialien, die einen negativen Imaginärteil der Permittivität und/oder Permeabilität in einem bestimmten Frequenz- und Raumbereich haben. Wie im Fall der Casimir–Polder–Kräfte eröffnen solche Medienanregungen verbesserte Manipulationsmöglichkeiten der Kraft. In der vorliegenden Dissertation wird das bereits auf den Fall der Verstärkung erweiterte Quantisierungsschema angewendet und

- die Casimirkraft zwischen (teilweise) verstärkenden Körpern ausgerechnet,

- der Zusammenhang zur resonanten Casimir–Polder–Kraft gezeigt, sowie

- die Kraft zwischen einer verstärkende Platte und einem dielektrischen Halbraum analytisch untersucht.

Zunächst wird der bereits bekannte Lorentzkraftansatz für die Casimirkraft auf verstärkende Körper angewendet und die entsprechenden Korrelationsfunktionen berechnet. Die gefundene Kraftformel hat einen nicht-resonanten Anteil, der formal mit dem der Casimirkraft auf einen Grundzustandskörper übereinstimmt. Ein neu gefundener, resonanter Kraftanteil tritt nur für verstärkende Körper auf. Es wird gezeigt, dass sich

die Casimirkraft für den Fall eines optisch dünnen verstärkenden Körpers als Summe von Casimir–Polder–Kräften auf die angeregten Atome im Körper darstellen lässt. Damit wird die Lifshitztheorie auf den Fall angeregter Systeme erweitert. Als Anwendung der allgemeinen Theorie wird die Kraft zwischen einer verstärkenden Platte und einem dielektrischen Halbraum untersucht. Im Fall der optisch dünnen, verstärkenden Platte zeigt sich, dass die Kraft für große Abstände zwischen den Platten oszilliert. Die Amplituden der Oszillationen nehmen mit steigender Dicke der verstärkenden Platte ab. Für kleine Abstände zwischen den Platten kann die Kraft anziehend oder abstoßend sein, in Abhängigkeit von der Permittivität und Permeabilität des Halbraums an den atomaren Übergangsfrequenzen. Über die Näherung des optisch dünnen verstärkenden Körpers hinaus wird gezeigt, dass die Kraft im nicht-retardierten Limes ebenfalls abstoßend ist wenn der Betrag der Permittivität des Halbraumes kleiner als eins ist. Für eine weiterführende numerische Berechnung der Casimirkraft auf die verstärkende Platte werden alle Grundlagen geliefert. Es werden insbesondere die Wahl der Wurzel im Wellenvektor in der verstärkenden Platte sorgfältig diskutiert, sowie obere Grenzen für die mögliche Verstärkung angegeben, so dass das Konzept der lineare makroskopischen Quantenelektrodynamik gültig bleibt.

Die in dieser Arbeit gefundenen Resultate können auf vielfältige Weise als Grundlage für weitere Rechnungen (und gegebenenfalls auch Experimente) dienen. Der Einfluss der Lokalfeldkorrekturen könnte beispielsweise auch für zylindrische Systeme untersucht werden. Die verwendeten Punktstreutechniken eignen sich auch um die Berechnung der Casimirkraft zwischen zwei kleinen Kugeln zu vereinfachen. Zudem wäre die Untersuchung von Casimir–Polder–Kräften in Anwesenheit verstärkender Medien denkbar.